EXPERIMENTAL STUDIES OF CHAR OXIDATION AND FUME FORMATION FROM PYRITE

Thesis by

Xiaoming Li

In Partial Fulfillment of the Requirements

for the Degree of

Doctor of Philosophy

Environmental Engineering Science

California Institute of Technology

Pasadena, California

1992

(Defended August 30, 1991)

ACKNOWLEDGEMENTS

I would like to express my deepest gratitude to my advisor, Professor Richard C. Flagan, and my co-advisor, Professor George R. Gavalas, for their invaluable guidance, timely suggestions, and understanding through my graduate studies. I would also like to express my thanks to Professor James J. Morgan and Professor Michael R. Hoffmann for their guidance as my committee members and their careful review of this thesis.

I am very grateful to Yiannis Levendis, Ranajit Sahu, and Scott P. Northrop for their help to start the experiments; Soojin Kim and Michael Tsapatsis for kindly sharing instruments with me; Chak Chan, Zezhong Fu, Zhengqiang Gao, Steven Rogak, Aaron Rulison, Guojun Shi, Shih-Chen Wang, and Brian Alan Wong for their assistance, helpful discussions and friendship. I express my special thanks to Joe Fontana, Rich Eastvedt, and Hai Duc Vu for their help in building the experimental apparatus, Carol Garland for analyzing the pyrite samples, Rayma Harrison and Gunilla Hastrup for their excellent library assistance, and to Evelina Cui, Fran Matzen, and Elaine Granger for all their kindly and timely help.

I would like to express my heartfelt thanks to my mother and my family. Nothing would have happened without their love and encouragement. The last thank-you goes to him, who has shared all happiness and sorrow with me and supported me with his whole-heart, my husband, Fangdong.

ABSTRACT

Pulverized coal combustion is nowadays the most commonly used technology for power generation from coal. The detailed understanding of the coal combustion process is of fundamental importance to the design of more economic and efficient combustion devices and to the control of gaseous and particulate pollutant emission. This thesis presents an experimental study of (a) thermally induced changes of char structure and their effect on its combustion reactivity and (b) the mechanism of ash formation under conditions pertinent to pulverized coal combustion.

Pyrolyzed or partially oxidized coal char was generated in a drop-tube furnace from a Pittsburgh seam hvA bituminous coal (PSOC 1451). The char was characterized by elemental analysis and N_2 adsorption for specific surface area and pore volume distribution to better understand the influence of oxygen and residence time on the char structure. The reactivities of chars produced under different oxygen contents and residence times were examined by oxidation in a thermogravimetric analyzer. The conversion of the combustible material at high temperature was measured using ash as a tracer.

The pyrolysis and combustion of pyrite particles were studied with an electrodynamic balance and a drop-tube reactor. Two types of pyrite were examined, a natural pyrite (85% purity) and a synthetic pyrite (99.9% purity). Fume particles formed from individual pyrite particles were observed directly in electrodynamic balance experiments. The drop tube reactor experiments allow measurements of the fume particle concentration and size distribution. The nature of the fume was characterized using a Transmission Electron Microscope equipped with energy dispersive X-ray analysis. Physical mechanisms that might lead to the release of iron rich fragments were investigated.

TABLE OF CONTENTS

LIST OF FIGURES

LIST OF TABLES

CHAPTER 1

INTRODUCTION

Advanced coal combustion and advanced safe nuclear fission are recognized to be the major sources of the energy for electricity generation in the U.S. for the foreseeable future (Heins, 1991). However, nuclear power remains a distant second to coal-generated power which provides about 55% of the nation's electricity requirements. Pulverized coal combustion was introduced in the United States in the 1920's. Nowadays it is still the most widely used technology for energy generation from coal. The detailed understanding of the coal combustion process is of fundamental importance to the design of more economic and efficient combustion devices and to the control of gaseous and particulate pollutant emission. Scaroni (1989) has pointed out that the burning of coal has been practiced for centuries and misunderstood for centuries. Therefore, the challenges facing the coal combustion community are as diverse and heterogeneous as coal itself.

Coal is formed by the slow decomposition of vegetation under high pressure. The great number of plant species and the wide variety of conditions under which they coalified determine the complex structure and varied composition of coal. When pulverized coal is blown into a boiler, it undergoes devolatilization, or pyrolysis, followed by the significant oxidation of carbonaceous residual char. Devolatilization is rapid, taking 10-100 ms, while char burnout requires as much as 1 second so that char oxidation is regarded as the rate limiting step for the overall process. Devolatilization, however, determines the initial physical and chemical properties of the char, e.g., particle density, surface area, porosity, as well as molecular structure. These properties, in turn, govern the char combustion kinetics. The current understanding of coal and its combustion is summarized in Chapter 2.

This thesis presents an experimental study of coal combustion under conditions pertinent to the pulverized coal combustion. The study was focused on the effects of combustion conditions on the char properties and the char combustion reactivity, as well

as on the mechanism of iron fume formation. The char characterization experiments are described in Chapter 3. Pyrolyzed or partially oxidized coal char was generated in a drop-tube furnace from a Pittsburgh seam hvA bituminous coal (PSOC 1451). The char was characterized by elemental analysis and N_2 adsorption for specific surface area and pore volume distribution to better understand the influence of oxygen and residence time on the char structure. The reactivities of chars produced under different oxygen contents and residence times were examined by oxidation in a thermogravimetric analyzer. The conversion of the combustible material at high temperature was measured using ash as a tracer.

Mineral impurities in coal produce many severe operation problems in utility and industrial combustors. Although these impurities typically account for only 10% of the total mass, they are the sources of particulate matter in the combustor stack gas, and can reduce thermal efficiency by deposition on heat-transfer surfaces. The environmental impact of flyash has caused increasing concern. Ash particles are formed by two mechanisms. Residual ash particles are formed directly from the mineral matter in the coal, although the size distribution of these particles is intermediate between that in the parent coal and that which would result if all of the mineral matter in each coal particle coalesced to form one ash particle (Sarofim et al., 1977; Flagan and Friedlander, 1978). The extent of coalescence is determined by the fragmentation behavior of the burning char and, hence, on the porous microstructure of the char (Helble and Sarofim, 1989). The particles, which are generally larger than 0.1 μm diameter, may be distributed into two modes (Kang et al., 1990). The second major mechanism of ash particle formation is nucleation of volatilized ash (Flagan and Friedlander, 1978). The nuclei grow by Brownian coagulation, producing a sharp peak in the size distribution between 0.01 and 0.1 μm diameter. The former particles have compositions that, on average, reflect that of the bulk mineral content of the parent coal. The latter particles reflect the volatilities of

the various ash constituents, at times leading to a sharp change in the ash compositions below 0.1 μm. Taylor and Flagan (1981) observed a dramatic increase in the iron content of ash particles smaller than 0.1 μm in laboratory pulverized coal combustion studies, and attributed these particles to the vaporization/condensation route. Helble and Sarofim (1989) provide strong evidence for iron volatilization in studies of particle formation from synthetic chars that had been doped with iron.

A conflicting picture of fine iron-containing particles has arisen from studies of the fate of pyritic iron during coal combustion. Baxter and Mitchell (1989) observed substantial iron loss at the end of the devolatilization phase and beginning of the char oxidation phase of coal combustion. An analysis of the thermochemistry of iron species in the combustion environment suggested that volatilization could not account for the iron loss. They postulated that pyrrhotite nodules, a product of pyrite decomposition, are entrained in gases leaving the char particles due to carbon oxidation. In Chapter 4, the experimental results of the fume formation in pyrite reactions and physical mechanisms that might lead to the release of iron-rich fragments are discussed, with the particular emphasis on the formation mechanism of iron-rich particles as postulated by Baxter and Mitchell (1989). The experiments were conducted with an electrodynamic balance and a drop-tube reactor at temperatures below 1420K. Two types of pyrite were examined, a natural pyrite (85% purity) and a synthetic pyrite (99.9% purity). Fume particles formed from individual pyrite particles were observed directly in electrodynamic balance experiments. The drop-tube reactor experiments allow measurements of the fume particle concentration and size distribution. The nature of the fume was characterized using a Transmission Electron Microscope equipped with energy dispersive X-ray analysis.

Chapter 5 summarizes the major conclusions from this study. The recommendations for future research studies are outlined.

REFERENCES

Baxter, L. L., and Mitchell, R. E. (1989), The Release of Iron during the Combustion of Illinois #6 Coal, *6th Ann. Int. Pittsburgh Coal Conf.*, University of Pittsburgh, 64-73.

Flagan, R. C., and Friedlander, S. K. (1978), Particle Formation in Pulverized Coal Combustion: A Review, *Recent Developments in Aerosol Science*, Shaw, D. T. (Ed.), Wiley-Interscience, New York, 25-59.

Heins, G. L. (1991), Perspectives on the U.S. Energy Situation and the Role of the Modular HTGR, *Energy*, 16, 1-6.

Helble, J. J., and Sarofim, A. F. (1989), Influence of Char Fragmentation on Ash Particle Size Distributions, *Comb.& Flame*, 76, 183-196.

Kang, S. G., Kerstein, A. R., et al. (1990), Simulation of Residual Ash Formation during Pulverized Coal Combustion: Bimodal Ash Particle Size Distribution, *Aerosol Sci. Tech.*, 13, 401-412.

Sarofim, A. F., Howard, J. B., and Padia, A. S. (1977), The Physical Transformation of the Mineral Matter in Pulverized Coal under Simulated Combustion Conditions, *Comb. Sci. Tech.*, 16, 187-204.

Scaroni, A. W. (1989), Coal Combustion-Old and New Challenges, *Preprints of Papers, Am. Chem. Soc., Fuel Chem.*, 34, 256.

Taylor, D. D., and Flagan, R. C. (1981), Laboratory Studies of Submicron Particles from Coal Combustion, *18th Symp. (Int.) on Comb.*, The Combustion Institute, Pittsburgh, PA, 1227-1237.

CHAPTER 2

BRIEF REVIEW OF COAL COMBUSTION LITERATURE

Coal was used to replace wood as the principal fuel in the United States during the period from 1880 to 1890 (Nash and Williamson, 1972). It has been and will remain one of the major energy sources to meet human energy demands for the foreseeable future. Questions about the nature of coal began to be asked before the end of the 16th century (Berkowitz, 1985)), but significant research in coal combustion did not start until the 1960's (Field, et al., 1967). It was not until the apparent reduction of oil and gas supplies in the mid-70's that coal combustion research became popular in the United States, profiting from advanced instrumental methods and other experimental techniques. These new tools opened new doors to the study of coal and also demonstrated coal and its combustion to be even more complex and varied than previously supposed.

2.1 Coal Characterization

It is now generally believed that coal is formed from prehistoric plants and trees by infinitesimally slow thermal transformation under high pressure. The difference in plant debris materials and in the extent of decay of these materials determine the *type* of coal (proportions of various macerals and minerals). The minerals most commonly encountered in coal are silicates, clays, carbonates, and sulfides (Hendrickson, 1975). *Macerals* are organic substances derived from plant tissues, cell contents, and exudates that are variably subjected to decay, incorporated into sedimentary strata, and then altered physically and chemically by natural (geological) processes (Neavel, 1981). The significant features of three major classes of macerals and of their important subclasses are summarized in Fig. 2.1.

The process of conversion of plant materials such as peat to coal is called *coalification.* The final product of this process is carbon, usually in the form of natural

graphite (Ubhayakar, 1977). The putative continuity of the sequence is

peat ⟶ lignite ⟶ subbituminous coal ⟶ bituminous coal ⟶ anthracite

The degree of coalification determines the *rank* of coal. During coalification, coal loses moisture, oxygen, bitumens and hydrogen. Carbon content and heating value are raised but reactivity is reduced. The color, hardness and other physical properties are also changed. A detailed description of the origin and characteristics of coal is given by Hendrickson (1975).

Differences in plant materials and in their extent of decay influence the components present in coals. Of more than 1200 coals categorized by petrographers at the Bituminous Coal Research Institute, no two coals were, however, found to have the same elemental composition. Typical coal compositions are given in Table 2.1. The highest values observed are given in the parentheses. The composition of coal is characterized by ASTM ultimate and proximate analyses. The ultimate analysis consists of measurements of the elemental composition of coal, generally presented as mass fractions of carbon, hydrogen, oxygen, nitrogen, sulfur, and ash. The proximate analysis identifies the degree of coalification. The air-dried coal sample is used to determine moisture, volatile matter, ash, and fixed carbon which is the difference between the initial mass of coal and the sum of masses of moisture, volatiles and ash.

2.2 Coal Combustion

Pulverized coal combustion basically involves three stages: coal pyrolysis or devolatilization, char oxidation, and ash formation, which to some extent may proceed simultaneously. The schematic of combustion process is shown in Fig. 2.2.

2.2.1 Devolatilization

Devolatilization or pyrolysis plays a significant role in coal combustion because volatile evolution rates have a profound effect on ignition, flame location, and later char oxidation and ash formation. Pyrolysis may be defined as the breaking down of complex organic substances into simpler compounds under the influence of heat. The combined chemical and physical processes in devolatilization have been reviewed by a number of investigators. The slow and rapid coal devolatilization was summarized by Badzioch (1967). Anthony and Howard (1976) described all aspects of devolatilization including experimental methods, composition of volatile products, chemical kinetics and fluid mechanical effects. Ubhayakar (1977) discussed the important parameters affecting coal pyrolysis and the modeling of coal pyrolysis kinetics. Gavalas (1982) summarized the results of experimental and theoretical studies and discussed the basic chemical and physical mechanisms in pyrolysis. Poutsma (1990) recently reviewed the mechanisms of thermal decomposition of selected hydrocarbons that serve as models for processing of coal. The studies have provided a useful research tool for understanding the major chemical changes when coal is heated above 350-400°C.

(1) Products

The products of devolatilization appear as vapors, liquids and a solid carbonaceous residue. They are known as *gases*, *tar*, and *char*. In general, char has a high carbon content, while gases and tar are enriched in hydrogen, relative to the original coal. Serio et al. (1987) presented a hypothetical picture of the organic structures for a Pittsburgh seam bituminous coal and the char formed at successive stages of devolatilization. The coal consists of aromatic and hydroaromatic clusters linked by aliphatic bridges. During pyrolysis, the weakest bridges break and produce molecular fragments. The fragments abstract hydrogen from the hydroaromatics or aliphatics, thus

increasing the aromatic hydrogen concentration. These fragments will be released as tar if they are small enough to vaporize under pyrolysis conditions and do not undergo retrograde reactions before escaping from the particle. The gases, such as, CO_2, CH_4, H_2O, and light hydrocarbons, are produced by the decomposition of molecules containing different functional groups.

(2) Important Parameters

a. Rank

Rank is defined as the stage of metamorphism in the series from lignite to anthracite. Rank classifications are based on varying combinations of volatile matter content, heating value, and agglomerating properties. The low-rank subbituminous coals and lignites manifest a higher degree of reactivity than do the higher rank bituminous coals, and do not agglomerate when the coal particles are heated to temperatures of 550°C or above. A canonical correlation analysis of the relationship between the reactivity and the chemical and physical properties revealed that rank was the most significant factor for coal reactivity (Well and Smoot, 1991). The direct observations of the devolatilization were reported that bituminous coals released a large amount of volatile matter (McLean, et al., 1981; Seekeer et al., 1981; and Beck and Hayhurst, 1990). The ejected volatiles formed a condensed phase surrounding the coal particles. Under reducing conditions, the condensed volatiles persisted throughout the flow reactor. In the oxidizing condition, they were burned near the surface of the particles. The heat released from the oxidation reactions increased the particle temperature above the bulk gas temperature. No condensed phase was formed for lignite or anthracite coal. The particle temperature for the lignite only slightly shifted above the bulk temperature at the same conditions because of the relatively low heat content of lignite. The low volatile content in anthracite caused the particle temperature to take 50 ms to reach the bulk gas temperature. Anthony, et al.

(1975) studied the rapid devolatilization of a lignite and a bituminous coal in helium. For the lignite coal, the volatile yield was found to depend only on temperature and residence time. But for the bituminous, it also increased with decreasing pressure and particle size. The analysis of the volatile composition revealed that lignite coals produced mostly CO, CO_2, H_2, H_2O, and light hydrocarbons, while the main volatiles from bituminous coals were tar and light hydrocarbons (Suuberg, et al., 1978; Solomon and Colket, 1979; and McLean, et al., 1981).

b. Temperature

Temperature is a measure of the internal energy. When coal particles are gradually heated to 350-400°C, some chemical bonds within the carbon matrix begin to break, releasing volatiles (Poutsma, 1990). Some molecular bonds are even broken at a temperature as low as 250°C to produce low molecular weight compounds (Nishioka and Larsen, 1988). For a particular coal, the amount of volatiles released increases with increasing temperature and heating rate.

c. Heating Rate

Experiments of coal pyrolysis are usually conducted in devices in which the heating is achieved by conduction from an ambient hot gas or by contact of a hot surface. Therefore, the heating rate is normally a function of the maximum temperature of the gas or surface and the size of coal particles. Since the effect of heating rate is coupled to the temperature of pyrolysis, rapid heating rate generally results in a higher volatile yield than slow heating rate. In addition, the size of coal particles, ambient gas composition and pressure may also have noticeable effect on the coal devolatilization process.

2.2.2 Char Oxidation

In pulverized coal combustion, char oxidation usually takes about 10 times or even longer time than devolatilization. Therefore, the burning of the char is the rate limiting step for the overall process. However, devolatilization determines the initial physical and chemical properties of the char, e.g., density, surface area, porosity, as well as chemical structure. These properties, in turn, govern the char combustion kinetics. Researchers have correlated char reactivity with oxidant concentration, particle size, external mass transfer, pore diffusion, and active surface area. The data still vary as much as four orders of magnitude at a given temperature for different kinds of chars (Smith, 1982). The primary problem is that the effects of coal structure on reaction characteristics are not characterized to a point useful to those modelling coal combustion since coal is a complex heterogeneous mixture of organic and inorganic materials (Wells and Smoot, 1991). The study of the structural changes of coal during coal combustion is very important in the need to improve the efficiency of coal conversion technology and to better model the coal combustion process. The discussion in this section is focused on the understanding of char oxidation process.

Wells and Smoot (1991) used canonical correlation analysis to determine the relationship between the reactivity and the chemical and physical properties. For different coals, rank had a significant correlation with reactivity. The same result was found for chars extracted by pyridine. For pyrolyzed chars, the relative importance of effective factors is: catalysis elements > porosity > total hydrogen. The cation activity in their study was in the order of Na > Mg > Ca >> K.

(1) Changes of Physical Structure

Anson et al. (1971) described, in great detail, the structural change of a low rank

and a medium rank bituminous coal burning in air. On being exposed to high intensities of radiation, coal particles typically soften. Rapidly generated volatiles cause the particle to swell and produce large holes on their external surfaces as they escape. With the completion of the devolatilization process, the swelling ceased, and after a short time interval (about 40 ms for 250 μm diameter particles) the particles underwent a marked contraction to form rigid skeletons. After contraction, the initial burning of the residue took place at approximately constant diameter. Reactions occurred around the pore mouths until the char particles fragmented. Samples of lithotypes of both low and medium rank coals were heat-treated in the furnace at a temperature of 1073K for 150 ms. The measurements of the surface areas of these samples by xenon adsorption confirmed the trend toward increasing surface with decreasing rank. The surface area for 53-63 μm Ackton Hall coal (CRC 502) burning in air at about 75 ms was about twice as that of the original coal. As the residence time increased to 85 ms, the surface area increased from 111 to 125 $m^2 g^{-1}$ on dry ash free basis. The surface area started to drop near the completion of devolatilization. It was 88.5 $m^2 g^{-1}$ at approximately 130 ms, while the devolatilization was ended at about 150 ms. Under the same conditions, the measured surface area of Rawdon coal (CRC 902) was almost constant at the residence time of 85 ms, then decreased progressively with time. The surface area dropped rapidly around the time of the completion of devolatilization (~150 ms), from 121 to 55 $m^2 g^{-1}$, corresponding to the time from 130 to 180 ms. The variation of surface area of semi-anthracite coal particles during combustion was measured by Smith and Tyler (1972) at temperatures of 1400K to 2200K and oxygen fractions about 0.1 and 0.2 atm. The surface areas first increased then steadily dropped with increasing burnout. The peak appeared between about 15 to 35% burnout, corresponding to the coal particle sizes 78 to 22 μm. The surface areas also decreased with increasing gas temperatures. The particle size and density were found both to reduce with burnout, indicating that the oxygen partially penetrated into the pore structure.

Particle size, density, porosity, pore size, and surface area have been found to have important influence on the combustion behavior of particles. When combustion is limited to the outer surface of the particle or to a shallow zone below the outer surface, particles burn with constant density but with a steady reduction in size. When oxygen penetrates completely within a porous particle, combustion occurs at constant size but with decreasing density. Thin-walled cenospheres were concluded to burn with reducing density but at constant size whether oxygen penetrated the pore or not (Smith, 1982). However, different results were obtained from the recent electrodynamic balance experiments (Wong, 1991). Two cenospheric chars were generated from PSOC 1451 bituminous coal at 1200K and 1600K in nitrogen for 2 seconds (Sahu et al., 1988). The char made at 1200K shrank and densified as it was oxidized, while the char made at 1600K oxidized at constant diameter and decreased in density. It would appear that the charring history has an effect on the subsequent oxidation behavior. The 1200K char was reported to have a bimodal distribution of pore volume and pore area with significant volume in the macropore region and significant area in the micropore region. The 1600K char contained similar micro- and macroporosity, in addition, it showed significant area and volume in the so-called transition pore region, around a pore diameter of 500 Å. The density and total porosity of two chars had only slight differences. The pore structure should have an effect on the oxygen penetration within the char, which, in turn, governed the char behavior during combustion. However, the reorganization of coal chemical structure at different temperatures is a totally unexploited issue.

(2) Chemical Structural Reorganization

Anson, et al. (1971) reported that the composition of coal had some effect on the morphology of hollow spheres formed during devolatilization. Particles of vitrain and clarain, composed mainly of vitrinite, produced spheres with thinner walls than durain

particles; and for the former there was a natural progression toward more extensive internal structures with decreasing rank.

The structural transformations that occur when carbons are heated to high temperatures have been studied extensively, but measurements of structural changes occurring on the short time scale of pulverized coal combustion are extremely limited. Smith and Tyler (1972) collected partially burned chars of a semianthracite from a laminar flow furnace and examined them by optical microscopy, porosimetry and X-ray diffraction. They found that micropore surface areas of char decreased, and a sharpening of a graphite band in the X-ray pattern indicated that some structural ordering took place. Such ordering was also observed after partial combustion of glassy carbons (Levendis and Flagan, 1987). It was also observed that oxygen catalyzed the structural transformation (Levendis, et al., 1989). Haussmann and Kruger (1988) measured the hydrogen and nitrogen to carbon ratios with carbon conversion at 1750K and 7.6% O_2, and at 1300K and pure argon, for 55 μm Montana Rosebud subbituminous coal. In oxidizing atmosphere, both H/C and N/C ratios decreased until around 50% carbon conversion, then varied very slowly. The pyrolyzed chars in argon showed the drop of H/C ratio, but almost constant N/C ratio with carbon conversion. The change of H/C ratio indicates the reorganization of carbon matrix. However, the understanding of the detailed chemistry will be very difficult.

(3) Ash Catalysis

Besides the various problems caused by the existence of ash, ash components have been found to catalyze coal gasification. Walker et al. (1968) were the first to correlate the reactivity with the chemical state of iron on graphite using the magnetic susceptibility technique. They found that the catalytic activity of iron decreased sharply as the metallic phase was oxidized to wustite. Magnetite was not active. The catalytic role

of calcium has been reported by a number of investigators (Jenkins, et al. 1973; Floess, et al. 1988; Mccollor, et al. 1988). Kopsel and Zabawski (1990a,b) investigated the influence of catalytically effective ash components on coal gasification. A lignite, which did not contain aluminium, was deashed with hydrochloric acid. The original coal had a much higher gasification rate than the deashed coal. The rate was increased by a factor of 30-50 in carbon dioxide gasification and by a factor of 19-35 in steam gasification. The gasification rate of the deashed coal was enhanced after impregnation with the catalytic elements of the ash. The degree of enhancement depended on the impregnated inorganic species. In their study, sodium was found more active than calcium. The rate by simultaneous impregnation of calcium and sodium was about the sum of the rates by impregnating only one of them with the same quantity.

In order to understand the catalytic structure and function of alkali-metal carbonate, the interaction between potassium carbonate and carbon substrata in an inert atmosphere was studied by using carbon black with an amorphous structure and graphite (Matsukata, et al., 1988). Potassium carbonate impregnated on carbon black decomposed to potassium oxide and CO_2 at the temperatures of 470-900K. Potassium species were found to migrate into the carbon matrix at the temperatures of 670-900K. At higher temperatures potassium oxide on the surface was reduced by reaction with carbon. The migration of potassium into bulk carbon was not observed on graphite. The mechanism of catalysis by iron and sodium investigated by a pulse technique with $^{13}CO_2$ was suggested to be (Suzuki et al., 1988)

$$Fe_nO_m + CO_2 \longrightarrow Fe_nO_{m+1} + CO \qquad (a)$$

$$Fe_nO_{m+1} + C \longrightarrow Fe_nO_m + CO \qquad (b)$$

$$2Na + CO_2 \longrightarrow Na_2O + CO \qquad (c)$$

$$Na_2O + C \longrightarrow 2Na + CO \qquad (d)$$

The apparent activation energies for reactions (a) and (c) were estimated as 77 and 44 kJ mol^{-1} at temperatures of 500 to 700°C, and 110 and 130 kJ mol^{-1} for the reactions (b) and (d) at temperatures above 750°C.

2.2.3 Ash Formation

Ash, as determined in the proximate analysis, represents the non-combustible residue that remains after coal is burned. It is formed as a result of the many chemical changes that take place in the mineral matter of coal during combustion. The minerals most commonly encountered in coal are silicates, clays, carbonates, and sulfides. Typical variations in the composition of coal ashes versus rank of coal is given in Table 2.2.

Mineral impurities in coal produce many severe operation problems in utility and industrial combustors. Although these impurities typically account for only 10% of the mass of the coal, they are the source of particulate loadings in the combustor stack gas, and can reduce thermal efficiency by deposition on heat-transfer surfaces. There have been numerous attempts to understand the transformation of inorganic coal constituents in combustion environments. About a decade ago, Sarofim et al. (1977) explored the fundamental mechanisms of ash particle formation in pulverized coal combustion. They first elucidated the role of ash coalescence in determining the nature of the ash particles, and clearly demonstrated that substantial quantities of ash can be vaporized in pulverized coal combustion. Flagan and Friedlander (1978) modelled the evolution of the aerosol formation due to nucleation of ash vapor. Their calculations have shown that a large number of very small particles can be formed from the volatilized species by homogeneous nucleation. Laboratory studies of the particle formation in pulverized coal

combustion show that the flyash size distribution is bimodal (Markowski, et al., 1980; Quann, et al., 1982). Typically, about 99 percent of the mass forms ash particles with diameter 1 to 20 μm diameter (Haynes et al., 1982). These larger particles consist of the major ash species, Al, Ca, Fe and Si. (Flagan and Taylor, 1981). Most of the ash surface area is provided by submicron particles (0.01~0.1 μm) even though they constitute only 1% of the total mass. Both kinds of particles are coated with volatile trace elements, such as As, Sb, and S (Haynes et al., 1982). Analysis of Montana lignite ash samples suggested that the submicron particles comprised a core of Mg and Fe oxides, covered by an inner layer of Si oxides and an outer layer of Na, As, and other volatile trace elements (Neville and Sarofim, 1982). Ash particle coalescence and vaporization followed by homogeneous nucleation are the two generally accepted mechanisms of ash particle formation. During combustion, coal minerals fuse, coalesce, and adhere to the receding carbonaceous material, forming 1 to 20 μm residual ash particles. The number of such particles formed from each coal particle is determined by their coalescence and growth on the receding char particles and the fragmentation of the char as burnout approaches completion. The small ash particles are believed to be formed by homogeneous nucleation. The nuclei then grow by coagulation and by condensation of additional ash vapors.

Iron is one of the major inorganic components of coal. Over 95% of iron in coal occurs as pyrite. Investigations of the submicron fume produced during pulverized coal combustion reveal the presence of substantial concentrations of iron in these fine particles. Combustion of Utah bituminous coal at 1500K (Flagan and Taylor, 1981) produced a fume of iron-rich particles with sizes as small as 20 nm. In the burning of a Montana lignite at 1750K (Quann, et al. 1982), 20.7% iron was recovered in the submicron fume (< 0.5 μm). These fine particles were hypothesized to be generated by homogeneous nucleation of volatilized mineral matter, although the mechanism of iron

volatilization was not identified. The size distributions of the fume closely approximate the so-called *self-preserving* size distribution that would be expected for particles grown by Brownian coagulation from ultrafine particles generated by homogeneous nucleation to a size much larger than that of the original nuclei.

Baxter and Mitchell (1989) examined the fate of pyrite iron in coal combustion. Their analysis of the thermochemistry of the iron/sulfur/oxygen system suggested that iron volatilization was probably not the source of the iron rich fume in their experiments. They reported a substantial loss of iron from coal particles just at the completion of devolatilization when the char surface was exposed to an oxidizing atmosphere. When oxygen attacked char particles, there was a net mass flux away from the surface if the gaseous product was CO. The iron-rich fume was postulated to be generated when iron or pyrrhotite nodules, the product of pyrite decomposition, detached from the surface of the char particles due to aerodynamic forces caused by the outflux. No direct measurements of the size of the fume particles that penetrated the filters were made, but they suggested that the iron fume produced consisted of particles in the range of 0.02 to 0.2 μm. Srinivasachar et al. (1990) studied the pyrite transformation under pulverized coal combustion conditions. They reported that a few submicron particles formed from pyrite particles. It is possible that there are different mechanisms of ash particle formation. Carefully designed experimental investigations may shed light on the origins of combustion-derived fine particles.

REFERENCES

Anson, D., Moles, F. D., and Street, P. J. (1971), Structure and Surface Area of Pulverized Coal During Combustion, *Comb. & Flame*, 16, 265-274.

Anthony, D. B., Howard, J. B., et al. (1975), *15th Symp. (Int.) on Comb.*, The Combustion Institute, Pittsburgh, PA, 1303.

Anthony, D. B., and Howard, J. B. (1976), Coal Devolatilization and Hydrogasification, *AICHE J.*, 22, 625-656.

Badzioch, S. (1967), Thermal Decomposition, Chapter 4, In *Combustion of Pulverized Coal*, Field, M. A., Gill, D. W., et al. (Eds.), The British Coal Utilization Research Association, Leatherhead, England.

Baxter, L. L., and Mitchell, R. E. (1989), The Release of Iron during the Combustion of Illinois #6 Coal, *6th Ann. Int. Pittsburgh Coal Conf.*, University of Pittsburgh, 64-73.

Beck, N. C., and Hayhurst, A. N. (1990), *Comb. & Flame*, 79, 47.

Berkowitz, N. (1985) (Ed.), *The Chemistry of Coal*, Elsevier: Amsterdam, The Netherlands.

Field, M. A., Gill, D. W., et al. (1967) (Eds.), *Combustion of Pulverized Coal*, The British Coal Utilization Research Association, Leatherhead, England.

Flagan, R. C., and Friedlander, S. K. (1978), Particle Formation in Pulverized Coal Combustion: A Review, *Recent Developments in Aerosol Science*, Shaw, D. T. (Ed.), Wiley-Interscience, New York, 25-59.

Flagan, R. C., and Seinfeld, J. H. (1988) (Eds.), *Fundamentals of Air Pollution Engineering*, Prentice Hall: Englewood Cliffs, New Jersey.

Flagan, R. C., and Taylor, D. D. (1981), Laboratory Studies of Submicron Particles from Coal Combustion, *18th Symp. (Int.) on Comb.*, The Combustion Institute, Pittsburgh, PA, 1227-1237.

Floess, J. K., Longwell, J. P., and Sarofim, A. F. (1988), *Energy & Fuels*, 2, 756.

Gavalas, G. R. (1982) (Ed.), *Coal Pyrolysis*, Elsevier: Amsterdam, The Netherlands.

Haussmann, G. J., and Kruger, C. H. (1988), *22nd Symp. (Int.) on Comb.*, The Combustion Institute, Pittsburgh, PA, 223-230.

Haynes, B. S., Neville, M., et al. (1982), Factors Governing the Surface Enrichment of Fly Ash in Volatile Trace Species, *J. Colloid and Interface Sci.*, 87(1), 266-278.

Hendrickson, T. A. (1975) (Ed.), *Synthetic Fuels Data Handbook*, Cameron Engineers, Inc., Denver, Colo.

Jenkins, R. G., Nandi, S. P., and Walkeer, Jr., P. L. (1973), *Fuel*, 52, 288.

Kopsel, R., and Zabawski, H. (1990a), *Fuel*, 69, 275.

Kopsel, R., and Zabawski, H. (1990b), *Fuel*, 69, 282.

Levendis, Y. A., and Flagan, R. C. (1987), *Comb. Sci. & Tech.*, 53, 117.

Levendis, Y. A., Flagan, R. C., and Gavalas, G. R. (1989), *Comb. & Flame*, 76, 221.

Markowski, G. P., Ensor, D. S., and Hooper, R. G. (1980), A Submicron Aerosol Mode in Flue Gas from a Pulverized Coal Utility Boiler, *Engineering Sci. & Tech.*, 14, 1400-1402.

Matsukata, M., Fujikawa, T., et al. (1988), *Energy & Fuels*, 2, 750.

Mccollor, D. P., Jones, M. L., and Benson, S. A. (1988), *22nd Symp. (Int.) on Comb.*, The Combustion Institute, Pittsburgh, PA, 59.

McLean, W. J., Hardesty, D. R., et al. (1981), *18th Symp. (Int.) on Comb.*, The Combustion Institute, Pittsburgh, PA, 1239.

Nash, R. T., and Williamson, J. W. (1972), Energy use in the United States: 1880-1966, *Fuel*, 51, 258.

Neavel, R. C. (1981), Coal Structure and Coal Science: Overview and Recommendations, In *Coal Structure*, Gorbaty, M. L. and Oucki, K., Am. (Eds.), Chem. Soc., Washington, D. C.

Neville, M. and Sarofim, A. F. (1982), The Stratified Composition of Inorganic Submicron Particles Produced during Coal Combustion, *19th Symp. (Int.) on Comb.*,

The Combustion Institute, Pittsburgh, PA, 1441-1449.

Nishioka, M, and Larsen, J. W. (1988), *Energy & Fuels*, 2, 351.

Poutsma, M. L. (1990), Free-Radical Thermolysis and Hydrogenolysis of Model Hydrocarbons Relevant to Processing of Coal, *Energy & Fuels*, 4(2), 113.

Quann, R. J., Neville, M., et al. (1982), Mineral Matter and Trace-Element Vaporization in a Laboratory-Pulverized Coal Combustion System, *Environ. Sci. Tech.*, 16, 776-781.

Sahu, R., Levendis, Y. A., et al. (1988), *Fuel*, 67, 275-283.

Sarofim, A. F., Howard, J. B., and Padia, A. S. (1977), The Physical Transformation of the Mineral Matter in Pulverized Coal under Simulated Combustion Conditions, *Comb. Sci. Tech.*, 16, 187-204.

Seekeer, W. R., Samuelsen, G. S., et al. (1981), *18th Symp. (Int.) on Comb.*, The Combustion Institute, Pittsburgh, PA, 1213.

Serio, M. A., Hamblen, D. G., et al. (1987), *Energy Fuels*, 1, 138.

Smith, I. W. (1982), *19th Symp. (Int.) on Comb.*, The Combustion Institute, Pittsburgh, PA, 1045.

Smith, I. W. and Tyler, R. J. (1972), *Fuel*, 51, 312.

Solomon, P. R., and Colket, M. B. (1979), *17th Symp. (Int.) on Comb.*, The Combustion Institute, Pittsburgh, PA, 131.

Srinivasachar, S., Helble, J. J., and Boni, A. A. (1990), Mineral Behavior during Coal Combustion, 1. Pyrite Transformation, *Prog. Energy Comb. Sci.*, 16, 281-292.

Suuberg, E. M., Perters, W. A., and Howard, J. B. (1978), *17th Symp. (Int.) on Comb.*, The Combustion Institute, Pittsburgh, PA, 117.

Suzuki, T., Inoue, K., and Watanabe, Y. (1988), *Energy & Fuels*, 2, 673.

Ubhayakar, S, K. (1977), *Pyrolysis of Coal*, AVCO Everett Research Laboratory, Inc., a Subsidiary of AVCO Co., Everett, Massachusetts 02149.

Walker, P. L., Shelef, M., and Anderson, R. A. (1968) (Eds.), *Chemistry and Physics of*

Carbon, Vol. 4, Marcel Dekker: New York, p 287.

Well, W. F., and Smoot, L. D. (1991), Relation between Reactivity and Structure for Coals and Chars, *Fuel*, 70(3), 454-458.

Wong, B. A. (1991), *The Oxidation of Individually Levitated Char Particles*, Ph. D. Thesis, California Institute of Technology.

Table 2.1 Typical Coal Composition (mass percentages)*

Component	Composition
Carbon	65-95
Hydrogen	2-7
Oxygen	≤ 25
Sulfur	≤ 10
Nitrogen	1-2
Inorganic Mineral	5-15 (≤ 50)
Moisture	2-20 (≤ 70)

* Essenhigh, R. H. (1977), Combustion and Flame Propagation in Coal Systems, *16th Symp. (Int.) on Comb.*, The Combustion Institute, Pittsburgh, PA, 1227-1237.

Table 2.2 Variations in Coal Ash Composition with Rank*

Rank	Lignite	Subbituminous	Bituminous	Anthracite
SiO_2 (%)	6-40	17-58	7-68	48-68
Al_2O_3 (%	4-26	4-35	4-39	25-44
Fe_2O_3 (%)	1-34	3-19	2-44	2-10
TiO_2 (%)	0-0.8	0.6-2	0.5-4	1.0-2
CaO (%)	12.4-52	2.2-52	0.7-36	0.2-4
MgO (%)	2.8-14	0.5-8	0.1-4	0.2-1
Na_2O (%)	0.2-28	-	0.2-3	-
K_2O (%)	0.1-1.3	-	0.2-4	-
SO_3 (%)	8.3-32	3.0-16	0.1-32	0.1-1

*Hendrickson, T. A. (1975) (Ed.), *Synthetic Fuels Data Handbook*, Cameron Engineers, Inc., Denver, Colo.

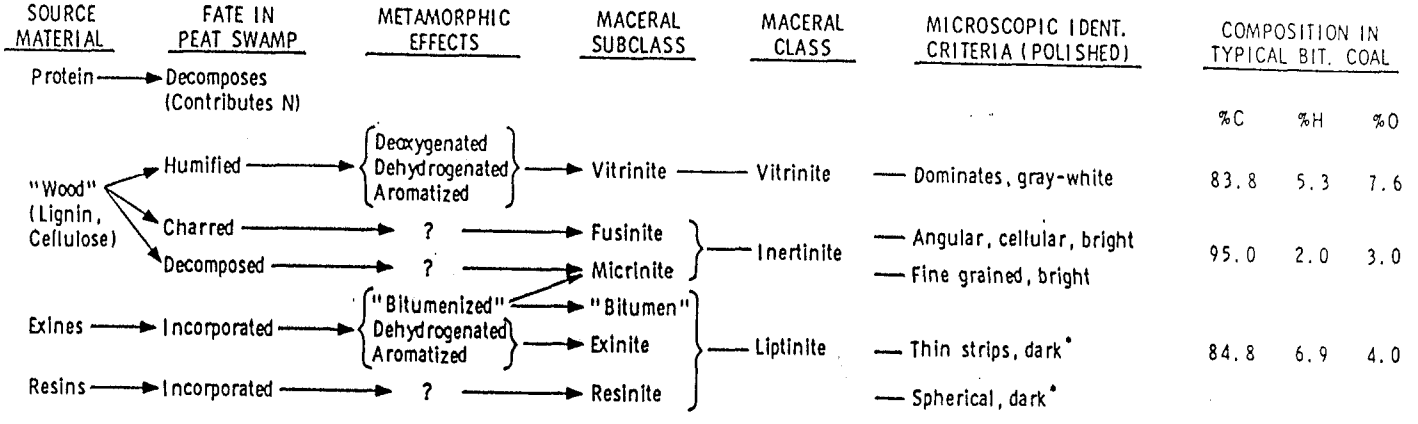

Fig. 2.1 Principal features of the major classes of macerals (Neavel, 1981)

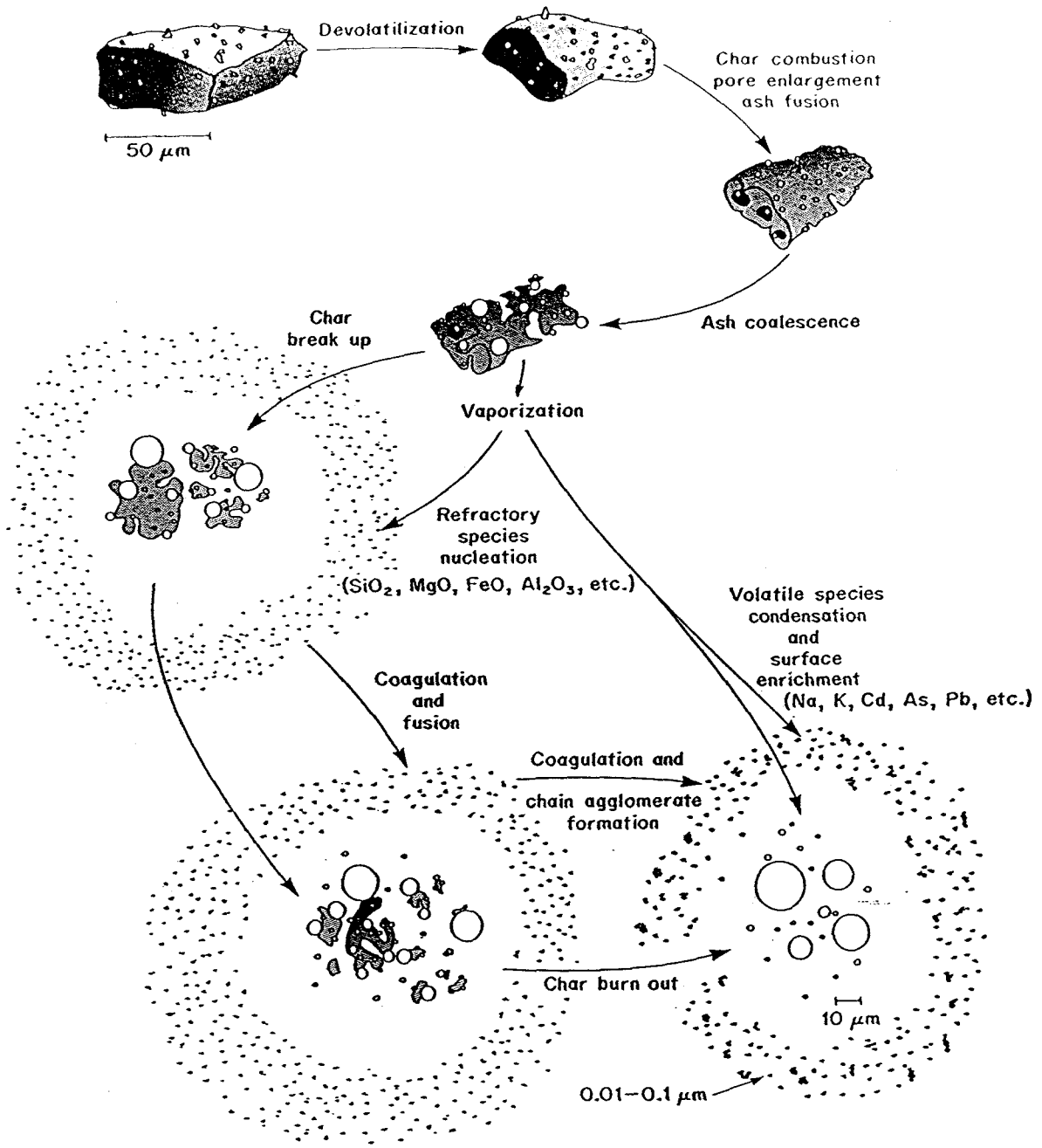

Fig. 2.2 Schematic diagram of coal combustion

(Flagan and Seinfeld, 1988)

CHAPTER 3

CHAR STRUCTURAL CHANGES IN PULVERIZED COAL COMBUSTION

CHAR STRUCTURAL CHANGES IN PULVERIZED COAL COMBUSTION

ABSTRACT

Chars were generated from a hvA bituminous coal in a drop-tube furnace in an atmosphere of N_2 or 1-5% O_2 in N_2 and at 1600K temperature. The chars were characterized by elemental analysis for carbon and hydrogen contents, N_2 adsorption for BET surface area and pore size distribution, and by oxidation in a thermogravimetric analyzer at a temperature of 773K. The effects of charring history on char structure and reactivity are discussed.

3.1 Introduction

Devolatilization and char oxidation are the two major steps involved in coal combustion. The first step is rapid and the second is slow. In pulverized coal combustion devolatilization takes 10-100 ms. Char burnout requires as much as 1 second, making it the rate limiting step for the overall process. However, devolatilization determines the initial physical and chemical properties of the char, e.g., particle density, surface area, porosity, as well as molecular structure. These properties, in turn, govern the char combustion kinetics.

The structural transformations that occur when carbons are heated to high temperatures have been studied extensively, but measurements of structural changes occurring on the short time scale of pulverized coal combustion are extremely limited. Smith and Tyler (1972) collected partially burned chars of a semianthracite from a laminar flow furnace and examined them by optical microscopy, porosimetry and X-ray diffraction. The micropore surface area was found to decrease with burnout. A sharpening

of a graphite band in the X-ray pattern indicated that some structural ordering took place. Such ordering was also observed after partial combustion of glassy carbons (Levendis and Flagan, 1987). Oxygen was observed to catalyze the structural transformation (Levendis et al., 1989). The decrease in the reactivity of the carbonaceous material that is expected to accompany these changes could have important implications to combustor design and operation. In the present work, we examine the structural changes occurring at combustion temperatures and times typical of pulverized combustion and probe the effect of the changes on the rate of char oxidation.

3.2 Experimental Methods

3.2.1 Char Formation

Chars were made from a high-volatile A bituminous coal (PSOC 1451). The properties of the coal are given in Table 3.1. The coal was pulverized in a mechanized mortar and pestle in air. It was then size classified by sieving on a mechanical shaker. The 45-53 μm coal size fraction was dried by heating in nitrogen at 100°C for one hour and then cooled to room temperature before char production. The experimental system has been described in detail elsewhere (Sahu, 1988) and is only briefly described here. Combustion experiments were conducted in a drop-tube furnace (Applied Test System, Series 3310) consisting of an alumina tube of 5 cm internal diameter and 71 cm length heated by Kanthal Super 33 elements. The gas temperatures were measured with a suction pyrometer. The isothermal zone of the reactor was about 30 cm long. The wall temperature was maintained at 1748K to 1773K, depending on the residence time, to produce a gas temperature of 1600K at the center of the isothermal zone in all experiments. The temperature at the ends of the isothermal zone dropped about 10%. Coal particles were injected into the alumina reactor through a water-cooled injector at a

rate of 3 gm hr^{-1}. Experiments were performed in pure nitrogen or in mixtures of 1 or 5% oxygen in nitrogen. The coal chars were collected on 0.4 μm nuclepore filters with a water-cooled, gas dilution quench probe. The residence times of the coal particles inside the furnace were varied by adjusting the gas flow rate and the position of the sampling probe. Both size classified, dried coal and the chars produced in the drop-tube furnace were stored under nitrogen atmosphere.

3.2.2 Char Characterization

(1) Elemental Analysis

The mass fractions of carbon, hydrogen, and nitrogen in various char samples were determined by a Model 240 Elemental Analyzer. These analyses were based on detecting and measuring the combustion products of carbon dioxide, water, and nitrogen in pure oxygen at a temperature of 860°C.

(2) Surface area

The surface areas of the chars were obtained by a modified volumetric adsorption technique described by Northrop et al. (1987). The gas adsorption isotherms were measured by continuous addition of adsorbate gas (N_2 at 77K) to the sample (see Appendix A). The apparatus was calibrated with γ-alumina. The relative measurement uncertainty is about ±15% for a surface area of 1 $m^2\,gm^{-1}$ and decreases with increasing sample surface area. The repeatability of the measurements was tested with duplicates using (1) the same sample; (2) or different samples of the same material. Each pair of measurements agreed to within 20% (Table 3.2).

(3) Pore volume distribution

The BET model is usually applied to a relative pressure range $0.04 < P/P^\circ < 0.30$, where P° is the vapor pressure of adsorbate. At higher relative pressure, capillary condensation occurs in porous solids due to the surface tension induced pressure difference across the curved meniscus of the condensed vapor. The size of the capillary can be calculated by the Kelvin equation,

$$ln\frac{P}{P^\circ} = \frac{2\gamma v\cos\theta}{LRT} \tag{3.1}$$

where γ is the surface tension, v is the molar volume, θ is the contact angle, L is the radius of a cylindrical pore. For a slit pore, L is half the distance between the walls. R is the gas constant and T is the absolute temperature.

Using the capillary condensation model including multilayer adsorption in cylindrical pores, Wheeler (1946) deduced that the specific pore volume $V(r)$ was related to the volume of nitrogen desorbed over a small segment on the desorption branch of the isotherm $v(r)$ by

$$v(r) = \left(\frac{r - t(r)}{r}\right)^2 V(r) + \frac{dt}{dr}\int_{r_0}^{r} \frac{2r' - t(r')}{r'^2} V(r')dr' \tag{3.2}$$

where r is the radius of the pore, t is the thickness of the adsorbed layer of gas. The first term on the right accounts for liquid evaporated from the pores, and the second term represents the amount of gas desorbed from free surfaces. However, Wheeler was not able to solve Eq. 3.2 for the unknown $V(r)$ at that time. Cranston and Inkley (1957) later developed a method to calculate $V(r)$. The volume of pores having radii, r, in the range $r_1 \le r \le r_2$ is estimated to be

$$V_{12} = R_{12}\left(v_{12} - k_{12}\sum_{r_2+\frac{\Delta r}{2}}^{r_{max}} \frac{r - t_{12}}{2r^2} V_r \Delta_r\right) \tag{3.3}$$

where

$$R_{12} = \left(\frac{1}{r_2 - r_1}\int_{r_2}^{r_1} \frac{r - t_1}{r}\, dr\right)^{-1}$$

$k_{12} = 4(t_2 - t_1)$, and $t_{12} = (t_2 + t_1)/2$. $V_r\Delta_r$ is the volume of pores having radii between r and $r+\Delta_r$, where Δ_r is very small compared with r. The quantity v_{12} is the total volume of nitrogen adsorbed during the adsorption step from pressure P_1 to pressure P_2, where P_1 corresponds to the critical radius r_1 and P_2 to radius r_2. The quantities t_1 and t_2 are the adsorbed layer thicknesses at the pressures P_1 and P_2, respectively. The t values were given by Lippens et al. (1964). We used Eq. 3.3 to estimate pore volume distributions from our adsorption measurements.

3.2.3 Char Reactivity

(1) High Temperature Conversion

To calculate the conversion of the chars generated under different atmospheres and residence times, the ash content of the samples was used as a tracer by assuming that the mass of the ash remains constant. Measured amounts of air-dried chars were burned in air at a temperature of 800°C for more than 5 hours. The ash content was then determined gravimetrically from mass measurements made before and after complete combustion. From the known ash content, the char conversion can be derived as follows:

$$M_{coal} = M_{ash} + M_c \tag{3.4}$$

$$M_{char} = M'_{ash} + M'_{c} \tag{3.5}$$

where M_c is the mass of combustible material. The relative ash contents of the coal and char samples, $R_{ash} = \frac{M_{ash}}{M_{coal}}$, and $R'_{ash} = \frac{M'_{ash}}{M_{char}}$, are determined experimentally. The measurement error is about ± 5%. The mass of char produced from a given mass of coal is,

$$M_{char} = M_{coal} \frac{R_{ash}}{R'_{ash}} \tag{3.6}$$

Combining Eqs. 3.4 to 3.6, the conversion of combustible material, η, becomes

$$\eta = \frac{M_{coal} - M_{char}}{M_c} = \frac{R'_{ash} - R_{ash}}{R'_{ash}(1 - R_{ash})} \tag{3.7}$$

(2) Low Temperature Conversion

Chars were oxidized under a flow of 5% O_2 in N_2 at 773K in a Dupont model 951 Thermogravimetric Analyzer (TGA). The typical sample size was about 5 mg. The sample was first heated in nitrogen at a rate of 30 K min^{-1} to the desired temperature. Oxygen was then immediately introduced. The measurements were conducted under isothermal conditions. The gas flow rate was 150 cm^3 min^{-1} for all runs. This flow rate was selected to avoid entrainment of the low density materials while eliminating diffusion resistance. The sample mass was continuously recorded using a data acquisition system. To correct for different ash contents of the various chars, the mass of ash was deducted from the total mass. Although the reaction was allowed to proceed for 2 hours,

some unreacted combustible material remained. The temperature of the TGA was increased to 1073K after about 90% conversion to burn out completely the residual carbon then reduced back to 773K when the ash mass was recorded. To discriminate between the TGA measurements and those obtained in drop-tube reactor experiments at high temperature, the TGA conversion is labeled χ, and defined separately as

$$\chi = \frac{M_{initial} - M_{measured}}{M_{initial} - M_{ash}} \tag{3.8}$$

where $M_{initial}$ is the sample mass at the moment oxygen was admitted.

3.3 Results and Discussion

Properties of chars produced under different conditions are listed in Table 3.3. The char morphology was examined by scanning electron microscopy. As Fig. 3.1 shows, the original coal particles were angular with a maximum aspect ratio about 5. Upon exposure to 1600K in nitrogen for 100 ms (Fig. 3.2), the particles started to change shape to spherical. At the same time the evolution of volatiles and trapped gases opened the pores on the particle surface (Fig. 3.2). These pores had a very broad size range from less than 1 μm to larger than 20 μm. Numerous ash particles appeared on the surface of char particles. When the residence time was increased to 200 ms, the particles became quite spherical (Fig. 3.3), and "Blow-holes" (following the terminology of Anson et al., 1971) appeared on the particle surface. As the residence time was further increased to 300 ms, the coal particles became cenospheres (Fig. 3.4). In 1% oxygen, the "blow-holes" appeared only for the 100 ms sample (Fig. 3.5). At 200 ms, the particles had lost a large fraction of their mass but kept their integrity by cross partitions (Fig. 3.6). Fragmentation occurred after 300 ms of combustion (Fig. 3.7). Raising the oxygen concentration increased the combustion rate. In 5% oxygen, the morphology of char particles collected

at 100 ms was similar to that of the particles generated at 200 ms in 1% oxygen (Fig. 3.8). At 200 ms residence time, the large loss of mass caused some particles to lose their integrity (Fig. 3.9). The fragmentation was significant after 300 ms residence time (Fig. 3.10). Comparing the original coal and the chars produced in nitrogen and oxygen, the char particles are more spherical as a result of the softening and swelling of the coal particles upon injection in the furnace. Although the original coal was sieved into a narrow size cut, the irregular particle shape prevents a direct evaluation of the degree of swelling. This irregular shape as well as the variation of the chemical composition among individual coal particles resulted in char particles possessing varied visible structures. The char particles seemed to burn at constant size until they fragmented. Comparison of the chars generated in nitrogen and oxygen showed some differences. Firstly, a great number of pores of less than 5 μm diameter appear on the surface of char particles produced at 100 ms in nitrogen. After devolatilization, cracks were formed at the thinner walls of the hollow particles (Figs. 3.3 and 3.4). Some particles were then broken into small fragments. In an oxidizing atmosphere, oxygen penetrated into the interior of the particles through the opened pores and mass removal by oxidation was observed around the pore mouths. Fragmentation took place only when almost all carbon was consumed (Figs. 3.6-3.8). Secondly, quite large ash particles appeared on the surface of nitrogen chars. The ash particles for oxygen chars were relatively small and adhered on the carbon skeleton. They grew gradually by coalescence as reactions proceeded.

Figs. 3.1 to 3.10 show the formation and growth of macropores. Information about the micropores ($15 \leq r \leq 120$ Å) and the total surface area was obtained by N_2 adsorption. For all of the chars, the surface area and the volume of micropores increased dramatically within the first 100 ms over the values for the original coal, indicating new pore formation and the pore growth (Figs. 3.11 to 3.15). The trends at later times, however, differed. The surface areas and pore volumes of nitrogen chars increased with

time. The peak observed at about 20 Å in the pore volume distribution of N2 char, and the change of C/H ratio (Table 3.3) suggested that there were still some small molecules released when the residence time was increased to 200 ms. In oxygen atmospheres, both surface area and volume of micropores first increased and then decreased after 100 ms. The decrease of micropores could be caused either by pore closure or pore growth to larger sizes. It should be noted that although the oxygen concentration in these experiments was only 1 to 5%, the bulk gas concentration did not change appreciably along the reactor because of the small coal feed rate.

Little information is available about the change of char surface area with the pyrolysis time of coal. Anson et al. (1971) and Smith and Tyler (1972) reported direct observation of surface area changes during coal combustion. The surface area for 53-63 μm Ackton Hall coal (CRC 502) particles burning in air at about 75 ms was about twice that of the original coal (Anson et al., 1971). As the residence time increased to 85 ms, the surface area increased continuously, from 111 to 125 $m^2 g^{-1}$ on dry ash free basis. The surface area started to drop near the completion of devolatilization. It was 88.5 $m^2 g^{-1}$ at approximately 130 ms, while the devolatilization ended at about 150 ms. Smith and Tyler (1972) measured the variation of surface area of semi-anthracite coal particles during combustion at temperatures of 1400K to 2200K and oxygen pressures about 0.1 and 0.2 atm. The surface areas first increased then steadily dropped with increasing burnout. The peak appeared between about 15 to 35% burnout, corresponding to the coal particle sizes 78 to 22 μm. The surface areas also decreased with increasing gas temperatures. The particle size and density were found both to reduce with burnout, indicating that the oxygen partially penetrated into the pore structure. The surface area of char generated in nitrogen for two seconds was also reported to decrease when burning in air (Sahu, 1988). Smith and Tyler (1972) collected partially burned chars and examined them by optical microscopy, porosimetry and X-ray diffraction. They reported that macropores (> 0.02

μm) increased with burnout, but micropores (< 0.02 μm) decreased. A sharpening of a graphite band in the X-ray pattern indicated that some structural ordering took place. The decrease in surface area was believed to be related to the closure of micropores associated with thermally induced alterations in solid structure.

The ash content and the carbon conversion (η as defined in Eq. 3.7) in chars produced under different conditions are plotted in the Figs. 3.16 and 3.17. In our drop-tube reactor experiments, the bulk of devolatilization of coal particles in nitrogen was completed within 100 ms as shown by the approximately equal ash contents of N1 and N2 chars, although there were some changes of C, H, and N contents measured by elemental analysis. The volatile yield was 10% higher than the value given by the ASTM proximate volatile analysis (Table 3.1) due to high temperature and the rapid mass and heat transfer. The weight loss, or conversion, increased with oxygen concentration. For the chars generated in oxygen, conversion also increased with residence time. The conversion calculated with initial carbon the carbon remaining after pyrolysis in N_2 for 100 ms, and excluding ash is given by

$$\eta' = \frac{\eta - \eta_{N1}}{(1 - \eta_{N1})} \tag{3.9}$$

are listed in Table 3.3. Even within 100 ms, there was 26% fixed carbon burned in 1% O_2 and 18% more in 5% O_2. By 300 ms, more than one third of the fixed carbon was lost in 1% O_2, and over 80% fixed carbon was consumed in 5% O_2. Jost et al. (1984) studied the devolatilization of pulverized coal in a flow tube reactor at gas temperatures between 1300K and 2000K and oxygen concentrations between 7% and 16%. They reported that the devolatilization rates increased with increasing oxygen concentration for a given gas temperature. They suggested that energy from the oxidizing volatiles was fed back to the coal particles, increasing their temperature and thereby the volatile release rate and yield.

An increase of the particle temperature due to the oxidation of volatiles was also reported by Seekeer et al. (1981). Devolatilization rates and yields increase with particle temperature have also been observed in experiments by Kimber and Gray (1967) and Kobayashi et al. (1977).

The char conversions, χ as defined in Eq. 3.8, are measured with the TGA and plotted in Figs. 3.18 to 3.20. The apparent reaction rates in Figs. 3.18 to 3.20 were obtained by differentiating the conversion curves. The char reactivities were obviously affected by the charring history. In all cases the char reactivity decreased with the content of oxygen. As shown in Figs. 3.18 to 3.20, the apparent rates increase sharply during the first 5 to 10% carbon conversion and then decrease. This phenomenon could result from the gradual chemisorption of oxygen. The sample was initially heated in nitrogen to reach the desired temperature. Oxygen was then immediately introduced. The gas composition over the sample, however, changes gradually from pure nitrogen to a final mixture of 5% oxygen in nitrogen. Jenkins et al. (1973) suggested that oxygen complex formation at the surface and char activation may also be important at this early stage of conversion. After the apparent rates reached the maximum, they decreased with time. The difference in apparent rate among the various chars decreased with conversion. After 60 to 70% carbon conversion, all the chars oxidized with quite similar rates. At the low temperature of the TGA experiments, the reaction is under kinetic control as it can be shown by an estimate of the Thiele modulus for the reaction. To achieve 70% conversion needs 40 to 60 minutes. During this long period, the more reactive fraction of the combustible material would have burned, leaving behind the more inert fraction. Significant reorganization of char structure could also have been completed. Therefore, the difference in chemical and physical properties of the various chars, which affect the reaction rate, could have been largely eliminated resulting in more uniform oxidation rates.

3.4 Conclusions

Structural changes of char and their effect on char reactivity have been examined under pulverized coal combustion conditions. When heated in neutral or oxidizing atmosphere, the great majority of the hvA bituminous coal (PSOC 1451) particles undergo a series of structural changes. Hollow sphere are formed, followed by particle fragmentation. In 1 or 5% oxygen, oxidation proceeds both externally and internally at approximately constant diameter until the onset of fragmentation. For all of the chars, the surface area and the pore volume in the size range 15 to 120 Å increased dramatically within the first 100 ms compared with the original coal. The ratio of carbon to hydrogen increases with residence time. Carbon conversion at 1600K also increases with increasing oxygen pressure. But the char reactivity measured at the low temperature TGA experiments was decreased. Significant structural reorganization occurred either simultaneously with devolatilization or continuously after devolatilization depending on the oxygen concentration. Oxygen appeared to accelerate the structural changes and to change the reactivity of the char.

ACKNOWLEDGEMENTS

This work was supported by the U.S. Department of Energy University Coal Research Program under grant number DE-FG22-89PC89765.

REFERENCES

Anson, D., Moles, F. D., and Street, P. J. (1971), *Comb. & Flame*, 16, 265-274.

Cranston, R. W., and Inkley, F. A. (1957), *Adv. In Cat.*, 9, 143.

Jenkins, R. G., Nandi, S. P. and Walker Jr., P. L. (1973), *Fuel*, 52, 288.

Jost, M., Leslie, I., and Kruger, C. (1984), *20th Symp. (Int.) on Comb.*, The Combustion Institute, Pittsburgh, PA, 1531.

Kimber, G. M., and Gray, M. D. (1967), *Comb. & Flame*, 11, 360.

Kobayashi, H., Howard, J. B., and Sarofim, A. F. (1977), *16th Symp. (Int.) on Combustion*, The Combustion Institute, Pittsburgh, PA, 411.

Levendis, Y. A., and Flagan, R. C. (1987), *Comb. Sci. & Tech.*, 53, 117.

Levendis, Y. A., Flagan, R. C., and Gavalas, G. R. (1989), *Comb. & Flame*, 76, 221.

Lippens, B. C., Linsen, B. G., and de Boer, J. H. (1964), *J. cat.*, 3, 32.

Northrop, P. S. (1988), *A Fundamental Study of Char Combustion: Changes in Particle Morphology during Oxidation*, Ph. D. Thesis, California Institute of Technology.

Northrop, P. S., Gavalas, G. R., and Flagan, R. C. (1987), *Langmuir*, 3, 300.

Sahu, R. (1988), *On the Combustion of Bituminous Coal Chars*, Ph. D. Thesis, California Institute of Technology.

Seekeer, W. R., Samuelsen, G. S., et al. (1981), *18th Symp. (Int.) on Comb.*, The Combustion Institute, Pittsburgh, PA, 1213.

Smith, I. W. and Tyler, R. J. (1972), *Fuel*, 51, 312.

Wheeler, A. (1946), *Catalyst Symposium, Gibson Island AAAS Conference.*

Table 3.1 Properties of Raw Coal

PSOC #	1451
Rank	HVAB
Location	Pennsylvania
Seam	Pittsburgh
Proximate Analysis (%)	
moisture	2.54
ash	13.32
volatiles	33.56
fixed carbon	50.58
Ultimate Analysis (%)	
ash	13.32
carbon	70.05
hydrogen	4.55
nitrogen	1.33
sulfur	1.33
chlorine	0.07
oxygen*	6.81
FSI	7.5

* moisture excluded

Table 3.2 Repeatability of the Surface Area Measurements

a. The measurements with the same sample:

Sample	Sample Size (gm)	Surface area (m^2)	Specific Surface Area (m^2/gm)	$\frac{\Delta S}{\overline{Si}}$
1% O_2	0.0596	0.412	8.28	0.259
200 ms		0.511	10.43	0.205
5% O_2	0.1066	0.378	3.54	0.198
200 ms		0.453	4.25	0.166
5% O_2	0.0908	0.410	4.51	0.176
300 ms		0.482	5.31	0.149
γ-Al_2O_3	0.0136	2.12	155.1	0.118
		2.37	173.9	0.105

b. The measurements with the same material:

Sample	Sample Size (gm)	Surface area (m^2)	Specific Surface Area (m^2/gm)	$\frac{\Delta S_{max}}{\overline{Si}}$
N_2*	0.2181	2.77	15.7	0.013
200 ms	0.2145	2.68	15.5	0.013
1% O_2	0.1164	0.811	8.36	0.248
200 ms	0.0596	0.511	10.43	0.198
	0.1405	24.0	170.8	0.092
γ-Al_2O_3	0.0497	8.39	168.8	0.093
	0.0136	2.12	155.1	0.101

*The char was 53-90 μm, and generated from 38-74 μm coal.

Table 3.3 Characterization of PSOC 1451 1600K Chars

char	time (ms)	name	R'_{ash} (%)	conversion (%)		S ($m^2\,gm^{-1}$)		mean mass fraction (%)			C/H
				η^1	η'^2	total	d.a.f.[3]	C	H	N	
N_2	100	N1	18.0 (21.6)[4]	46.6	-	4.15 (3.04)[4]	4.58 (3.27)[4]	68.02	0.86	1.14	79.09
	200	N2	17.7 (22.63)[4]	45.5	-	14.2 (12.7)[4]	16.8 (15.7)[4]	83.49	0.98	1.08	85.19
	300	N3	-	-	-	-	-	82.97	0.81	0.845	102.4
1% O_2	100	O11	22.9 (21.7)[5]	60.5	26.0	10.2 (9.33)[5]	12.6 (11.3)[5]	73.96	0.80	1.32	93.03
	200	O12	22.5 (27.5)[4]	59.6	24.3	6.97 (5.01)[4]	8.36 (6.08)[4]	74.51	0.69	1.30	108.0
	300	O13	25.5	65.7	35.8	-	-	74.99	0.65	1.20	115.4
5% O_2	100	O51	28.3	70.3	44.4	17.2	23.1	64.63	0.88	1.21	73.17
	200	O52	37.2	80.2	62.9	3.54	4.34	60.04	0.73	1.12	82.81
	300	O53	58.4	91.6	84.3	4.51	7.77	48.16	0.64	0.835	75.83

*1. R_{ash} = 10.5 (%); 2. η_{N1} = 46.6 (%); 3. S_{ash} = 2.19 ($m^2\,gm^{-1}$)

4. The char was 53-90 μm, and generated from 38-74 μm coal; the coal feed rate is 5 gm $hour^{-1}$.

5. The char was generated from 53-61 μm.

Fig. 3.1 Unreacted PSOC coal particles

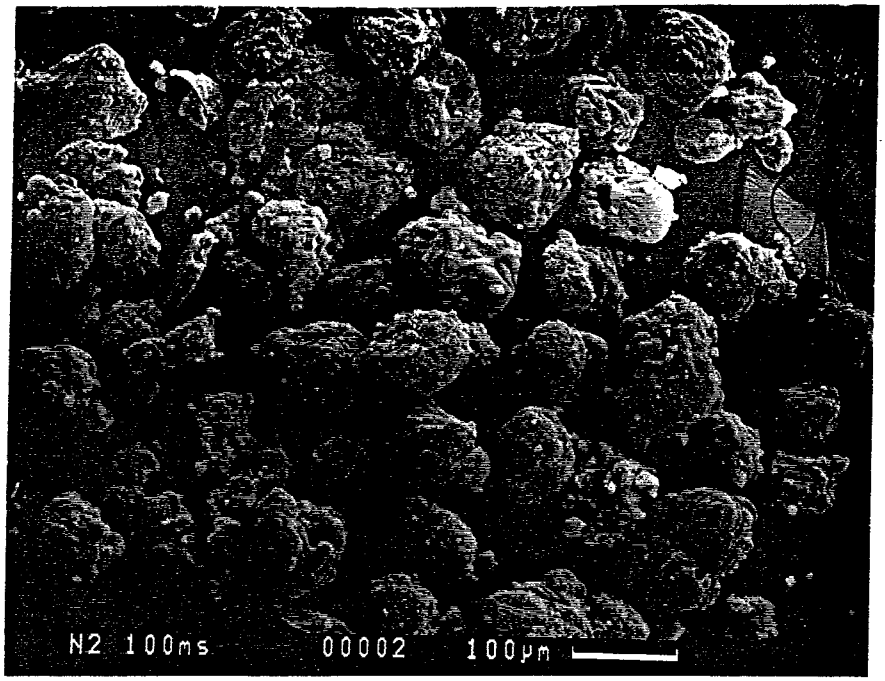

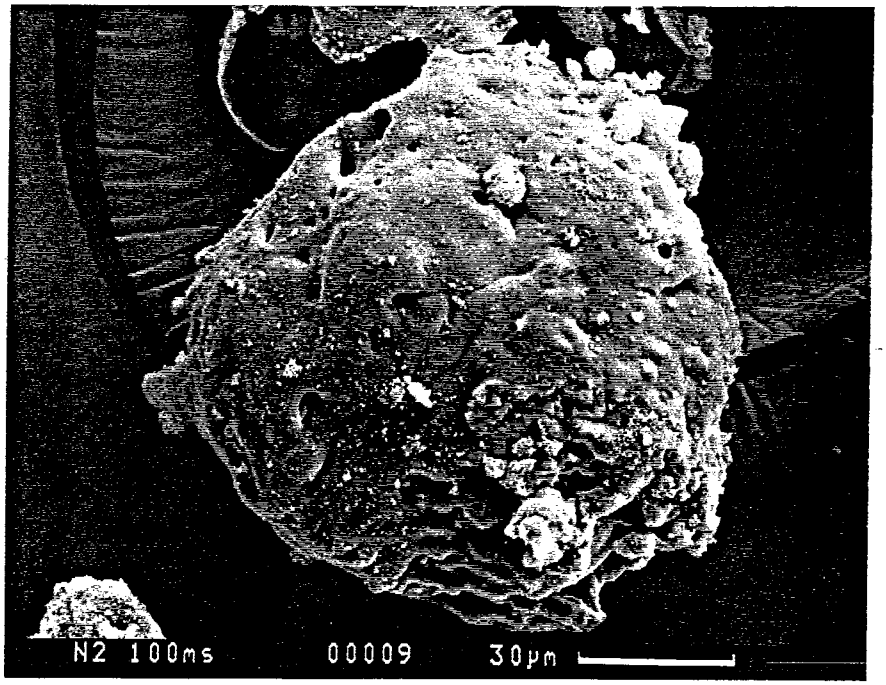

Fig. 3.2 Char particles produced in N_2 at 100 ms

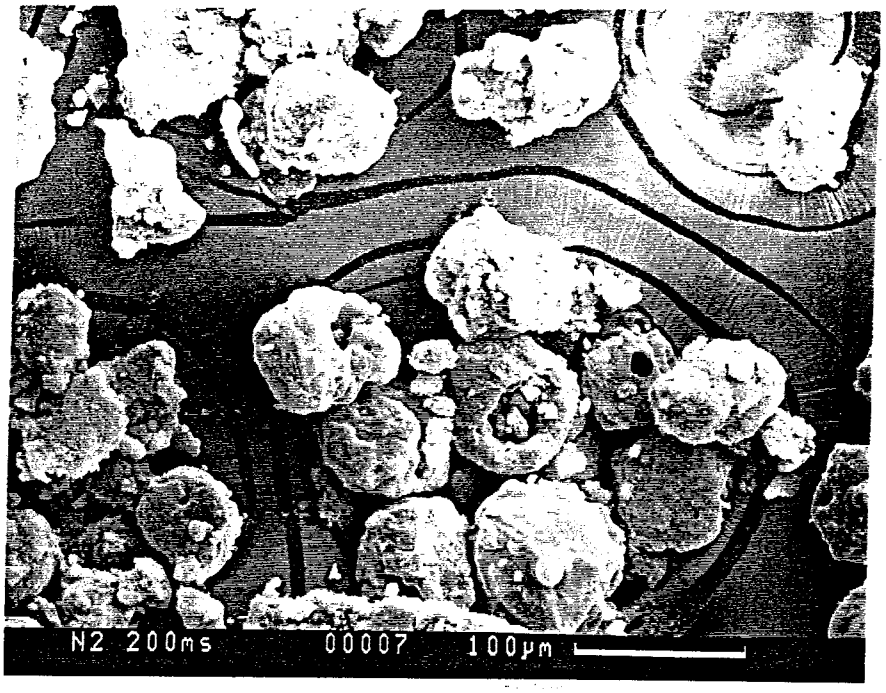

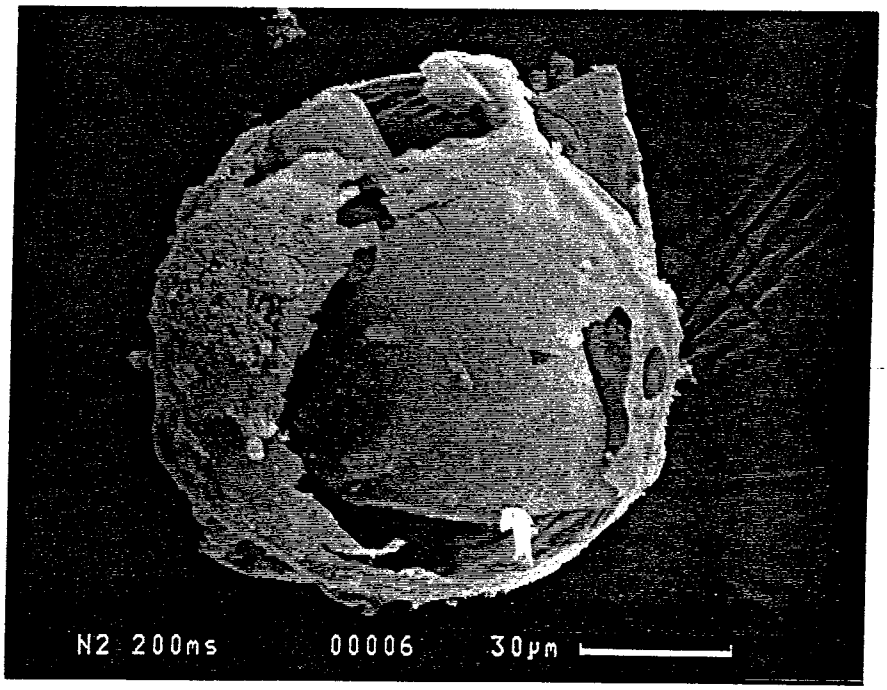

Fig. 3.3 Char particles produced in N_2 at 200 ms

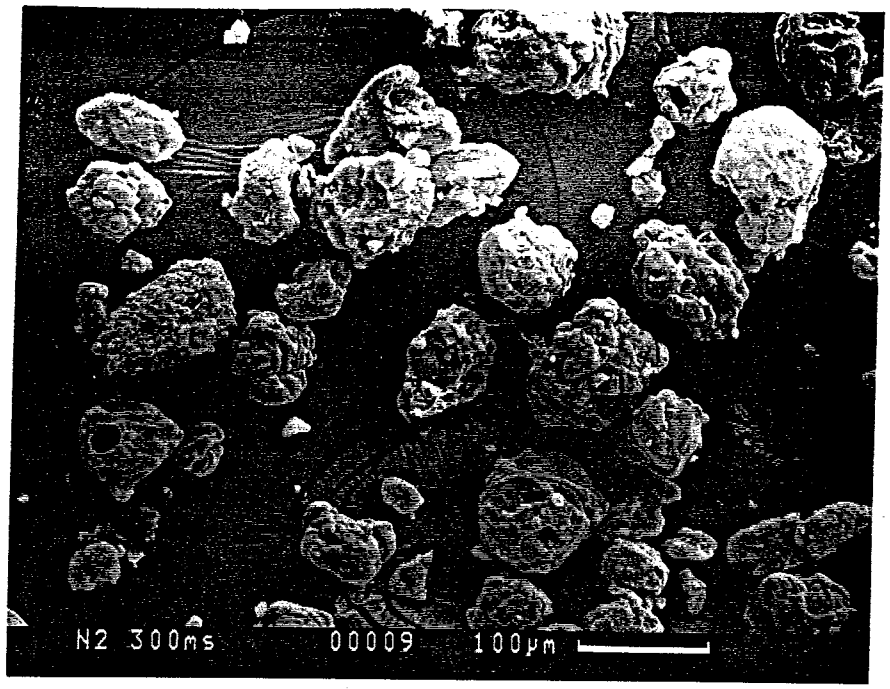

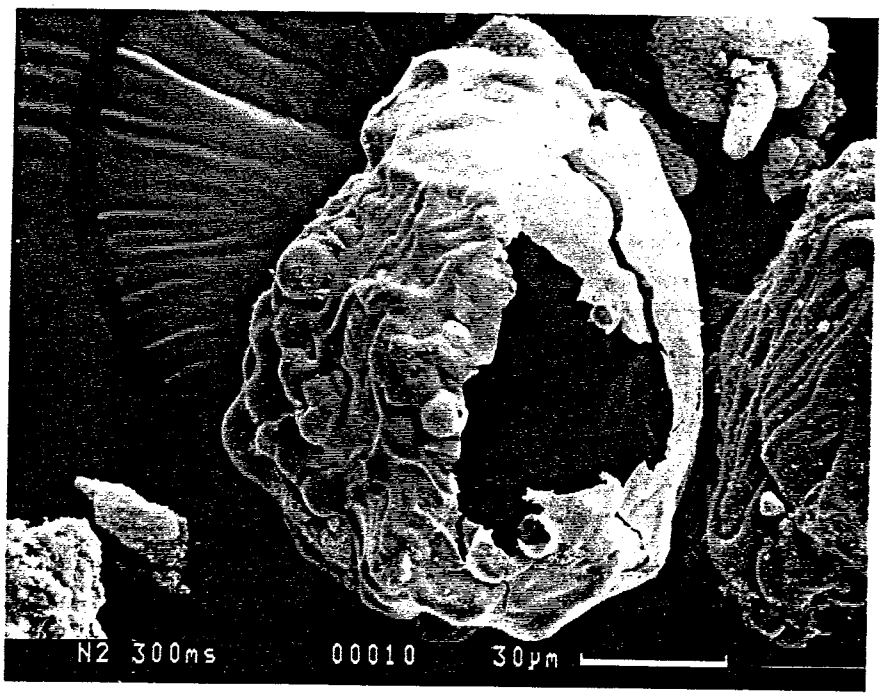

Fig. 3.4 Char particles produced in N_2 at 300 ms

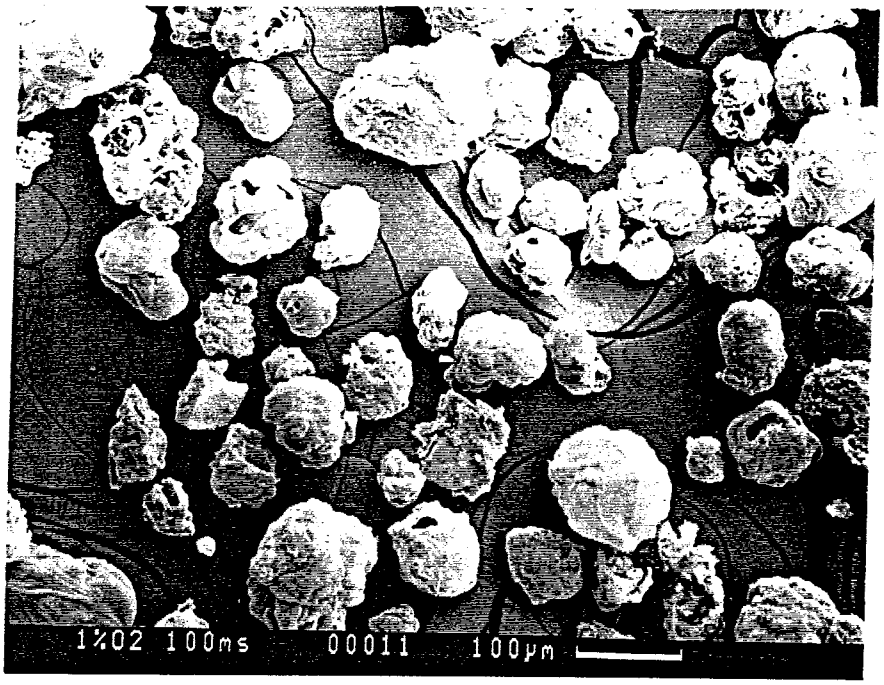

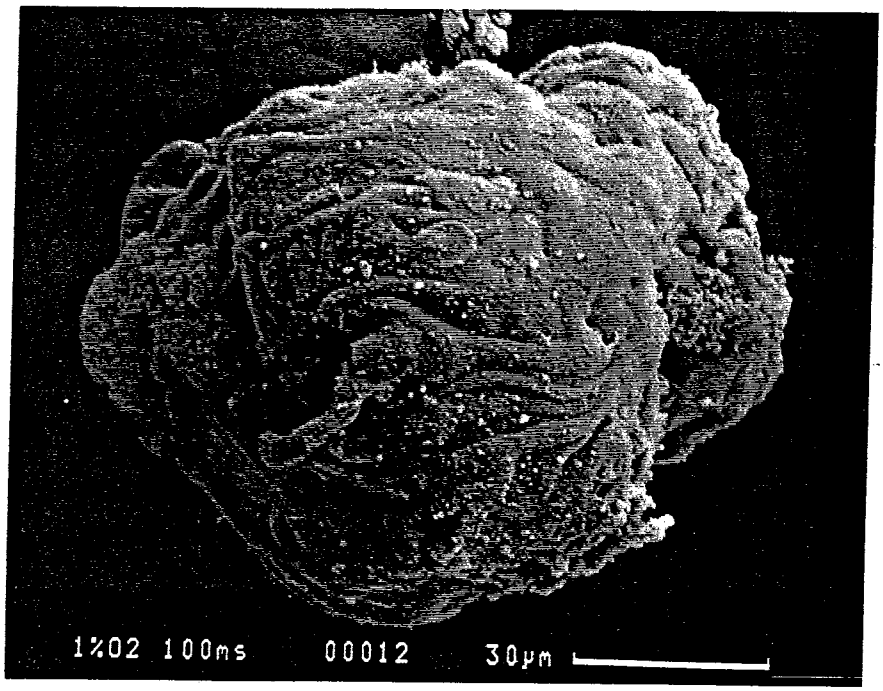

Fig. 3.5 Char particles produced in 1% O_2 at 100 ms

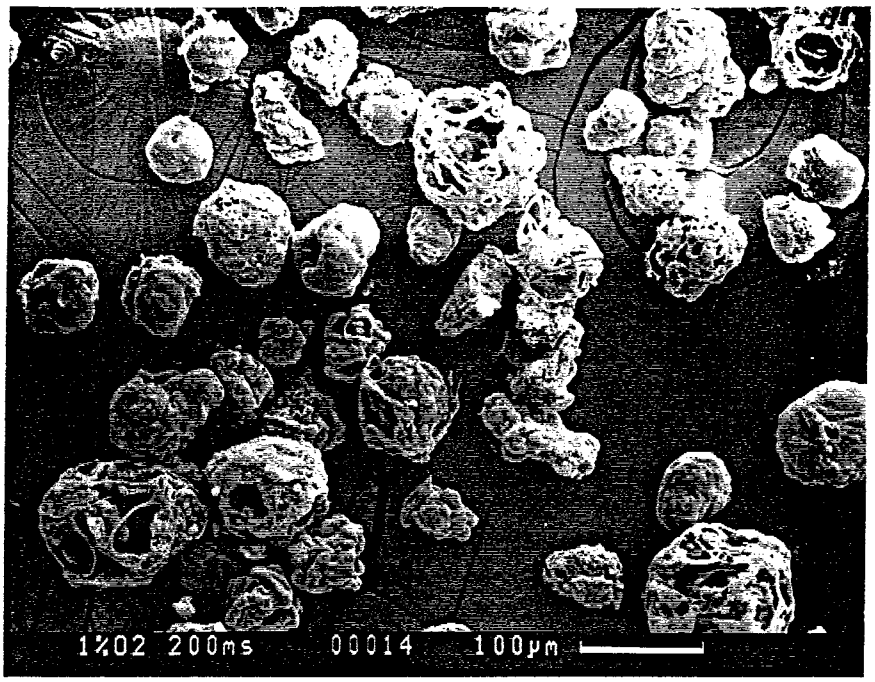

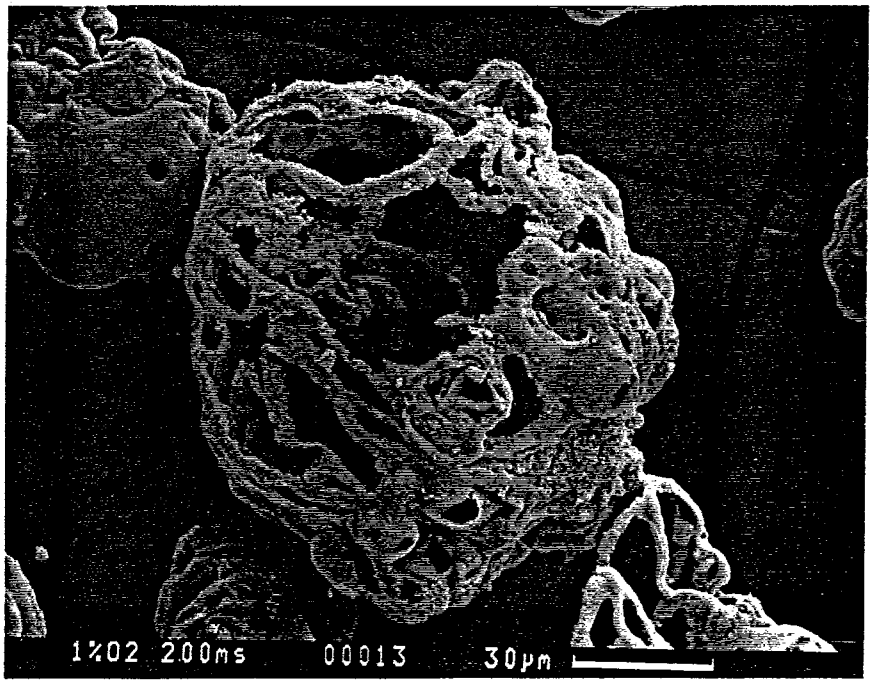

Fig. 3.6 Char particles produced in 1% O_2 at 200 ms

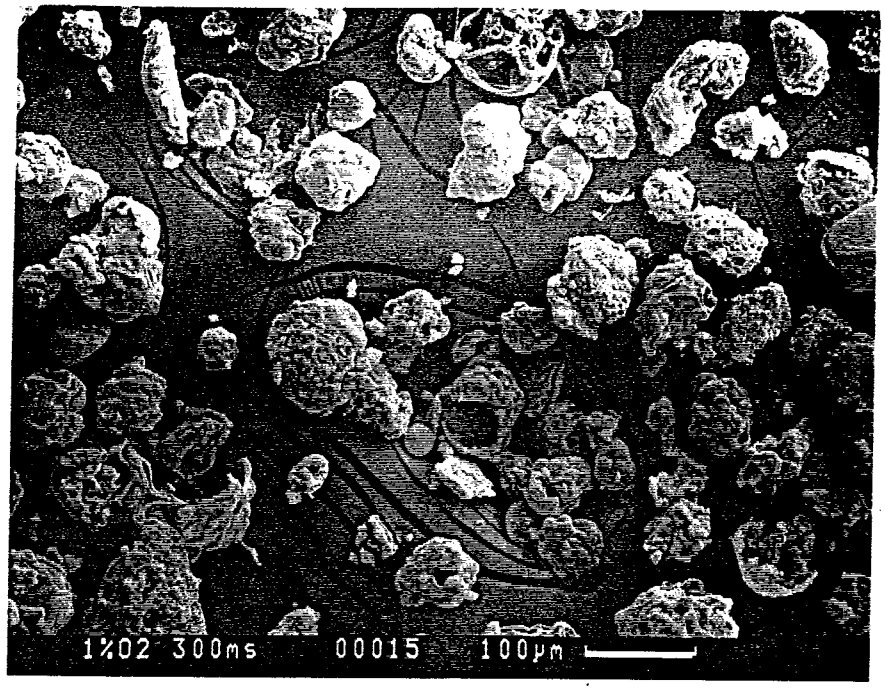

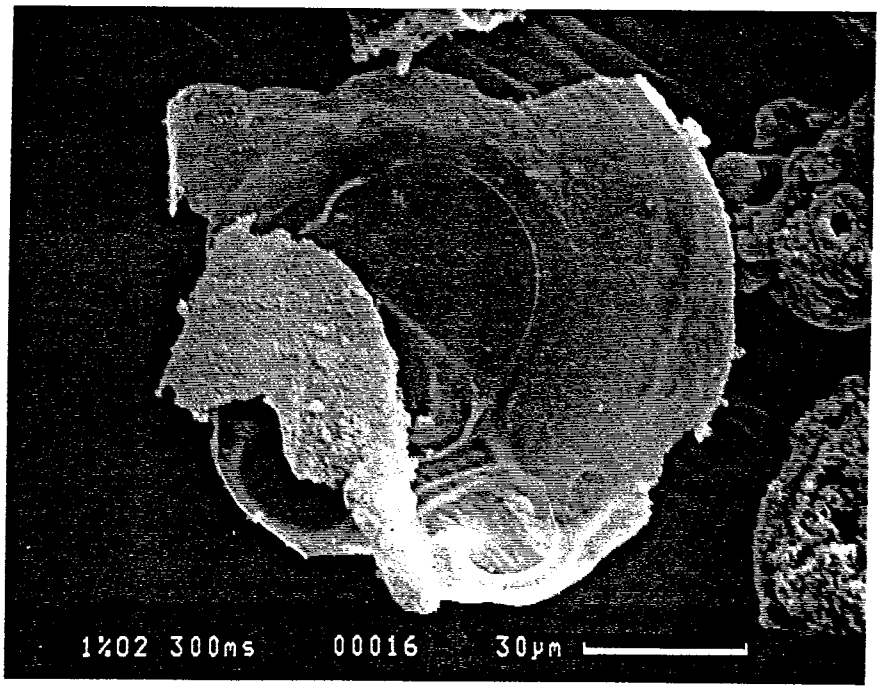

Fig. 3.7 Char particles produced in 1% O_2 at 300 ms

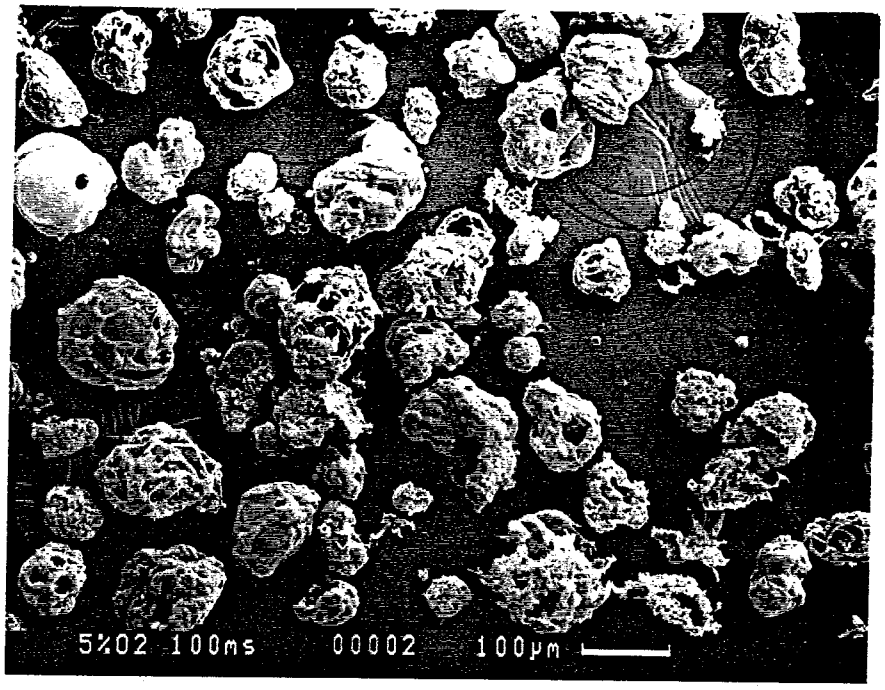

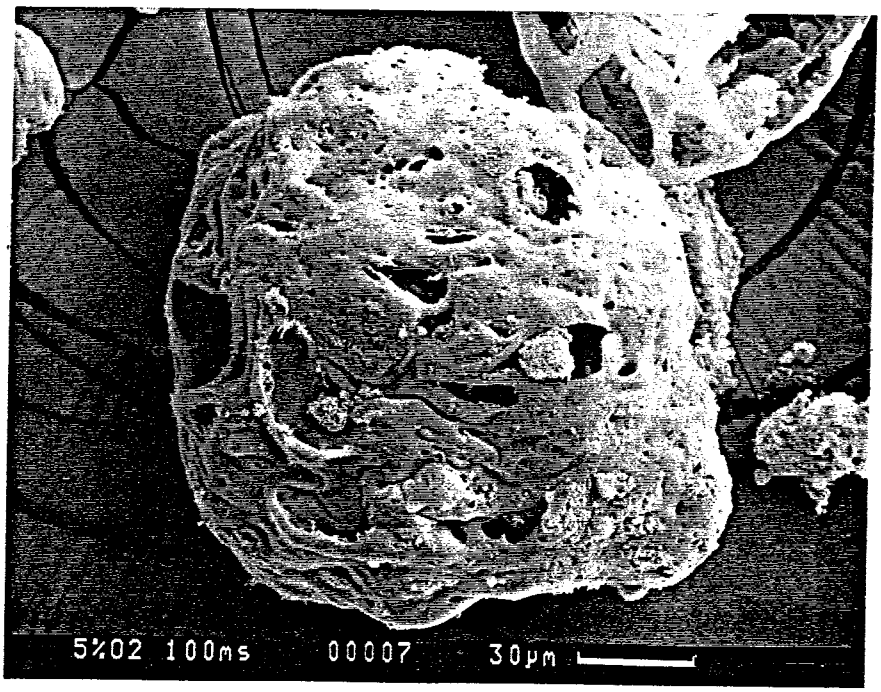

Fig. 3.8 Char particles produced in 5% O_2 at 100 ms

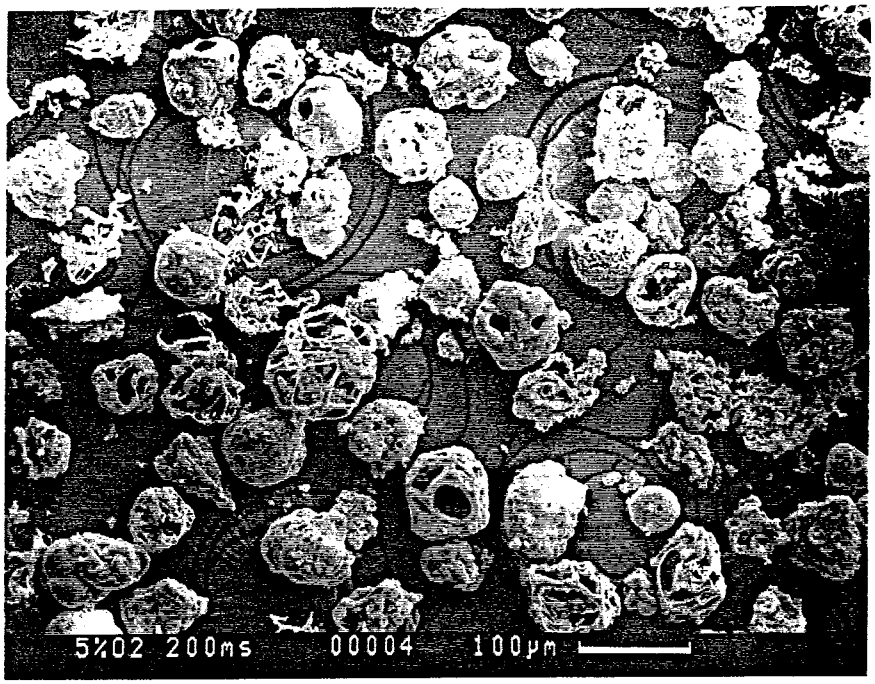

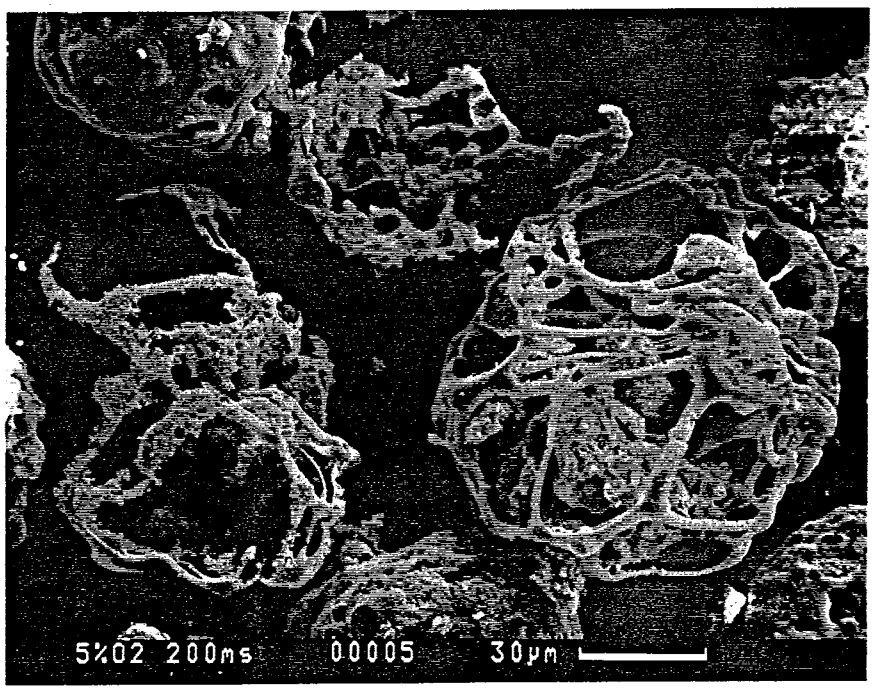

Fig. 3.9 Char particles produced in 5% O_2 at 200 ms

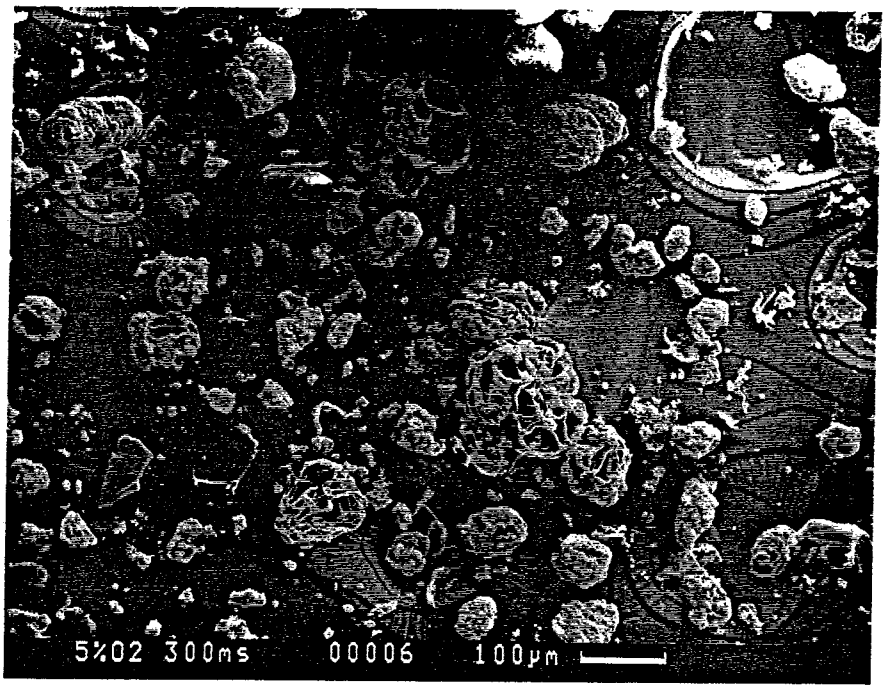

Fig. 3.10 Char particles produced in 5% O_2 at 300 ms

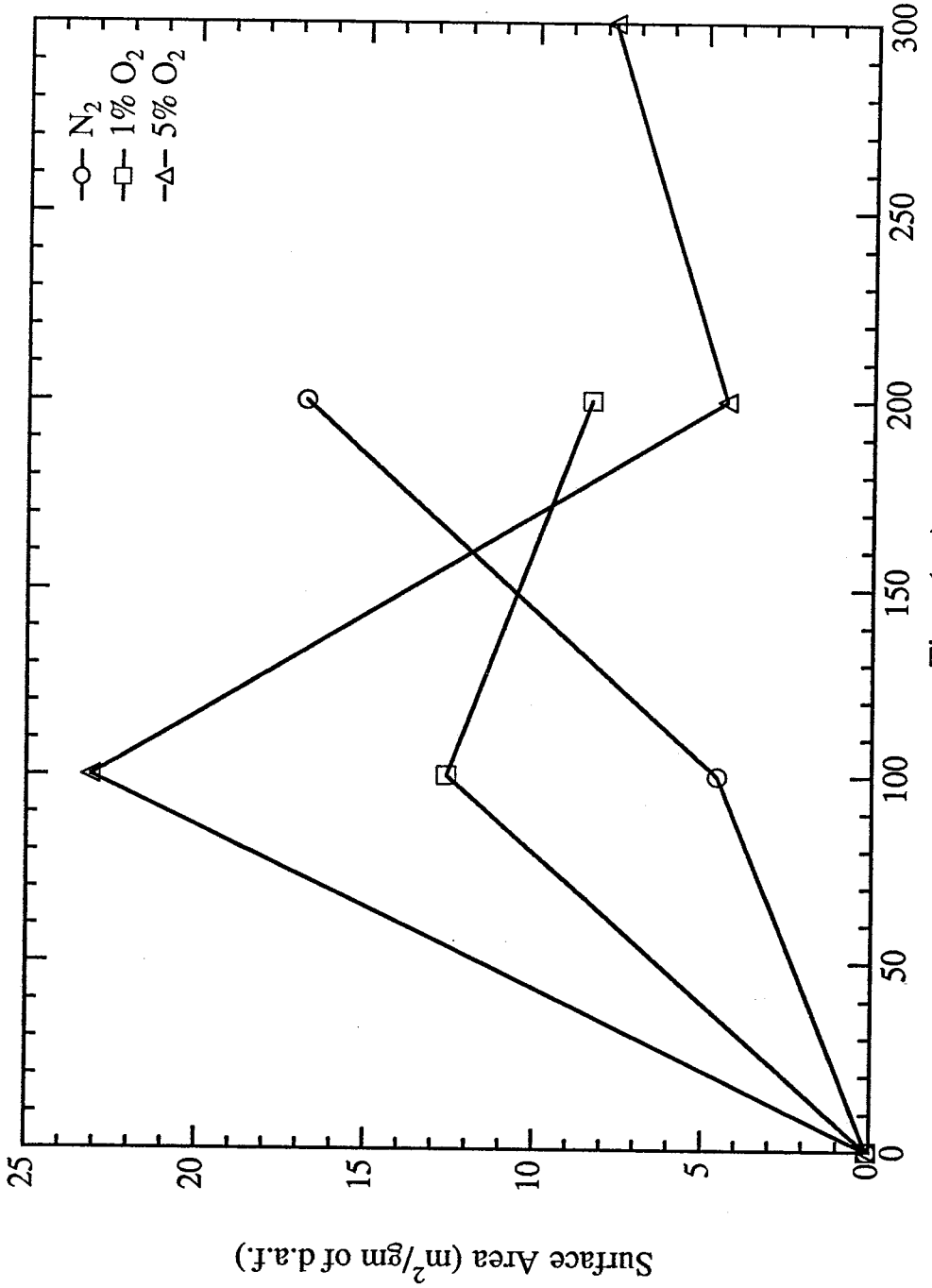

Fig. 3.11 Surface area of various chars at 1600K derived from drop-tube reactor experiments (dry ash free basis)

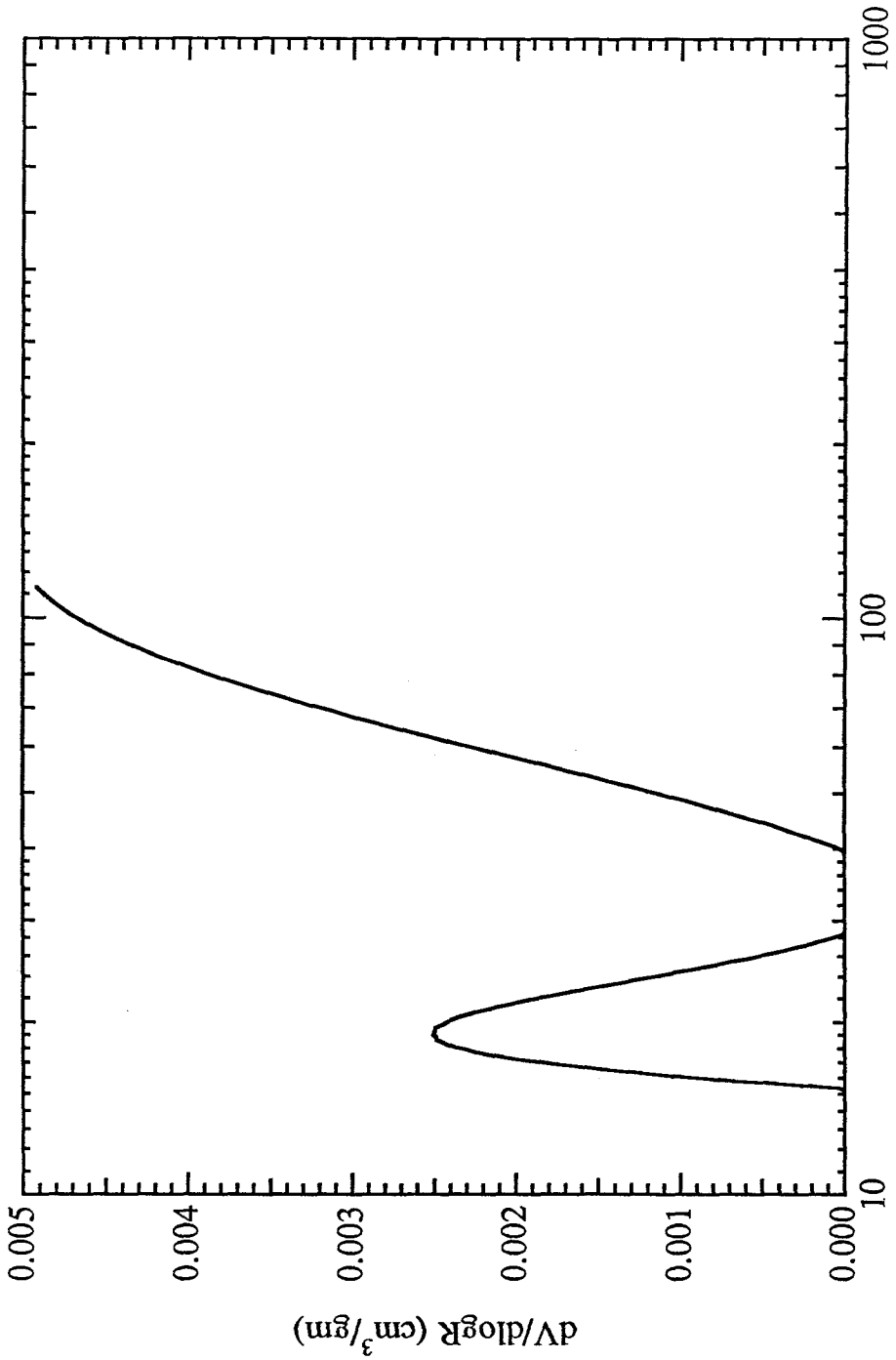

Fig. 3.12 Pore volume distribution of coal (PSOC 1451)

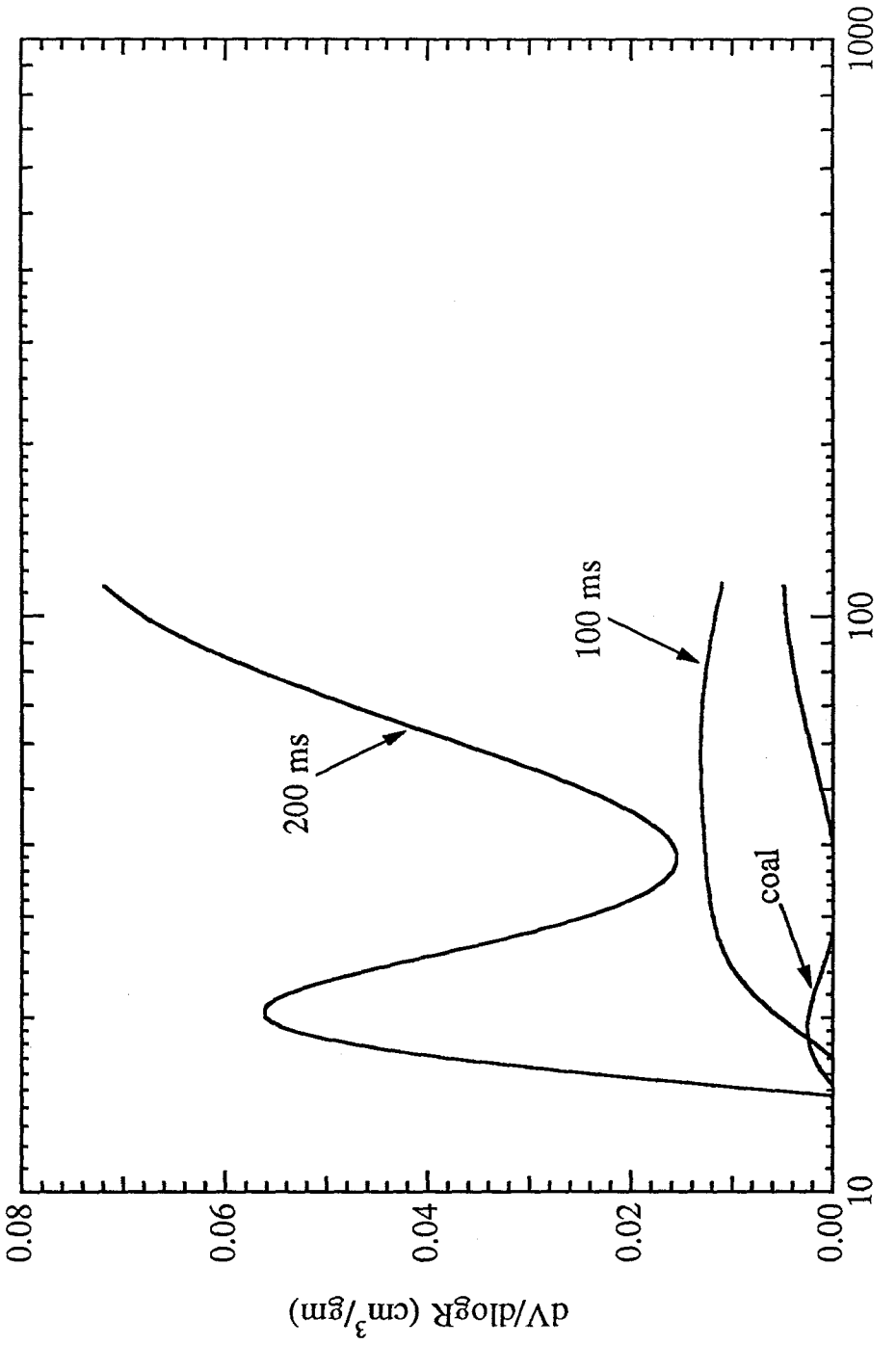

Fig. 3.13 Pore volume distribution of chars generated in N_2

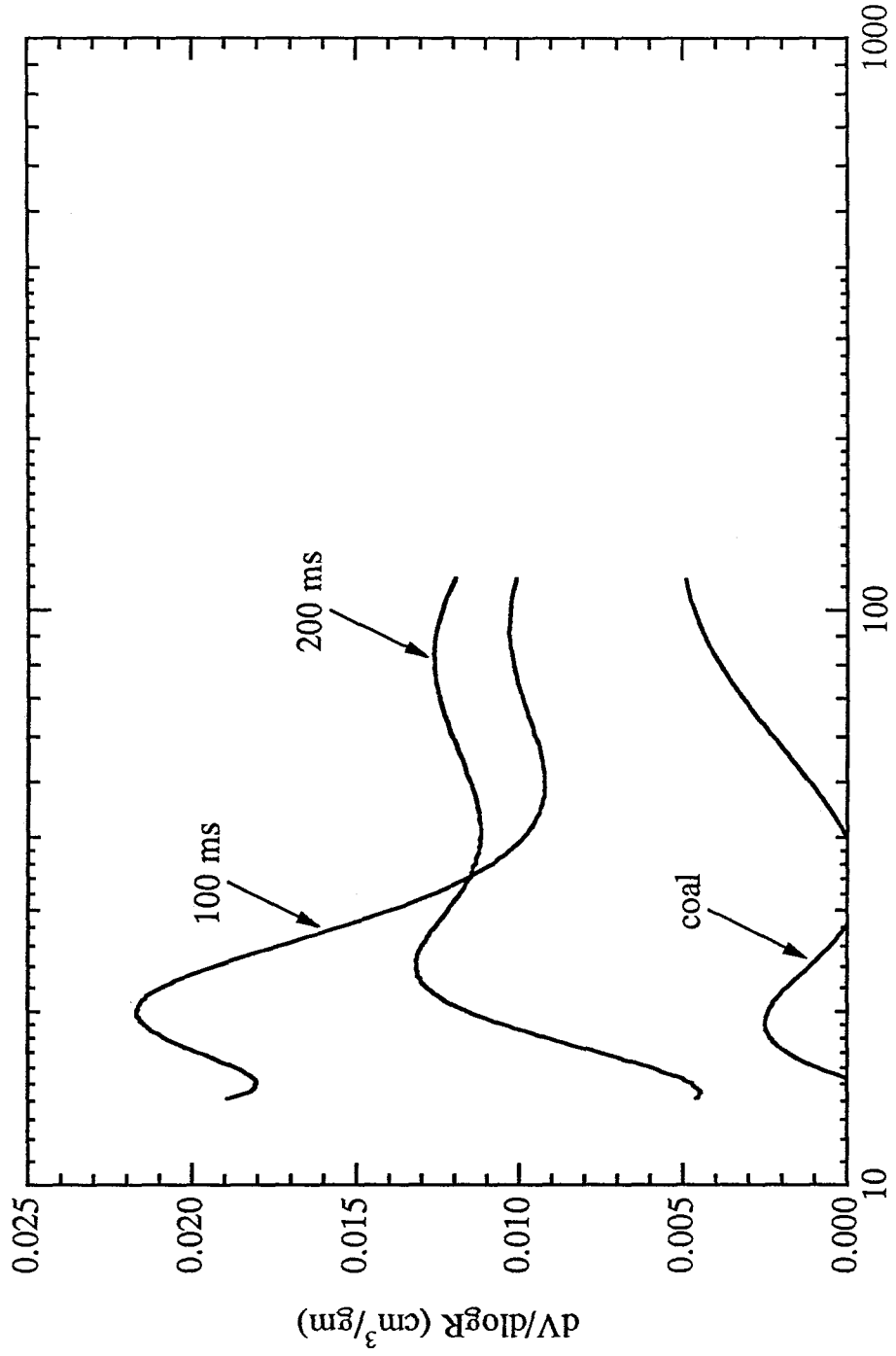

Fig. 3.14 Pore volume distribution of chars generated in 1% O_2

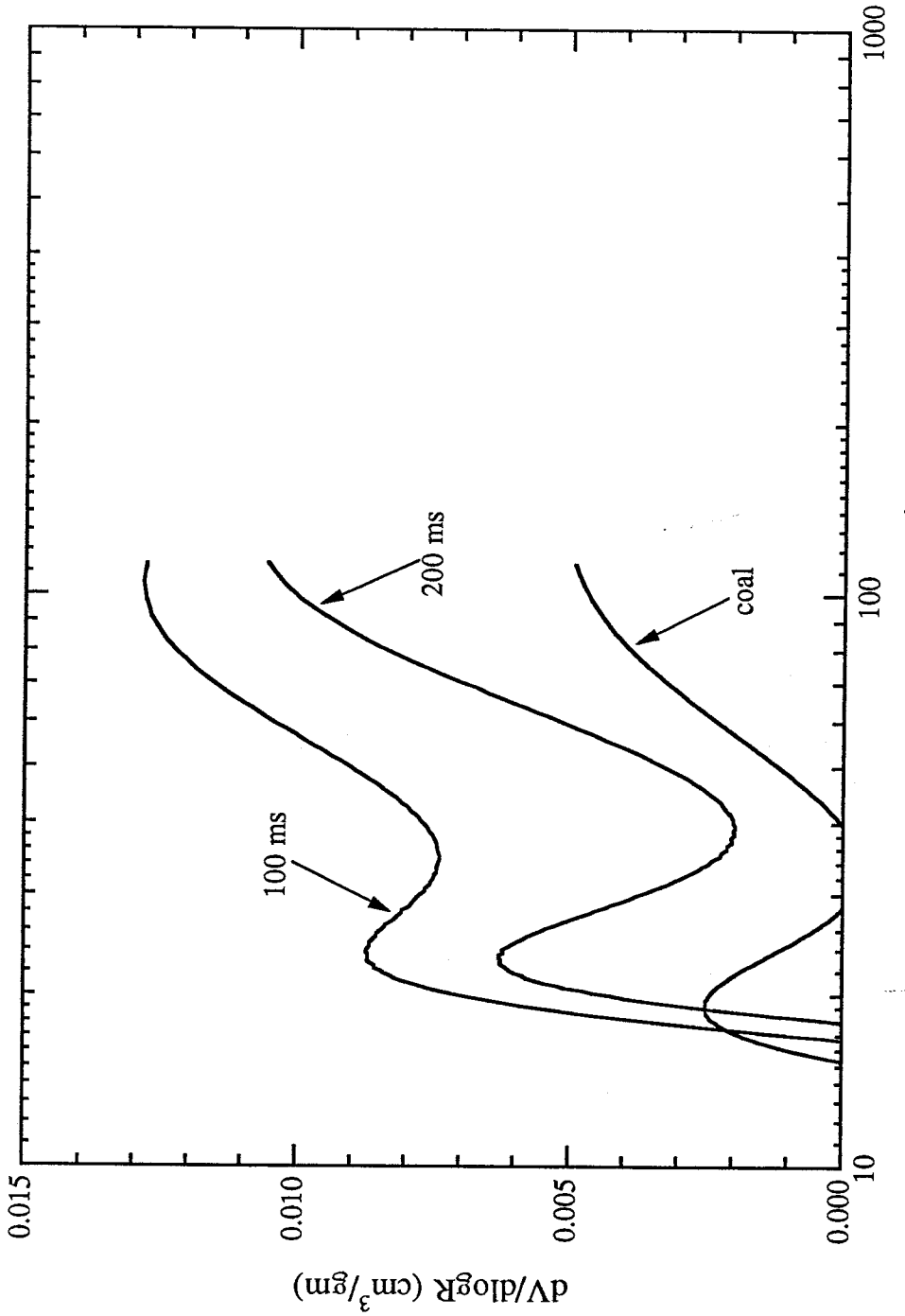

Fig. 3.15 Pore volume distribution of char generated in 5% O_2

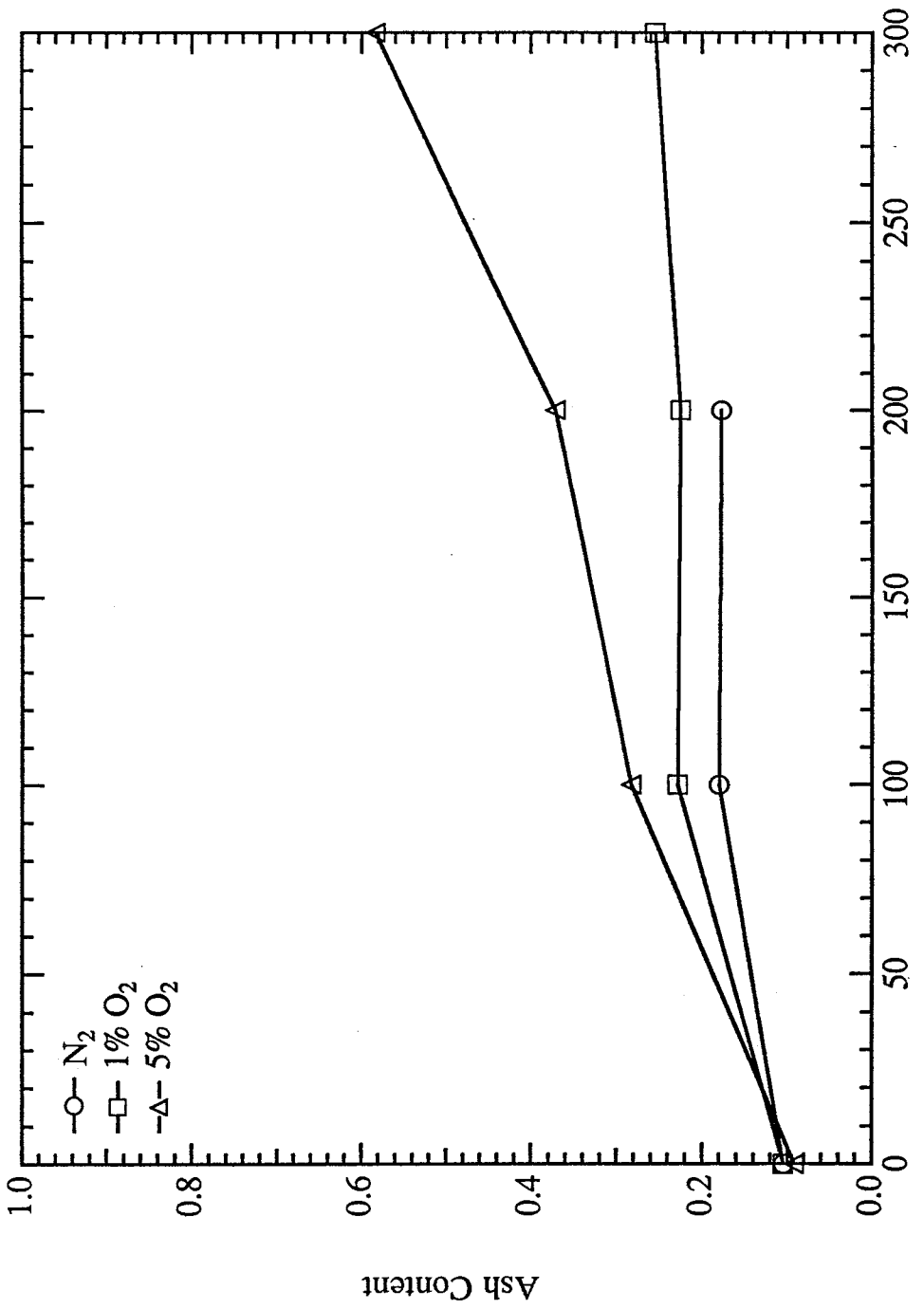

Fig. 3.16 Ash content of various chars at 1600K derived from drop-tube reactor experiments

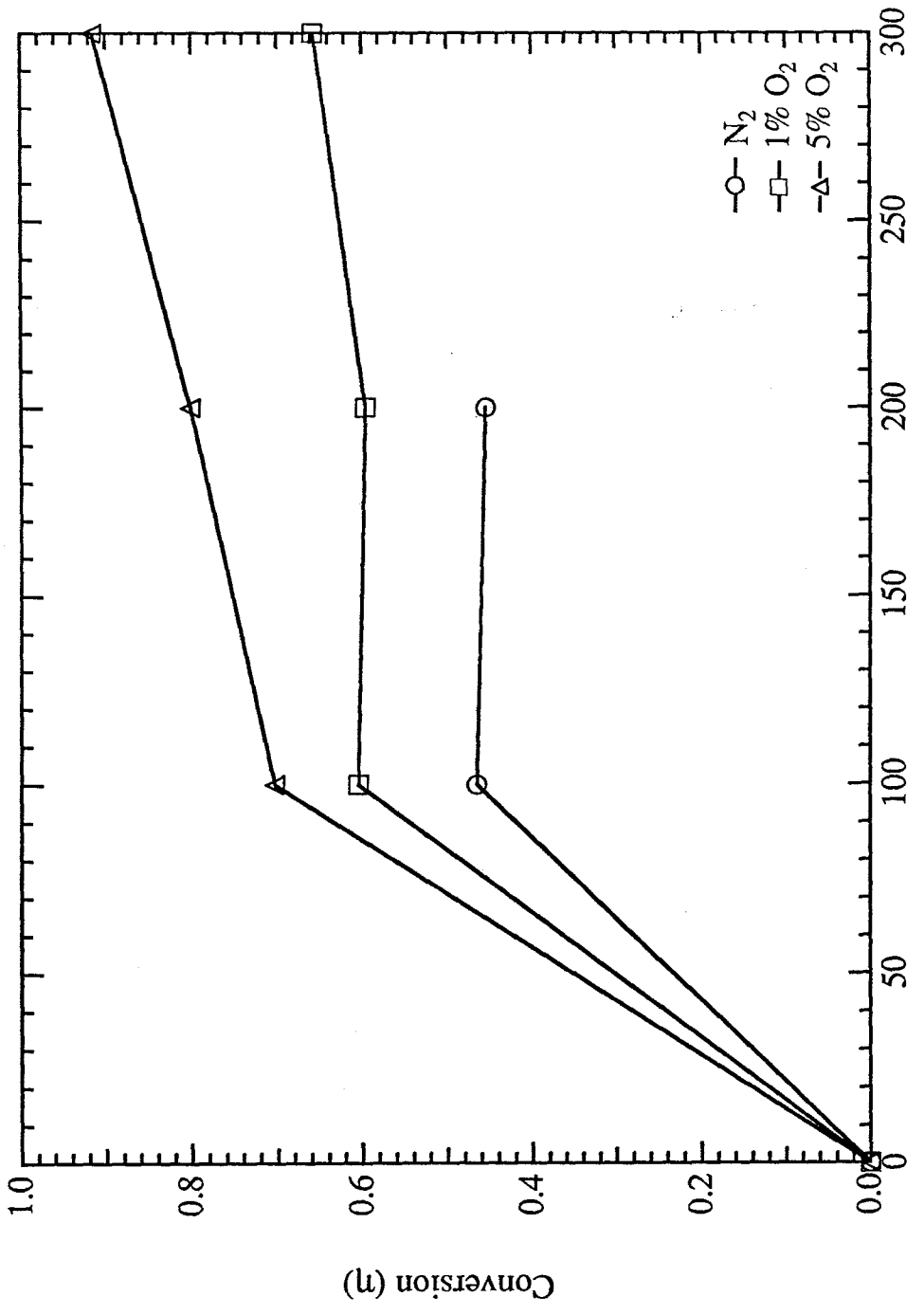

Fig. 3.17 Conversion of various chars at 1600K derived from drop-tube reactor experiments (dry ash free basis)

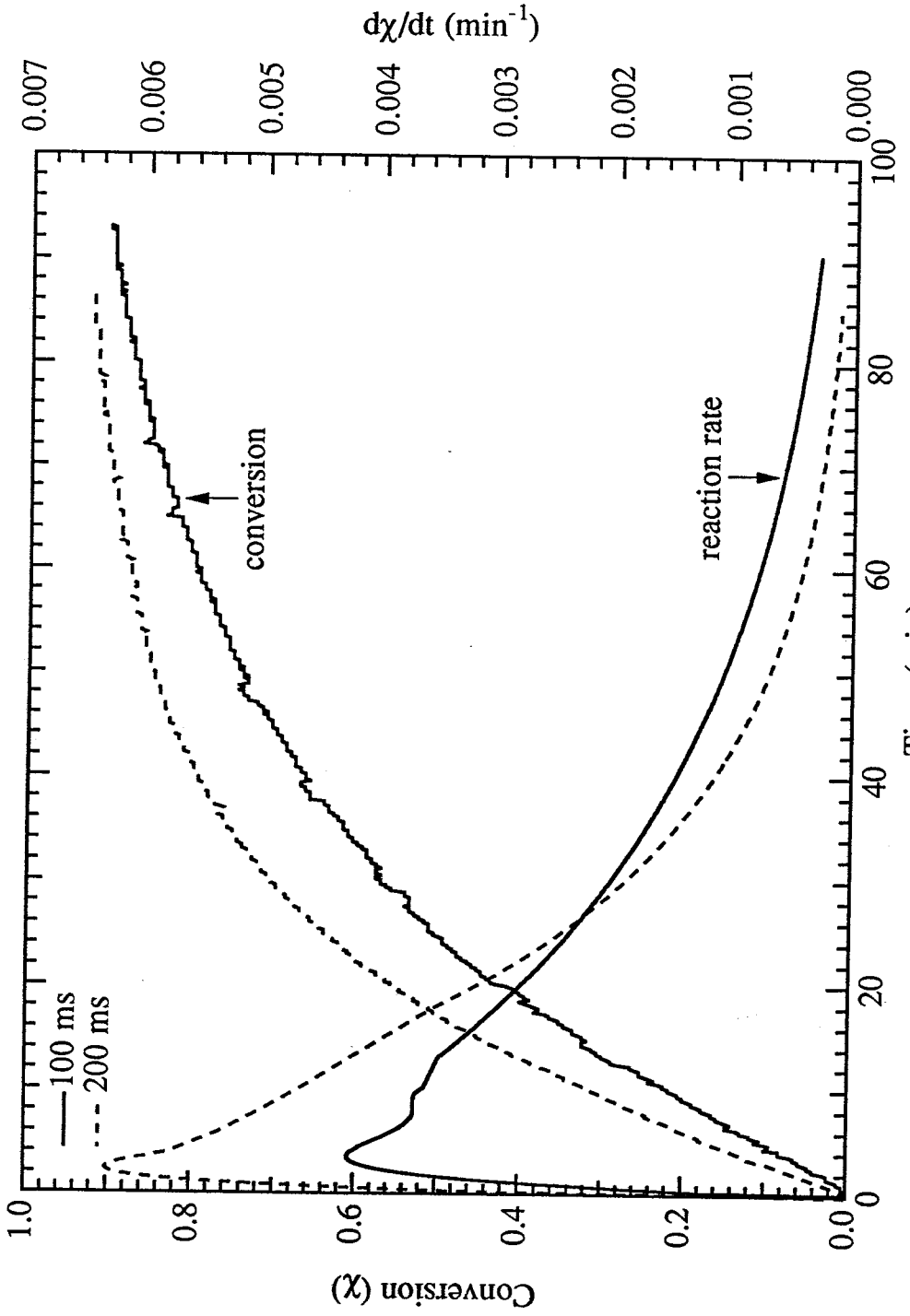

Fig. 3.18 TGA measurements of conversion and low temperature reactivities of chars generated at 1600K in N_2

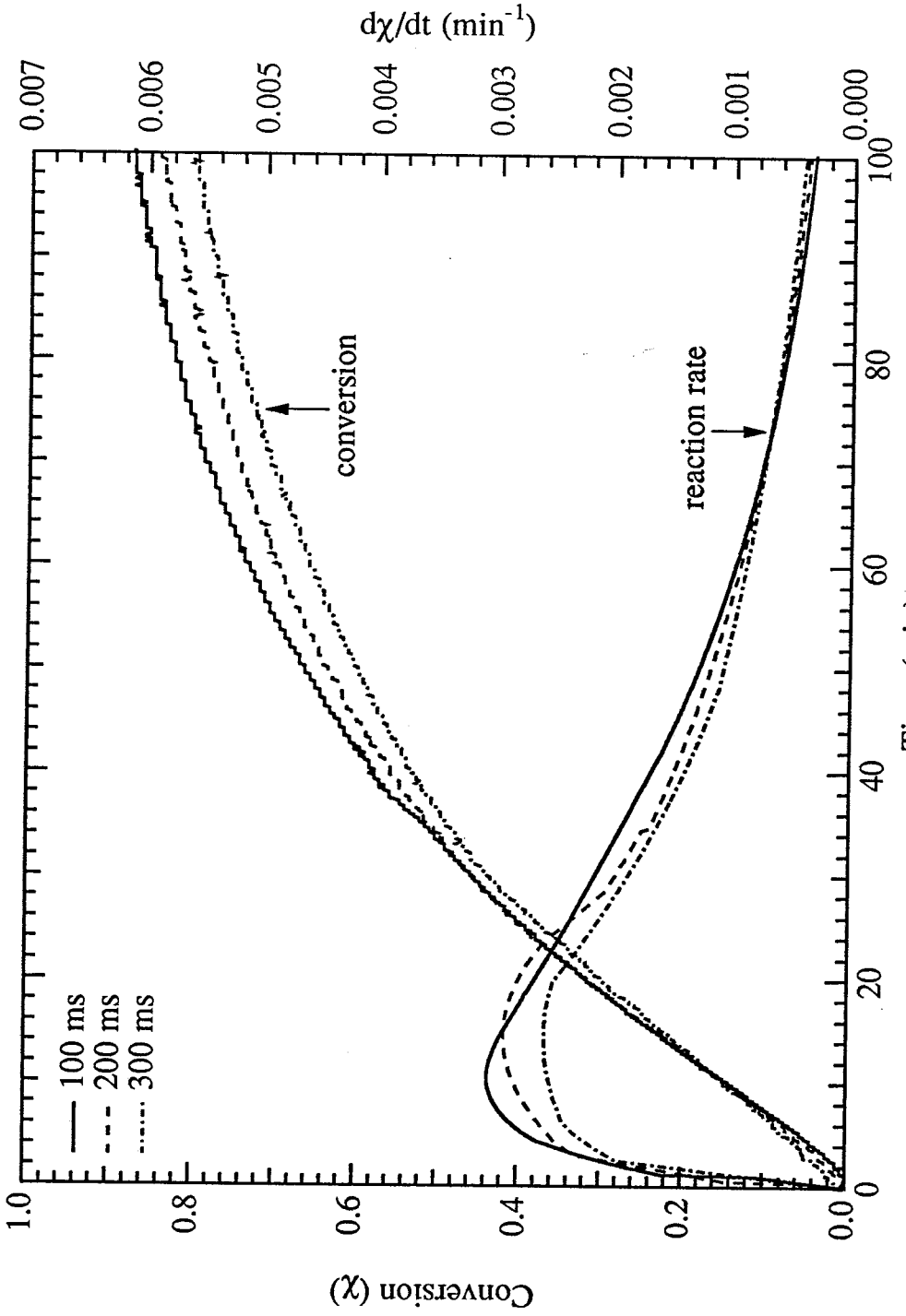

Fig. 3.19 TGA measurements of conversion and low temperature reactivities of chars generated at 1600K in 1% O_2

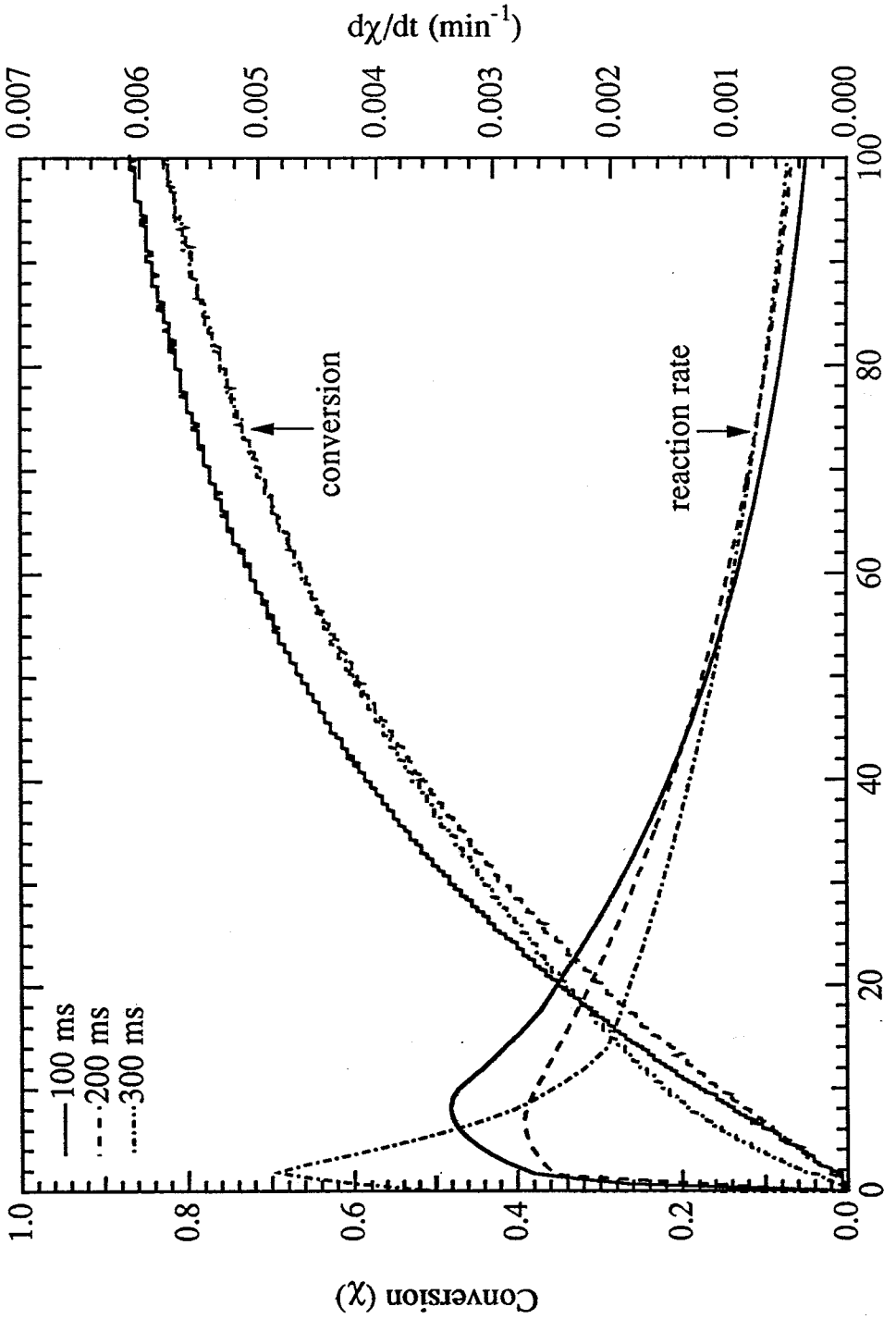

Fig. 3.20 TGA measurements of conversion and low temperature reactivities of chars generated at 1600K in 5% O_2

CHAPTER 4

A SEARCH FOR IRON FUME FORMATION IN PYRITE REACTIONS BELOW 1420K

A SEARCH FOR IRON FUME FORMATION IN PYRITE REACTIONS BELOW 1420K

Xiaoming Li, Brian Wong, and Richard C. Flagan*

Department of Environmental Engineering Science

*Department of Chemical Engineering

California Institute of Technology

Pasadena, CA 91125

ABSTRACT

An electrodynamic balance and a drop-tube reactor were used to study the fume formation in pyrite reactions below 1420K with particular emphasis on the formation mechanism of iron-rich particles as postulated by Baxter and Mitchell (1989). Fume particles were observed directly in electrodynamic balance studies of individual pyrite particles. The drop-tube reactor experiments allow measurements of the nature of the fume. No evidence was found for the formation of previously hypothesized small iron-rich particles under our experimental conditions. A large number of sulfur particles were collected due to the condensation of sulfur vapor. Physical mechanisms that might lead to the release of iron-rich fragments were also investigated.

4.1 Introduction

Investigations of the submicron fume produced during pulverized coal combustion reveal substantial concentrations of iron in these fine particles (Flagan and Taylor, 1981; Quann et al. 1982). Analysis of Montana lignite ash samples suggested

that the submicron particles comprised a core of Mg and Fe oxides, followed by an inner layer of Si oxides and an outer layer of Na, As, and other volatile trace elements (Neville and Sarofim, 1982). The presence of so much iron in the fume has generally been thought to result from homogeneous nucleation of volatilized iron species. Under combustion conditions, the temperature of coal particles is several hundred degrees higher than the surrounding gas temperature. That some minerals evaporate and then form fine particles due to the rapid temperature drop is well documented (Flagan and Friedlander, 1978; Neville and Sarofim, 1982). The size distribution of the fume closely approximates the so-called *self-preserving* particle size distribution, that would be expected for free molecular particles grown by Brownian coagulation, from ultrafine sizes generated by homogeneous nucleation to sizes much larger than the original nuclei (Flagan and Taylor, 1981). However, detailed mechanisms for iron volatilization have not been presented.

Baxter and Mitchell (1989) recently examined the fate of pyrite iron in coal combustion. Their analysis of the thermochemistry of the iron/sulfur/oxygen system suggested that iron volatilization was probably not the source of the iron-rich fume in their experiments. They reported substantial loss of iron from coal particles just at completion of devolatilization when the char surface is exposed to an oxidizing atmosphere. During devolatilization, pyrite decomposes to form highly porous pyrrhotite (FeS_{1+x}). There is a net mass flux away from the surface when oxygen attacks char particles. They postulate that the iron-rich fume results when iron or pyrrhotite nodules detach from the surface of the char particles due to aerodynamic forces caused by the outflux. No direct measurement of the sizes of the fume particles that penetrated the filters (1.0 μm pore size, polycarbonate nuclepore filters) was made, but they suggested that the iron fume produced consisted of particles in the 0.02 to 0.2 μm range. The filtration velocity was about 12 to 14 cm sec^{-1} (Baxter, 1990; personal communication). Some insight into the nature of the particles that escape collection can be gained by

examining the filtration efficiencies. Liu et al. (1983) have measured the size dependent penetration for the same polycarbonate filters. Their data for a velocity of 13 cm sec^{-1}, shown in Fig. 4.1, indicates a minimum collection efficiency of 50% at 0.1 μm, with smaller particles being more efficiently captured due to Brownian diffusion. These data suggest that the particles that apparently penetrated the filter in Baxter and Mitchell's experiments were indeed smaller than 1 μm, and probably larger than 0.01 μm. Without more direct measurements, it is impossible to make more definitive statements about the particle sizes.

The present study explores fume formation during pyrite pyrolysis and combustion, with particular emphasis on the supposed formation of iron-rich particles in the 20 to 100 nm size range. We report direct observations of fume formation during reactions of individual particles, as well as drop-tube reactor experiments that allow measurements of the nature of that fume. A theoretical investigation of the possibility of release of iron-rich fragments is also described.

4.2 Experiments

4.2.1 Electrodynamic Balance

The Electrodynamic Thermogravimetric Analyzer (EDTGA) utilizes a modern version of the Millikan oil-drop experiment known as the electrodynamic balance to levitate a single charged particle within a tightly constrained space for the study of high temperature processes. The traditional electrodynamic balance (EDB) design utilizes a bihyperboloidal electrode system, although a variety of much simple electrode designs have been used successfully. For the present study, the end caps are hemispherical and the ring is a right cylinder. The system diagram is illustrated in Fig. 4.2.

The particles to be injected into the EDTGA are charged by applying a high voltage pulse between a small cup containing these powders and the bottom electrode of the EDB. Electrostatic forces then accelerate the charged particles upward into the EDB. An AC potential on the ring electrode traps one or more particles in the electrodynamic balance. The DC potential is then adjusted to bring one particle to the center of the chamber. By reducing the AC strength, all other particles are released from the chamber. The AC is then applied to the ring electrodes so that the selected particle is stably trapped throughout the experiment. An optical servo system is used to adjust the DC potential continuously such that the particle is maintained at the center of the chamber as its mass changes or when it is otherwise disturbed. The control voltage provides a continuous record of the force required to hold the particle at the center of the chamber. It should be noted that during heating, this force does not correspond directly to the charge to mass ratio. The drag forces due to the buoyancy induced flow around a hot particle levitated in a cold gas, and photophoretic forces must also be taken into account (Spjut et al., 1985).

The trapped particle is illuminated by a helium neon laser (Melles-Griot Model 05-LPH-151) that is directed down through a hole in the top electrode. The light scattered from the particle is imaged by an f/1 lens. Light scattered at 90° is also focussed onto a 1×3 mm silicon position sensitive detector (Hamamatsu S1543). An interference filter is used to block wavelengths other than that of the HeNe laser (632.8 nm) to reduce spurious signals as the particle is heated. The output of the position sensitive detector is amplified and then transmitted to a proportional-integral-differential (PID) controller. The controller continuously adjusts the output of the high voltage amplifier (TREK Model 603) that controls the DC voltage applied to the end caps of the electrodynamic balance. The particle is also monitored with a video system consisting of a Questar QM1 long range microscope and a Cohu CCD video camera, and recorded on a Panasonic super-VHS AG1830 video recorder. Two modes of particle illumination were employed. Bright

field illumination was provided by placing a diffusing screen outside the window opposite the viewing window and illuminating the screen with a white light source. In this case, an interference filter was mounted outside the viewing window to eliminate scattered light from the HeNe laser. The particle appeared as a dark shadow in the bright field image until ignition raised the temperature sufficiently high for the thermal emission from the particle to become visible. Dark field images of the laser light scattered from the particle made the clouds formed around reacting particles visible.

The levitated particle was heated by a 20 W Advanced Kinetics flowing gas CO_2 laser. A refractory shutter was installed at the laser output to allow the laser to run until stable operation was achieved before introducing the beam into the EDTGA. The beam from the CO_2 laser was directed through a beam combiner, where it was combined with the HeNe laser beam that facilitated tracking of the invisible CO_2 beam, as well as optical alignment. Laser alignment problems were minimized by directing a single laser beam through the top of the electrodynamic balance. A large bore laser tube was used so that the laser could be operated in TEM 01^* mode (the so-called "donut" mode), simplifying the retention of the particle in the laser beam. For the experiments described in the present study, the laser was operated at constant output with the intensity delivered to the particle being controlled by the degree of focussing of the beam. A Zn-Se lens above the top of the EDTGA was mounted on a motorized translation stage to facilitate rapid heating of the particle. The non-Gaussian laser beam and the incompletely determined optical properties of the pyrite particles precluded quantitative theoretical predictions of the particle temperature. The particle temperature was estimated using a two color pyrometer operating at wavelengths of 1.8 and 3.4 μm, illustrated in Fig. 4.3a. Radiation emitted by the particle was collimated by a CaF_2 lens. The collimated radiation was divided by a grating-type beam splitter which reflected the infrared radiation through two narrow band pass filters (1.48 μm with bandwidth 70 nm, and 3.42 μm with bandwidth

130 nm). CaF_2 lenses then focused the beams onto separate solid state detectors, an InGaAs detector that was active from 1.1 to 1.8 μm, and an InSb detector that was active from 2 to 5 μm. The signals from the two detectors were amplified and then processed with a log-ratio amplifier. The resulting signal was a function of the temperature of the emitting material. Because the pyrite particles were irregularly shaped, and the optical properties of the pyrite were not well known, the optical pyrometer response was determined empirically. A type R (Pt - Pt/13% Rh) thermocouple was coated with silica (Fristrom and Westenberg, 1965) and then with fine pyrite particles ($d_p < 4$ μm). The thermocouple bead was then heated with the CO_2 laser. Monitoring the thermocouple response, an empirical calibration of the optical pyrometer response as a function of temperatures was obtained. Fig. 4.3b shows the pyrometer response as a function of indicated thermocouple temperature. Note that the pyrometer response changed with repeated heating, indicating a change in the optical properties of the coating material. This is not surprising since the pyrite decomposition to pyrrhotite is expected at the highest temperatures encountered. Thus, temperatures reported below are subject to an uncertainty of ± 40°C.

Several different approaches to particle heating and data acquisition were used over the course of the pyrite EDTGA experiments. (1) *Pulse heating*: The particle was initially heated by the laser at very low power to a temperature below the threshold of the pyrometer (280°C). The pyrometer signal was sampled at about 2500 Hz. After establishing the pyrometer baseline, the laser power was increased in a pulse. (2) *Ramped pulse heating*: The basic method was the same as (1), except that the initial low level of heating was slowly increased until fume formation was observed. (3) *Ramped heating - laser control*: The laser power was externally controlled by a circuit which slowly increased the laser power. Data acquisition was conducted at the slow rate. (4) *Ramped heating - focus control*: Rather than change intensity of the laser beam at the particle by

changing laser power, the intensity was changed by moving the laser focusing lens with respect to the particle.

4.2.2 Drop-Tube Reactor

The electrodynamic balance makes it possible to observe some of the transformations of a single particle directly. However, uncertainties in the particle temperature, possible effects of nonuniform laser heating, and the inability to make direct measurements of the products of reaction, limit our ability to make quantitative measurements with the present system. Hence, parallel experiments were performed using a drop-tube reactor to characterize the nature of the fume produced by reactions of pyrite at elevated temperatures.

The experimental system illustrated in Fig. 4.4 has been described in detail elsewhere (Sahu, 1988) and is only briefly described here. The drop-tube furnace is an Applied Test Systems Series 3310 tube furnace with a maximum temperature of 1650°C. The reactor tube is a 99.8% alumina tube of 5 cm ID. and 71 cm length. A water-cooled stainless steel injector was used to inject the reactant particles directly into the hot zone of the reactor. Low density zirconia refractory insulation in the cooled injector reduces the load on the furnace and allows the gas that enters coaxially with the injection stream to be preheated upstream of the particle injection point. The isothermal zone of the reactor is about 30 cm long. In the present experimental conditions, the centerline temperature differs from the wall temperature about 40K to 50K. The gas temperature in nitrogen agrees with that in air within 40K or less. Aerosol samples were extracted with a water-cooled, gas dilution quench probe. The dilution gas was injected into the sample through a number of small holes near the probe entrance. A portion of the aerosol flow was extracted from the sampling probe, through a dilution system, and into the aerosol

measurement instruments. The aerosol sample flow was controlled by the critical orifice of Condensation Nucleus Counter (CNC, TSI Model 3760). The sample was diluted by recycling part of the sample through an absolute filter (MSA Ultra Filter, type H cartridge) using a two-stage diaphragm pump to keep particle concentrations within the operating limit of the CNC. The aerosol concentration and size distribution were measured with a Scanning Electrical Mobility Spectrometer (SEMS) (Wang and Flagan, 1990) based on a computer controlled Differential Mobility Analyzer column (DMA) (TSI, Model 3071) with the Condensation Nucleus Counter as a detector. Particles were also collected on silver grids for structure and chemical composition analysis using Transmission Electron Microscope (TEM, Phillips EM 430) equipped with energy dispersive X-ray analysis (EDX). The mass feed rates of the different experiments were adjusted so that the particle number concentrations could be kept below the upper detection limits of the aerosol instruments.

Two types of pyrite were examined, a natural pyrite (85% purity, EM Science) and a synthetic pyrite (99.9% purity, AESAR). Scanning electron microscope pictures of both types of pyrite particles are shown in Fig. 4.5. The pyrite compositions are summarized in Table 4.1. Both the supplier's analysis and qualitative analysis obtained using a Kevex EDS X-ray fluorescence spectrometer (XFS) are reported. The predominant impurity species in the natural pyrite are calcium and silicon, with small quantities of copper and zinc. The natural pyrite was first size classified to 53-74 μm. The pyrite particles were reacted in high purity N_2 or in clean dry air at temperatures ranging from 750K to 1220K. Due to agglomerate nature and the fine particle size of the synthetic pyrite, it was not possible to size classify sufficient material for the experiments performed. Hence, polydisperse particles of this material were used for drop-tube furnace experiments. The fine synthetic pyrite particles tended to cake upon exposure to air, so it was necessary to dry the powder in the feed test tube by heating mildly ($\leq 40°C$) and to

evacuate the sample for 5 to 12 hours prior to the experiments. Polydisperse particles of the synthetic pyrite were reacted at 873K to 1420K in either high purity N_2 or dry clean air.

4.3 Experimental Results

4.3.1 Electrodynamic Balance

(1) Fume Formation

When some pyrite particles were heated, a spherical cloud of very fine particles was formed around the particle as illustrated in Fig. 4.6. The cloud was observed to start from the particle, expand quickly to several particle diameters, and generally maintained its slightly elongated spherical shape as it rose, out of view due to buoyancy. The fume formation was affected by the heating rate and oxygen concentrations. The fume was occasionally observed when the particle was heated slowly by a ramping procedure, but was more often seen when the particle was hit by a sudden laser pulse; the temperature of the particle just prior to fume formation in air was in the range of 300 to 400°C, but in a nitrogen atmosphere, some fume formation was observed when particles were heated at temperatures up to 500°C. The mass changes in the particles during fume formation were generally very small. In many cases, mass changes were undetectable to a resolution of 1 part in 10^5. In experiments where particle temperature was maintained at 300 to 350°C, for 30 seconds to 3 minutes, the particle mass was reduced by 6 to 8%. The mass loss that would be observed if pyrite is completely converted to pyrrhotite is 23%.

Figs. 4.6a and 4.6b show the darkfield images of a pyrite particle of approximately 100 μm size prior to laser heating and after it was heated to about 320°C by a single laser pulse of approximately 10 ms duration. The cloud that formed was

approximately 4 particle radii in size. Fig. 4.6c shows the corresponding temperature trace. The laser was operated at a steady state that maintained the particle at a steady temperature below the threshold of the pyrometer and briefly pulsed to heat the particle. The charge-to-mass ratio change during this initial pulse was less than 1 part in 10^5.

(2) Particle Fragmentation

Fragmentation of pyrite particles was observed at temperatures between 300 and 700°C. The pyrite particle occasionally broke into two or more particles when the particles were hit by a sudden laser pulse. No fragmentation was observed in any of the ramped experiments, when the pyrite particles were subjected to a slow rate of heating. At temperatures higher than 700°C, ignition was observed. The rapid particle loss due to charge loss from the burning particle precluded direct observations of fragmentation, although in some cases a fragment remained captured in the balance.

(3) Ignition

Ignition was usually the terminal event in a pyrite experiment conducted in air. In general, a denser cloud was formed around the particle than for the lower temperature reactions. Occasionally, a small remnant particle would remain trapped. Smoke remained visible in the chamber for several seconds after the ignition event. Fig. 4.7a shows a typical ignition event, with a cloud forming in streaks both above and below the particle due either to jetting of released material or, more likely, to oscillations induced by the AC field as the particle loses charge. The corresponding temperature profile is shown in Fig. 4.7b, with maximum temperatures of the particle, reaching nearly 1000K.

During some of the ramped heating experiments, fume formation and ignition were observed nearly simultaneously. As the pyrite particle was heated, a fume cloud suddenly formed around the pyrite particle and gradually rose out of view which the

particle dropped down, due either to charge loss, or to the position control system's attempt to track the rising cloud. The focus of the lens was usually below the initial starting point of the particle, so as it dropped down into a region of higher intensity, it ignited, generating a much larger cloud of smoke.

4.3.2 Drop-Tube Reactor

Drop-tube reactor studies of pyrite reactions were undertaken to probe the nature of the fume produced during the reactions of pyrite at relatively low temperatures. The particle number concentration and size distribution of produced fume were measured by SEMS under different conditions. Figs. 4.8 and 4.9 show typical particle volume distributions obtained in N_2 or in air at different temperatures, using either natural pyrite or synthetic pyrite. In order to compare the effects of temperature and oxygen concentration, the particle volume distributions in Figs. 4.8 and 4.9 were normalized by the volumetric feed rates. The contribution of the original polydisperse synthetic pyrite to particles in the measured size range was examined by measuring the size distribution of the entrained particles in air at room temperature by SEMS. Few small particles were detected under this condition. The detailed experimental conditions and average results are summarized in Table 4.2.

(1) Natural Pyrite

Initial experiments were performed using natural pyrite in the 53-74 μm sieve fraction at temperatures ranging from 750K to 1220K. At the temperature of 750K, most of the fume particles were smaller than a few tens of nanometers in diameter (Fig. 4.8), although a small but significant aerosol volume was observed above 50 nm diameter. The minimum detectable particle size of SEMS used for these measurements was 13 nm. The data suggest that the number concentration increased further at smaller sizes. The total

mass of fume produced with sizes ranging from 13 nm to 190 nm at this low temperature in air amounted to about 40 parts per million of the original pyrite mass. Similar experiments done in nitrogen resulted in a somewhat smaller number of fine particles. The total mass of fume produced in N_2 was estimated about one-half of that in air. This difference increased with temperature. The fume yield also increased with temperature as indicated by the volume distribution for the reactions of pyrite. The peak at about 70 nm in the particle volume distribution obtained at 1220K is the result of coagulation of the large numbers of extremely fine particles produced in the initial nucleation burst. The estimated mass of fume generated in air at 1220K was about 7% of the original pyrite mass (assuming the particles to be dense spheres), whereas, that in N_2 was only around 0.3% of the original pyrite mass.

Samples of particles produced during these experiments with the natural pyrite were collected directly on silver TEM grids. They were then characterized by TEM with EDX. Fig. 4.10 shows small crystalline particles with sizes of 20 to 50 nm typical of the samples collected from the reaction of the natural pyrite in air. The primary constituents of these particles were silicon, calcium, copper, and zinc. Neither sulfur nor iron were detected except for one sample shown in Fig. 4.10. Within the circle in Fig. 4.10, small amounts of iron and sulfur were found, as indicated by the EDX spectrum.

(2) Synthetic Pyrite

Additional experiments were conducted with synthetic pyrite to reduce the influence of impurities. The particle volume distributions at 873K both in nitrogen and oxygen are shown in Fig. 4.9. The quantity of fume generated in air was much larger than that in nitrogen. The occurrence of coagulation due to the presence of many small particles was indicated by the peak at 70 to 100 nm in the particle volume distribution obtained in air. The fume particles were analyzed by TEM with EDX. Reaction in air at

1420K produced particles similar to those generated from the natural pyrite both in morphology and chemical composition. The particles consisted of the major impurities present in the original material (Table 4.2), e.g., silicon, calcium, copper and zinc, together with a very small amount of sulfur. Although the particles produced in N_2 at 1420K had similar chemical compositions to those produced in air, the collected particles appeared to be extensively agglomerated and lack the crystalline particles produced in air (Fig. 4.11). The sulfur content of the fume particles increased with decreasing temperature. Analysis of the fume produced by reaction in air at 873K and 1220K revealed fume particles consisting of elemental sulfur. Fig. 4.12 illustrates numerous particles with crystalline shapes. During analysis of the samples, the portion of them were damaged by the electron beam, which could be seen from the formation of bubbles in the crystals (Fig. 4.12). Some small particles even disappeared completely.

The mass of the fume generated from pyrite was very low in our experiments. The fume particles had a very broad size distribution and varied significantly in morphology and chemical composition depending on the experimental conditions. Elemental analysis of the fume particles ($d_p < 50$ nm) revealed the predominance of sulfur and impurities present in the original pyrite. No evidence was found for the formation of small iron-rich particles under our experimental conditions. Hence, the cloud observed in EDB experiments (Fig. 4.6b) is thought to consist mainly of impurities released during pyrite decomposition and condensed due to the dramatic temperature drop from the particle to the surrounding gas. These observations differ from the iron fume formation in coal combustion as reported by Flagan and Taylor (1981) or by Baxter and Mitchell (1989). They both reported that small iron-rich particles were generated when burning pulverized coal. Flagan and Taylor measured the composition-size distribution of ash particles generated during combustion and found a pronounced peak in the iron mass distribution below 0.1 μm diameter. The differences between the previous results and our

experiments may be caused by the materials and gas temperatures of the various experiments. Gas temperatures in the coal combustion experiments were about 100K to 300K higher than the highest temperature used in our experiments. The reactions of pyrite within coal particles could differ significantly from those of pure pyrite because of the locally reducing atmosphere at the surface of the burning carbon and because of modified surfaces of the included pyrite. Particle temperatures may also exceed the surrounding gas temperature during char oxidation.

We have found no direct evidence for the formation of an iron-rich fume in particle size of 20-50 nm during pyrolysis or oxidation of isolated pyrite particle. However, iron has been detected in particles larger than a few microns. The low temperatures of our experiments makes iron vaporization unlikely. Fragmentation does not appear to generate large numbers of fume particles. Baxter and Mitchell (1989) suggested that gases evolved during coal devolatilization entrain fine iron-rich particles. Reactions of isolated pyrite particles or of coal chars will not generate the same high velocities. The formation of soot or impurity-derived fumes would interfere with our present methods of estimating pyrite derived fume production. For these reasons, we turn to theoretical arguments to examine whether the fragmentation/entrainment mechanism suggested by Baxter and Mitchell (1989) could be expected to generate significant quantities of submicron fume. The key question is whether the aerodynamic forces are sufficient to dislodge small particles from the surface of the burning char.

4.4 Theoretical Considerations

To dislodge a solid particle from a surface requires a removal force provided by the drag and lift of the gas stream on the particle. Experimental studies of the reentrainment of sand particles by wind (Bagnold, 1960) showed that the velocity must exceed a limiting value for entrainment to occur, and the value varies with particle size.

The velocity increases due to particle-to-particle cohesive forces as the particles become smaller. For submicron particles, the intermolecular attraction force is dominant. Electrostatic effects have been observed to be much smaller than the intermolecular attraction force (Lipinski et al., 1985). The force needed to separate two spherical particles of radii r_1 and r_2 from one another was given by Bradley (1932),

$$F_{adhesion} = 4\,\pi\,\sigma \frac{r_1\,r_2}{r_1 + r_2} \tag{4.1}$$

where σ is the surface free energy of the particles. σ is equal to one-half of the (van der Waals) energy needed to separate two surfaces from contact to infinity, and can be estimated by (Israelachvili, 1985)

$$\sigma = \frac{A}{24\,\pi\,D_0^2} \tag{4.2}$$

where D_0 is the distance between two surfaces in contact. The value of $D_0 = 0.165$ nm yields surface energy estimates in close agreement with measured values (Israelachvili, 1985). A is the Hamaker constant,

$$A = \pi^2\,C\,\rho_1\,\rho_2 \tag{4.3}$$

where C is the coefficient in the atom-atom pair potential, ρ_1 and ρ_2 are the number of atoms per unit volume in the two bodies. Typical values of A are 7×10^{-13} erg, with values ranging as high as 3×10^{-12} erg. A more rigorous method of calculating the Hamaker constant in terms of the macroscopic properties of the media is based on the Lifshitz theory (Israelachvili, 1985). For two identical phases 1 interacting across medium 2,

$$A = \frac{3}{4} kT \left(\frac{\varepsilon_1 - \varepsilon_2}{\varepsilon_1 + \varepsilon_2}\right)^2 + \frac{3h\upsilon_e}{16\sqrt{2}} \frac{(n_1^2 - n_2^2)^2}{(n_1^2 + n_2^2)^{3/2}} \tag{4.4}$$

The estimated value A of ferrous oxide in air at the temperature of 1600K is 3.3×10^{-12} erg. Thus, the surface energy σ calculated from Eq. 4.2 is 160.8 erg cm^{-2}.

The primary forces acting to remove the particles from the surface result from aerodynamic drag. For the small particles of interest here, the drag force acting on a free spherical particle moving at a velocity v relative to the gas in which it is immersed is

$$F_{drag} = \frac{3 \pi \mu d_{p_1} v}{C_c(Kn)} \tag{4.5}$$

where the slip correction factor C_c

$$C_c = 1 + Kn\{1.257 + 0.4 \exp(-\frac{1.1}{Kn})\}$$

corrects the Stokes drag for noncontinuum effects when the particle diameter d_{p_1} is small compared to the mean free path of the gas molecules l, i.e. Knudsen number ($Kn = \frac{2l}{d_{p_1}}$) is greater than 1 .

In the following calculations, we assume that the drag force exerted by the fluid is the only force acting to remove a particle from a surface, and that the drag can be calculated as though the particle were immersed in the flow. This is illustrated in Fig. 4.13. The critical velocity required to separate particle 1 from particle 2 is that for which

$$F_{adhesion} = F_{drag}$$

We find

$$v_{crit} = \frac{2\, C_c\, \sigma\, d_{p_2}}{3\, \mu (d_{p_1} + d_{p_2})} \tag{4.6}$$

The critical velocities thus depends on fluid and particle properties as well as the sizes of particles to be separated. The calculated results for a 100 μm coal particle are shown in Fig. 4.14. For the larger Hamaker constants, indicated by the dashed lines in Fig. 4.14, the velocities required to separate the particle from the surface are too high to be achieved at normal conditions. The critical velocities decrease with the increasing ash particle diameters for submicron particles (d_{p_1}), and are proportional to the surface free energy. The maximum value of v_{crit} corresponds to the removal of a very small particle from a much large one, i.e., $d_{p_1} \ll d_{p_2}$,

$$v_{crit,\, max} = \frac{2\, C_c\, \sigma}{3\, \mu} \tag{4.7}$$

The minimum critical velocity is that for which $d_{p_1} = d_{p_2}$, and amounts to

$$v_{crit,\, min} = \frac{1}{2}\, v_{crit,\, max} \tag{4.8}$$

There are few experimental measurements of v_{crit}. Corn and Stein (1965) studied the reentrainment of glass beads by high velocities of air flow. They found that particles with sizes less than 0.5 μm could not be removed from a surface even by a flow with a free stream velocity of 150 m sec^{-1}. The reentrainment velocities of particles in a broad range has been studied by Lipinski et al. (1985). The minimum velocity for particle resuspension from a dry surface is about 1.8 m sec^{-1} for 10 μm particles. Although the drag force we consider is valid for a free particle of spherical shape, it provides an estimate of the force acting on a spherical particle adhering to a substrata. These results of previous studies are consistent with our estimates.

From Baxter and Mitchell's report (1989), there was a significant fraction of the

iron in the coal lost in the 25 ms time period just after the completion of coal devolatilization. During the iron release, the peak particle temperature measured was 1710K in the 6% oxygen environment. The estimated carbon consumption rate is 0.006 gm cm^{-2} sec^{-1}, using the char particle combustion model developed by Sahu (1988). Thus, the estimated velocity of releasing gas is 70 cm sec^{-1}. Comparing this value with those in Fig. 4.14 calculated by Hamaker constant of 3.3×10^{-12} erg, we can find that the velocity of the releasing gas is much smaller than the critical velocities required to release the particles with sizes less than 1 μm to the surrounding gases. It is even smaller than the required velocities calculated by the abnormally low value of Hamaker constant (Hamaker, 1937).

Besides lifting, a particle has two other modes of incipient motion on a surface, sliding and rolling, depending upon the magnitude, direction, and the position of the applied force (Hubbe, 1984). Wang (1990) examined the possibility of a particle removed by these two motions. A dimensionless force parameter, F^*, is defined as

$$F^* = \frac{F_{drag}}{F_{adhesion}} \tag{4.9}$$

The force to start a particle to slide (see Fig. 4.13),

$$F_{slide} = \alpha (F_{adhesion} + F_{drag} \sin\theta)$$

where α is the coefficient of friction. Since $F_{slide} = F_{drag} \cos\theta$,

$$F^*_{slide} = \frac{\alpha}{\cos\theta - \alpha \sin\theta} \tag{4.10}$$

The minimum force parameter for sliding is

$$F^*_{slide,\,min} = \frac{\alpha}{\sqrt{1+\alpha^2}} \tag{4.11}$$

with $\theta_{min} = -arctan\ (\alpha)$. The α values listed in CRC book (1990) are in the range of 0.02 to 5. α is 0.1 for graphite on steel, and 1.2 for iron on iron. Hence, the minimum drag force required to slide a pyrrhotite particle on the char surface should not be less than $0.01F_{adhesion}$.

The onset of rotation of a particle is determined from the balance of moments at point B in Fig. 4.13.

$$F_{drag}\{(a_y + r - \beta)\cos\theta - (a_x + x)\sin\theta\} = F_{adhesion}x$$

where β is the deformation. (a_x, a_y) is the coordinate of the applied drag force, and $a_x = r\cos\varphi$, $a_y = r\sin\varphi$. So we have

$$F^*_{roll} = \frac{x/r}{(1 - \frac{\beta}{r})\cos\theta - \frac{x}{r}\sin\theta + \sin(\varphi - \theta)} \tag{4.12}$$

A similar equation can be obtained for point C. The minimum force parameter for rolling is

$$F^*_{roll,\,min} \approx \frac{x}{2r} \tag{4.13}$$

The upper-limit to the size of detached particles postulated by Baxter and Mitchell (1989) is 0.2 μm. For hexagonal pyrrhotite, FeS_{1+x} ($0 < x < 0.12$), the cell dimensions are 3.446 and 5.848 Å (Lowson, 1982). Therefore, the minimum drag force required to start rotation of a pyrrhotite particle on the char surface is about $10^{-3}F_{adhesion}$. The calculated results show that the critical removal force and, hence, the critical velocity can be reduced up to two to three orders of magnitude by sliding or rolling. The estimated velocity of the escaping gas is, however, still more than one order of magnitude lower than that required

(Fig. 4.14), to dislodge the submicron pyrrhotite particles from the char surface.

As coal particles are heated to sufficient high temperature, devolatilization starts. Gaseous jets of volatiles effusing from the particle give rise to high-frequency char particle rotation (Helble and Sarofim, 1989). Rotation frequencies may reach 1000 revolutions per second for 100 μm particles at the beginning of char combustion, as measured by two-color pyrometry traces of burning particles. The centrifugal and gravitational forces may cause the shedding of ash particles from the surface of the burning char. The centrifugal and gravitational forces can be presented as,

$$F_c = m_{ash}\, r_{char}\, \omega^2 \tag{4.14}$$

$$F_g = m_{ash}\, g \tag{4.15}$$

where $\omega = 2\pi f$, f is the frequency of rotation (s^{-1}). g is gravitational acceleration. There are two limit cases. If an ash particle adheres on the side of the char surface, lift-off is the only motion to initiate ash particle movement. Therefore the sum of F_c and F_g must be at least equal to the adhesion force to remove the ash particle. If the ash particle adheres on the top or bottom of the char particle surface, gravitational force will increase or decrease the resistance to remove ash particle. But the ash particle may also be removed by slide or rotation. As shown above, slide or rotation could reduce the required external force two to three orders of magnitude to remove a 0.2 μm particle. Therefore, the minimum dimensionless force parameter, F^*_{min}, required to move a pyrrhotite particle by centrifugal and gravitational force is,

$$F^*_{min} = \frac{F_c + F_g}{F_{adhesion}} = 10^{-3} \sim 10^{-2} \tag{4.16}$$

Neglecting the contact angle of the ash particle with the char surface considered by

Helble and Sarofim (1989), the maximum mass of an ash particle is

$$m_{ash,\,max} = \frac{3}{4}\pi r_{ash}^{3} \rho_{ash}$$

Combining Eqs. 4.1, 4.14 and 4.15, then

$$F^{*} = \frac{r_{ash}^{2} \rho_{ash} (4\pi^{2} f^{2} r_{char} + g)(r_{ash} + r_{char})}{3\sigma r_{char}} = \frac{3.1\times10^{-5}}{\sigma} \qquad (4.17)$$

where r_{ash} = 0.1 μm, r_{char} = 50 μm, density of pyrrhotite is about 4.74 g cm^{-3} (Lowson, 1982). The estimated σ is 160.8 erg cm^{-2}. Then $F^{*} = 2\times10^{-7} \ll F^{*}_{min}$. If using smallest Hamaker constant, 0.7×10^{-14} erg, the calculated σ is 0.34 erg cm^{-2}. Thus, $F^{*} = 9.1\times10^{-5}$, which is still lower than F^{*}_{min}. Helble and Sarofim (1989) examined the possibility to separate a molten (i.e., liquid phase) ash particle from a solid char surface due to high-frequency rotation. Their results indicated that the ash particles must grow to 80 μm diameter on a 100 μm char particle before they can be shed at a gas temperature of 1750K and a rotational frequency of 1000 s^{-1}. We considered the initial motion of pyrrhotite particles detached from the char surface. Although the force required to start the rotation of an ash particle is smaller than that to separate a molten ash particle from the char surface calculated by Helble and Sarofim, the force supplied by high-frequency rotation is still too small to dislodge even a 0.2 μm pyrrhotite particle, which is the up-limit of detached particles postulated by Baxter and Mitchell (1989). Therefore, the mechanical mechanism of iron fume formation proposed by Baxter and Mitchell does not appear to be viable.

4.5 Discussion

An experimental investigation of the reactions of pyrite has been undertaken to

seek the sources of iron-rich fume in coal combustion. A fume was formed in low temperature reactions, but it contained virtually no iron. The primary constituents of the fume were impurities derived from the starting mineral and sulfur. When pyrite was oxidized in air at temperatures below 1220K, or pyrolyzed in nitrogen at temperatures up to 1420K, a sulfur rich fume was generated. Some of the particles were crystalline. During electron microscope analysis, the beam damaged some of the crystallites. The sulfur-rich particles are thought to be elemental sulfur. Due to the low vapor pressure of sulfur at room temperature, it probably condensed in the cooled sampling probe in the drop-tube reactor experiments. The observed fume particle size distribution is, therefore, determined by the sample extraction system and is not directly related to the pyrite reaction. Similarly, a cloud is formed around the laser heated particles when the temperature drops to near ambient levels. The persistence of elemental sulfur to temperatures as high as 1220K suggests relatively slow reaction of the predominant S_2 species. Sulfur was not found in the higher temperature oxidation experiments, presumably due to SO_2 formation.

Baxter and Mitchell (1989) have observed significant iron loss in the early phases of coal combustion when temperatures are too low for volatilization to be significant. They provide no data on the size, structure, or composition of the iron containing particles that escaped their collection system. Examination of the filters used in their measurements by Liu et al. (1983) reveals that a broad range of particle sizes might penetrate. The large fractional loss they report suggests that the particles are near the minimum of the collection efficiency curve, i.e., between 0.04 and 0.2 μm. They hypothesize that pyrrhotite nodules, which are observed to be of order 0.1 μm diameter, are entrained by the gases released during devolatilization or the early phases of oxidation. Our experiments show no evidence for such release during reactions of pyrite alone. Similar experiments have been conduced by Srinivasachar et al. (1990). They

reported that little submicron particle formation was observed.

We have examined the ability of aerodynamic and centrifugal forces to remove particles held on a surface by van der Waals force. The velocities required to entrain submicron particles are too large for this mechanism to produce significant quantities of fine particles directly. However, fragments of order 1 to 10 μm in size or larger might be released. Two mechanisms might allow fine iron particles to be formed by fragmentation. If a carbonaceous bridge holding a mineral inclusion on the parent particle were consumed by oxidation, the separation distance might be large enough to allow even a very small particle to be removed aerodynamically. On the other hand, oxidation of a large carbonaceous fragment could have left behind relatively small residual ash particles. The former mechanism could generate a large number of fine fragments since the apparent surface free energy scales inversely as the square of the separation distance. It would likely appear early in the oxidative phase of coal combustion when temperatures are low enough for the pyrrhotite to be solid and when sufficient oxygen reaches the coal surface to consume carbon bridges. These conditions are consistent with the observations of Baxter and Mitchell (1989), as well as with the lack of fine fragment in the present study. The latter mechanism would require that a significant amount of carbon be associated with each fine particle and would, therefore, limit the number of fine fragments generated. Moreover, it would likely occur late in the combustion process when pore enlargement causes the entire char particle to disintegrate.

Previous coal combustion studies have shown substantial evidence for iron volatilization (Taylor and Flagan, 1981; Flagan and Taylor, 1981; Quann et al. 1982; and Neville and Sarofim, 1982). The evidence from these pyrite studies suggest that more than one mechanism may be responsible for the production of fine ash particles of all types in coal combustion. The distribution of a mineral in the parent coal and the

transformation that the mineral experiences will influence the extent of fine particle formation by fragmentation. Carefully designed experimental investigations of mechanical generation of fine particles from pyrite in coal combustion may shed light on the origins of other combustion-derived fine particles.

ACKNOWLEDGEMENTS

This work was supported by the United States Department of Energy under grant number DE-ACC22-86PC90751.

NOMENCLATURE

A	Hamaker constant (erg)
d_p	particle diameter (μ)
h	Planck's constant = 6.626×10^{-27} erg sec
k	Boltzmann's constant = 1.381×10^{-16} erg K^{-1}
l	mean free path of the gas
n_i	refractive index of the medium i in the visible
r	particle radius (μm)
T	absolute temperature (K)
v	fluid velocity
ε_i	static dielectric constants of the medium
υ_e	plasma frequency of the free electron gas, typically in the range 3 to 5×10^{15} sec^{-1}
σ	free surface energy (erg cm^{-2})
μ	fluid viscosity (gm cm^{-1} sec^{-1})

REFERENCES

Bagnold, R. A. (1960), The Re-entrainment of Settled Dusts, *Int. J. of Air Pollution*, 2, 357.

Baxter, L. L., and Mitchell, R. E. (1989), The Release of Iron during the Combustion of Illinois #6 Coal, *6th Ann. Int. Pittsburgh Coal Conf.*, University of Pittsburgh. 64-73.

Bradley, R. (1932), The Cohesive Force between Solid Surface and the Surface Energy of Solids, *Phil. Mag.* 13, 853-862.

Corn, M, and Stein, F. (1965), Re-entrainment of Particles from a Plane Surface, *Amer. Ind. Hyg. Assoc. J.*, 26, 325-336.

Flagan, R. C., and Friedlander, S. K. (1978), Particle Formation in Pulverized Coal Combustion: A Review, *Recent Developments in Aerosol Science*, Shaw, D. T. (Ed.), Wiley-Interscience, New York, 25-59.

Flagan, R. C., and Taylor, D. D. (1981), Laboratory Studies of Submicron Particles from Coal Combustion, *18th Symp. (Int.) on Comb.*, The Combustion Institute, Pittsburgh, PA, 1227-1237.

Fristrom, R. M., and Westenberg, A. A. (1965), (Eds.), *Flame Structure*, McGraw-Hill, New York.

Hamaker, H. C. (1937), The London-van der Waals Attraction between Spherical Particles, *Physics*, 4(10), 1058-1072.

Helble, J. J., and Sarofim, A. F. (1989), Influence of Char Fragmentation on Ash Particle Size Distributions, *Comb.& Flame*, 76, 183-196.

Hubbe, M. A.. (1984), Theory of Detachment of Colloidal Particles from Flat Surfaces Exposed to Flow, *Colloids and Surfaces*, 12, 151-178.

Israelachvili, J. N. (1985), (Ed.), *Intermolecular and Surface Force with Applications to Colloidal and Biological Systems*, Academic Press Inc., London.

Lipinski, R. J., Bradley, D. R., et al. (1985), "Uncertainty in Radionuclide Release under

Specific LWR Accident Conditions", Appendix G on Resuspension & Reentrainment, SAND84-0410, 2, R5.

Liu, B. Y. H., Pui, D. Y. H., and Rubow, K. L. (1983), Characteristics of Air Sapling Filter Media, *Aerosols in the Mining and Industrial Work Environments, Vol. 3, Instrumentation and Arbor Science*, Marple, V. A. and Liu, B. Y. H. (Eds.), Ann Arbor Science, Ann Arbor, Michigan.

Lowson, R. T. (1982), Aqueous Oxidation of Pyrite by Molecular Oxygen, *Chem. Rev.*, 82, 462-497.

Neville, M., and Sarofim, A. F. (1982), The Stratified Composition of Inorganic Submicron Particles Produced during Coal Combustion, *19th Symp. (Int.) on Comb.*, The Combustion Institute, Pittsburgh, PA, 1441-1449.

Quann, R. J., Neville, M., et al. (1982), Mineral Matter and Trace-Element Vaporization in a Laboratory-Pulverized Coal Combustion System, *Environ. Sci. Tech.*, 16, 776-781.

Sahu, R. (1988), On the Combustion of Bituminous Coal Chars, Ph. D. Thesis, California Institute of Technology.

Spjut, R. E., Sarofim, A. F., and Longwell, J. P. (1985), Laser Heating and Particle Temperature measurement on an Electrodynamic Balance, *Langmuir*, 1, 355-360.

Srinivasachar, S., Helble, J. J., and Boni, A. A. (1990), Mineral Behavior during Coal Combustion: 1. Pyrite Transformation, *Prog. Energy Comb. Sci.*, 16, 281-292.

Taylor, D. D., and Flagan, R. C. (1981), Aerosols from a Laboratory Pulverized Coal Combustion, *Atmospheric Aerosols-Source/Air Quality Relationships*, Macias E. S. and Hopke, P. K. (Eds.), ACS Symposium Series No. 167.

Wang, H. C. (1990), Effects of Inceptive Motion on Particle Detachment from Surfaces, *Aerosol Sci Tech.*, 13(3), 386-393.

Wang, S. C., and Flagan, R. C. (1990), Scanning Electrical Mobility Spectrometer, *Aerosol Sci Tech.*, 13(2), 230-240.

Table 4.1 Impurities in Pyrite Samples

Element	Natural Pyrite		Synthetic Pyrite	
	Supplier (%)	XFS (%)	Supplier (ppm)	XFS (%)
B			10	
Ca		~ 10	< 10	trace
Cu	0.5	~ 1	100	
Cr		trace		≤ 0.1
K		< 1		
Mg		trace	< 10	trace
Mn		< 5	< 10	
Mo			10	
Ni			10	
Pb	0.04			
Si			700	
Ti			10	
Zn	0.03	~ 5-10%		
Zr			100	

Table 4.2 Experimental Conditions and Average Results

Natural Pyrite:

T_{wall} (K)	750		873		1220	
Gas	N_2	air	N_2	air	N_2	air
Q_{mass} (gm hr^{-1})	1.08	0.94	0.22	0.022	0.87	0.016
$Q_{in,total}$ (lpm)	4.0	4.0	4.0	4.0	4.0	4.0
Q_{probe} (lpm)	5.0	5.0	5.0	5.0	5.0	5.0
$Q_{dilutor}$ (lpm)	0.0	0.0	28.0	28.0	28.0	28.0
N_{tot} (No.cm^{-3})	1.9×10^6	4.1×10^6	2.0×10^6	1.3×10^6	3.2×10^6	7.2×10^6
V_{tot} (μm^3 cm^{-3})	3.4	6.9	7.7	8.8	96	39
$C_{FeS_2,reacted}$ (based on ρ_{FeS_2})	16ppm	38ppm	0.1%	1%	0.3%	7%

Synthetic Pyrite:

T_{wall} (K)	873		1220		1420	
Gas	N_2	air	N_2	air	N_2	air
Q_{mass} (gm hr^{-1})	0.23	0.072	0.46	0.034	0.43	0.048
$Q_{in,total}$ (lpm)	4.0	4.0	4.0	4.0	4.0	4.0
Q_{probe} (lpm)	4.5	4.5	4.5	4.5	4.5	4.5
$Q_{dilutor}$ (lpm)	20.0	20.0	20.0	20.0	20.0	20.0

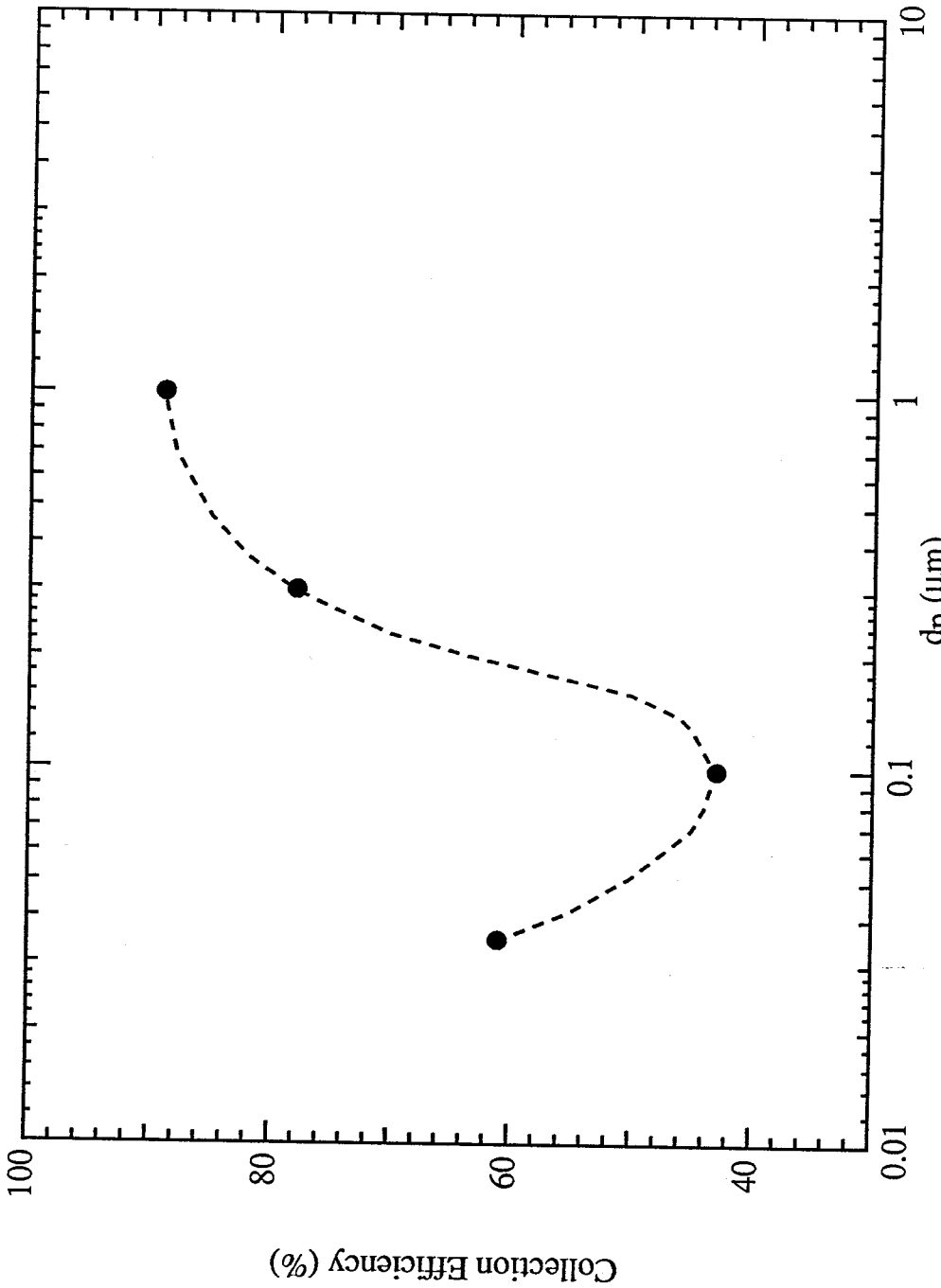

Fig. 4.1 Collection efficiency of 1.0 μm nuclepore filter (Liu, et al., 1983)

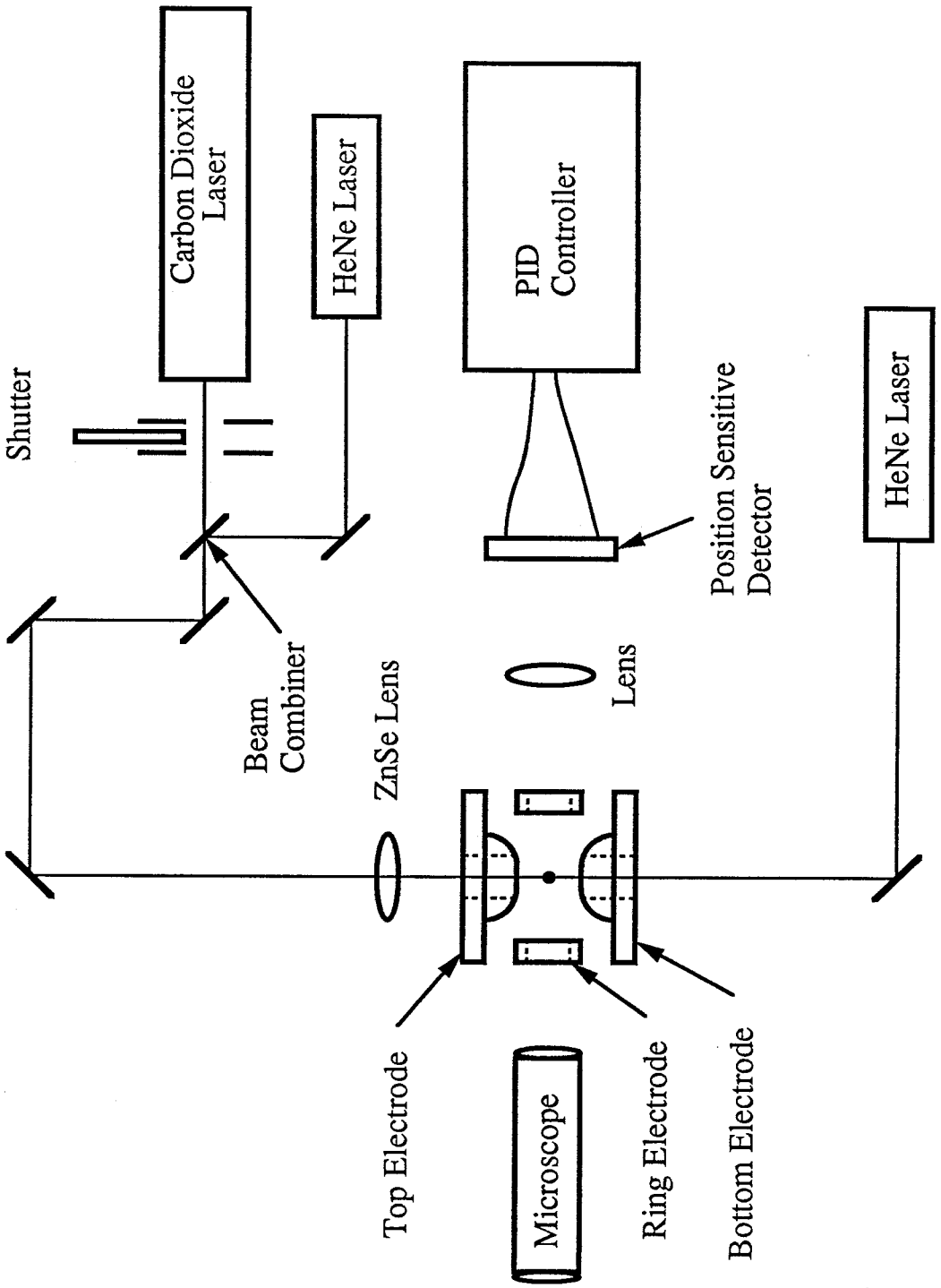

Fig. 4.2 Schematic of the EDTGA

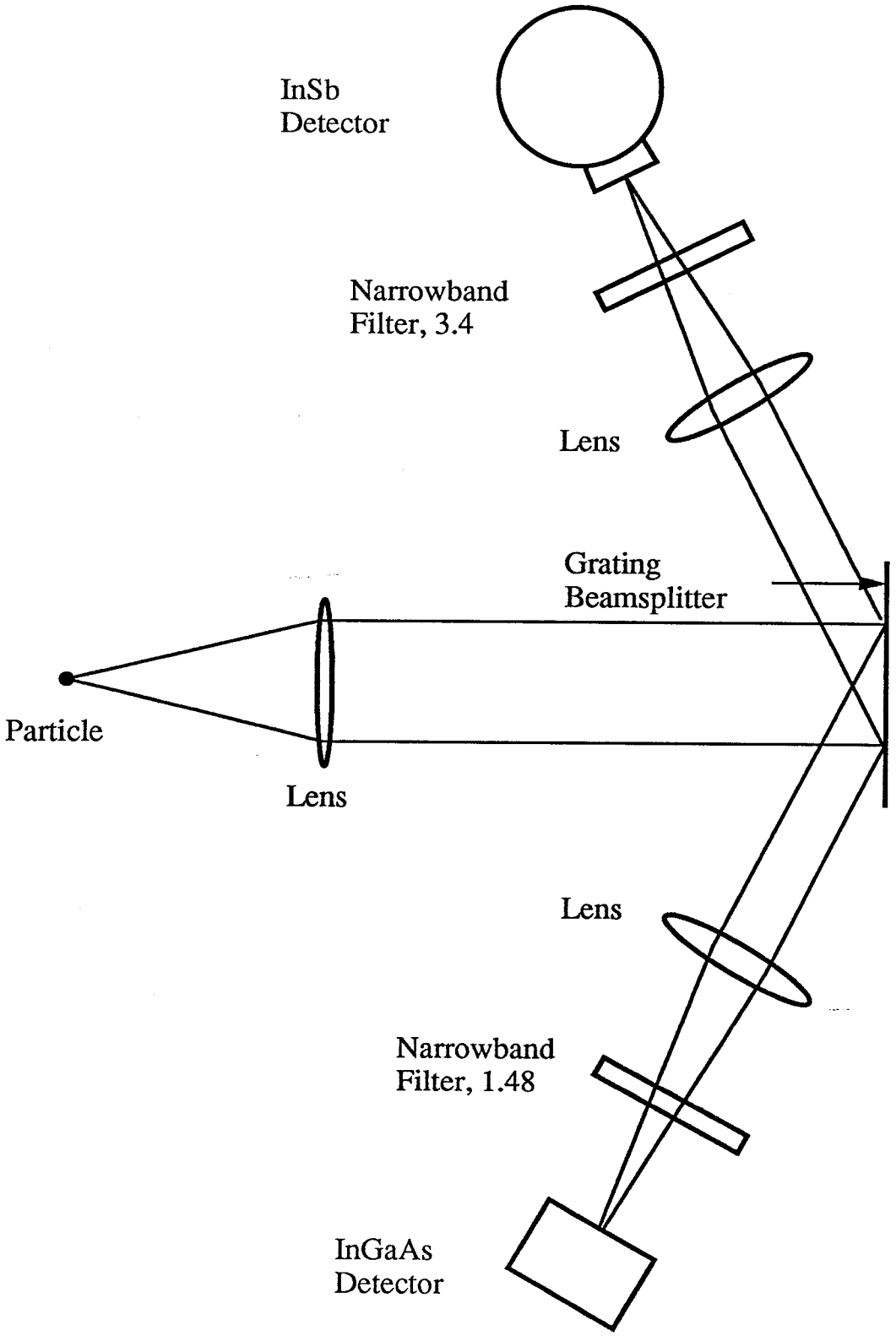

Fig. 4.3a Pyrometer Schematic

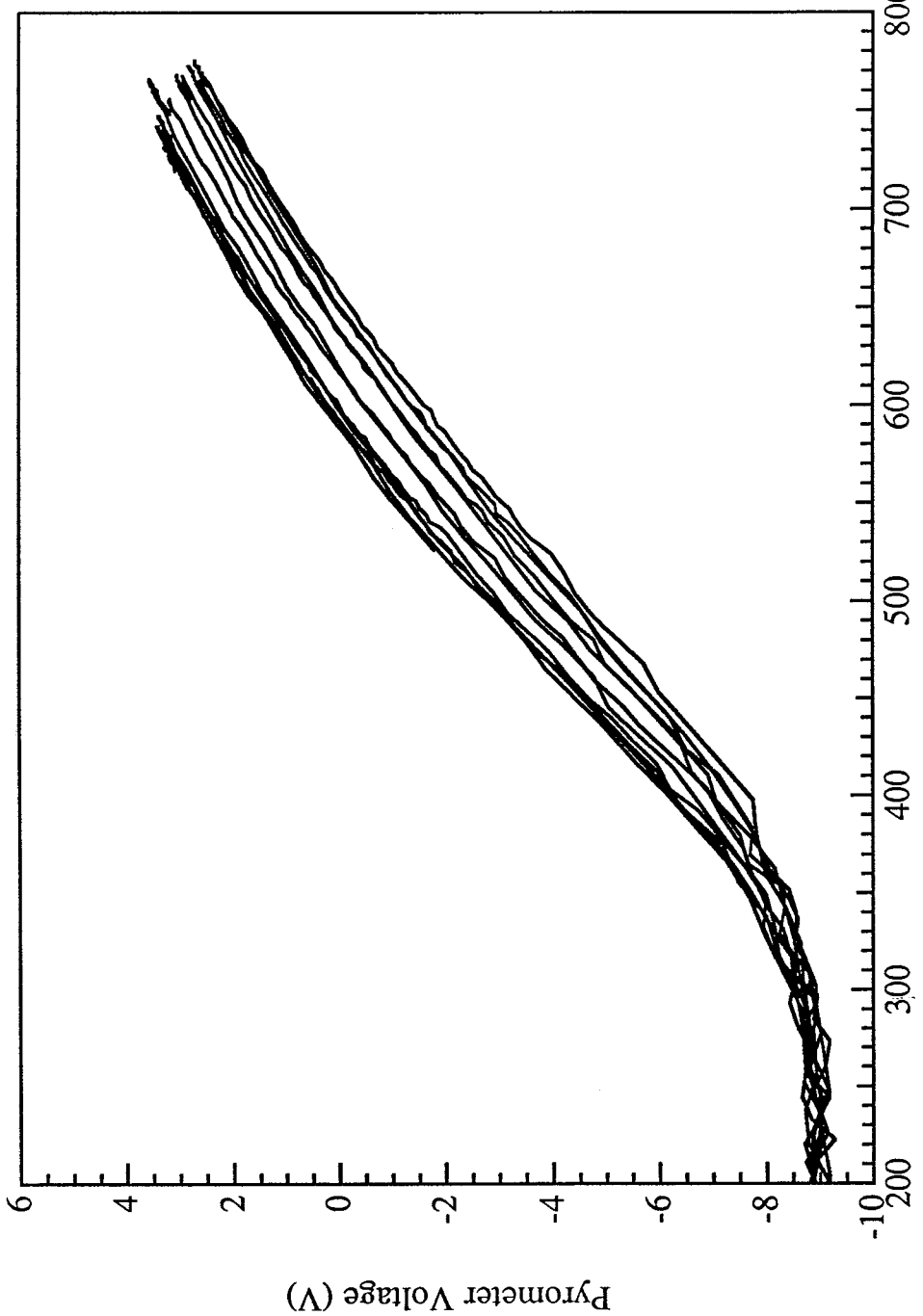

Fig. 4.3b Optical pyrometer calibration data obtained using a pyrite coated thermocouple bead

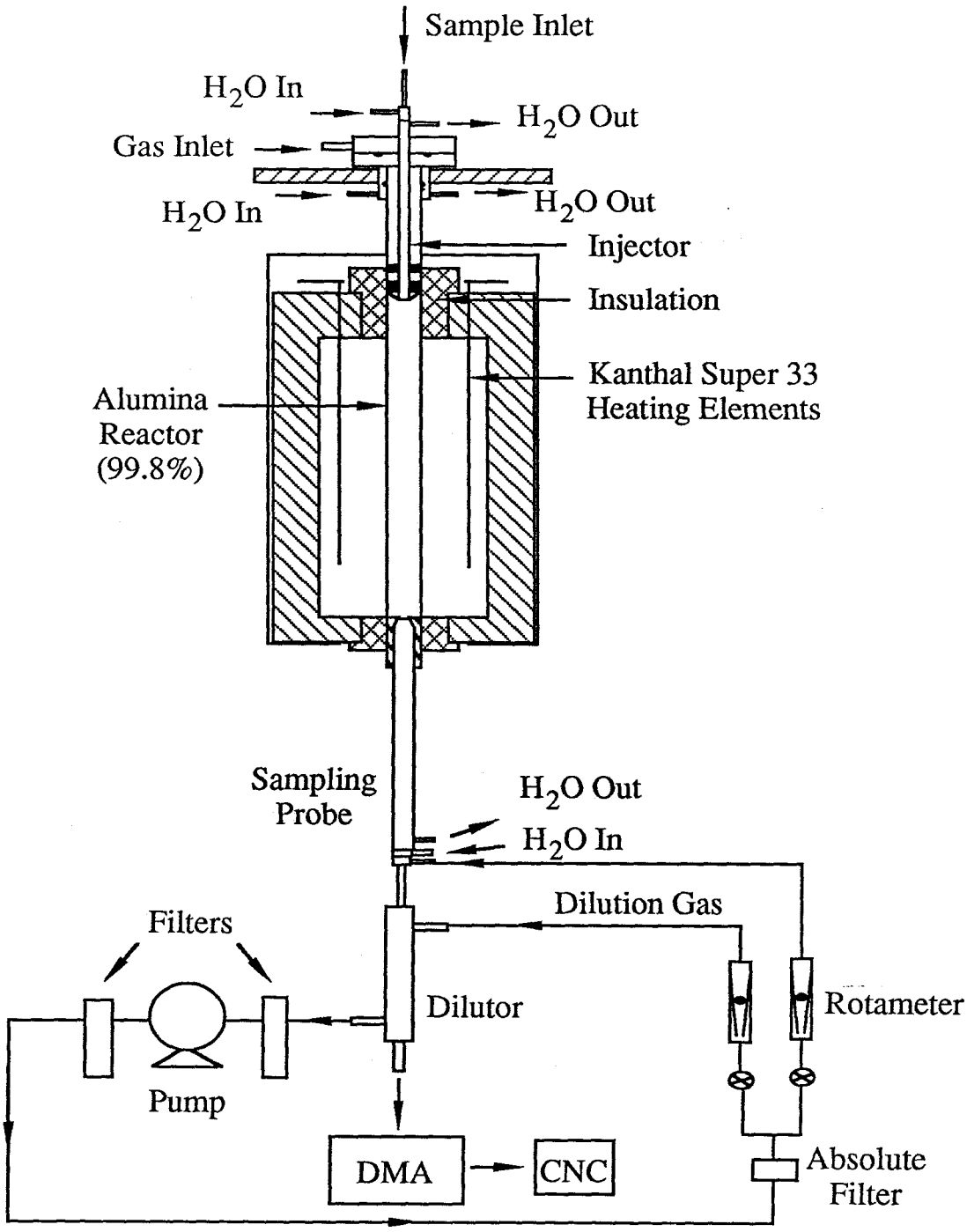

Fig. 4.4 Schematic of experimental system

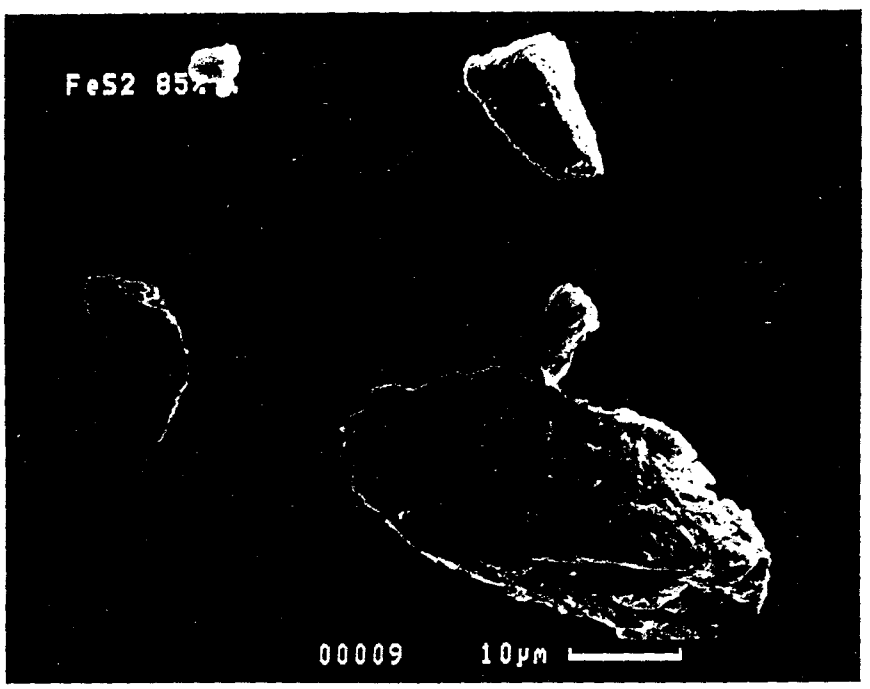

Fig. 4.5a SEM pictures of natural pyrite

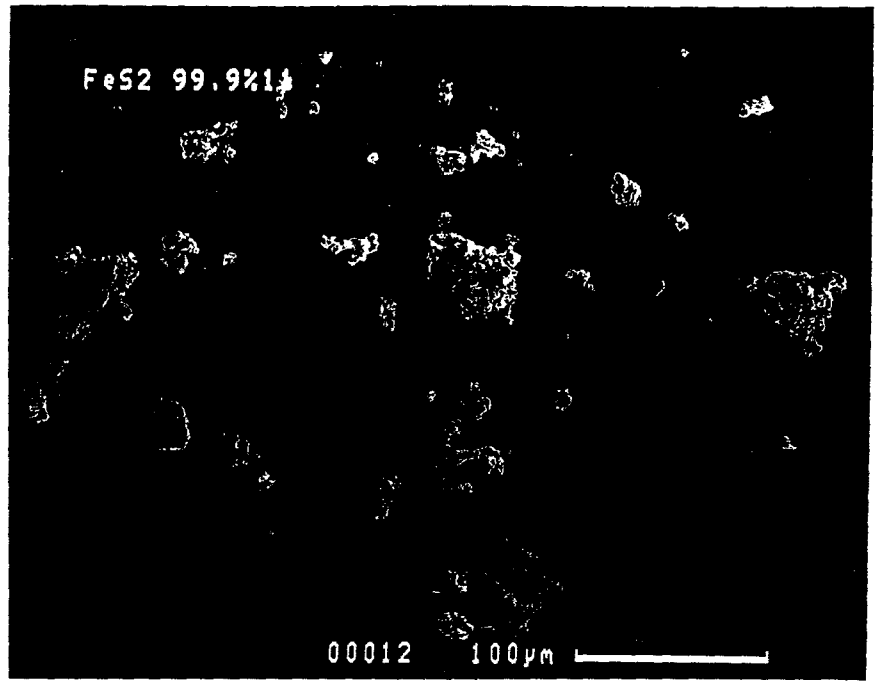

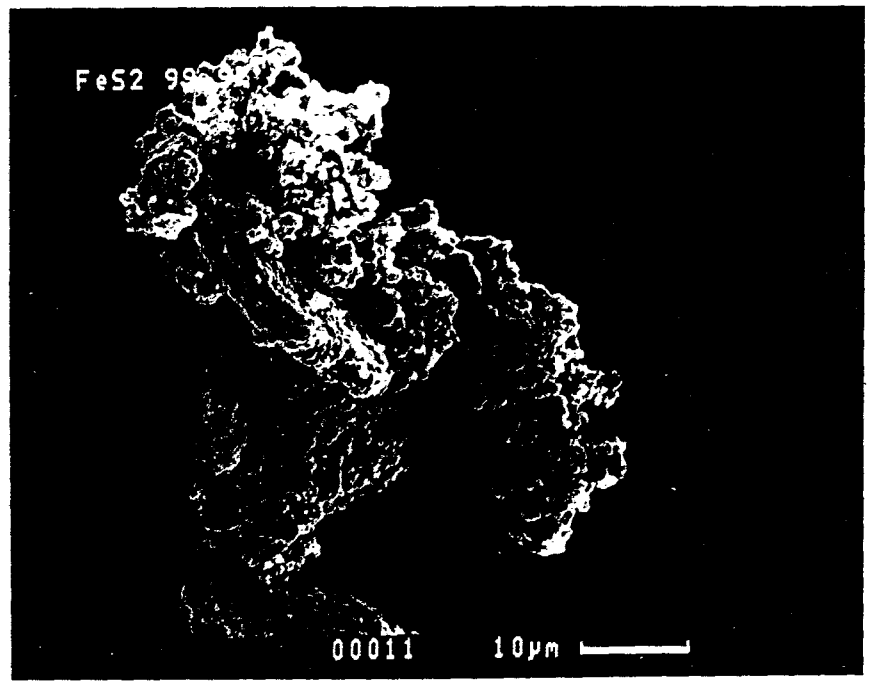

Fig. 4.5b SEM pictures of synthetic pyrite

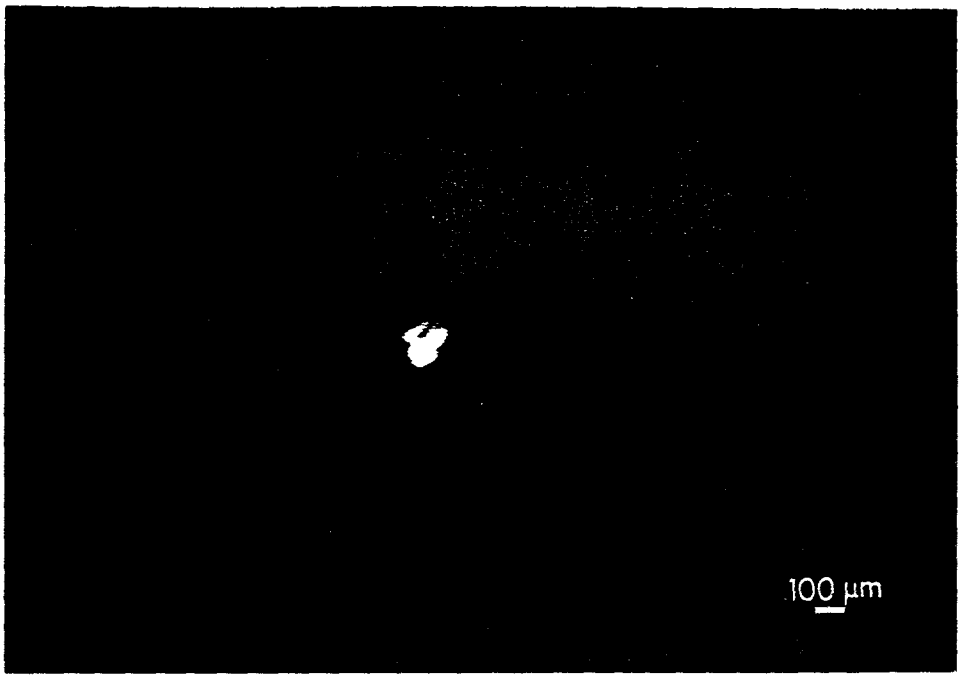

(a)

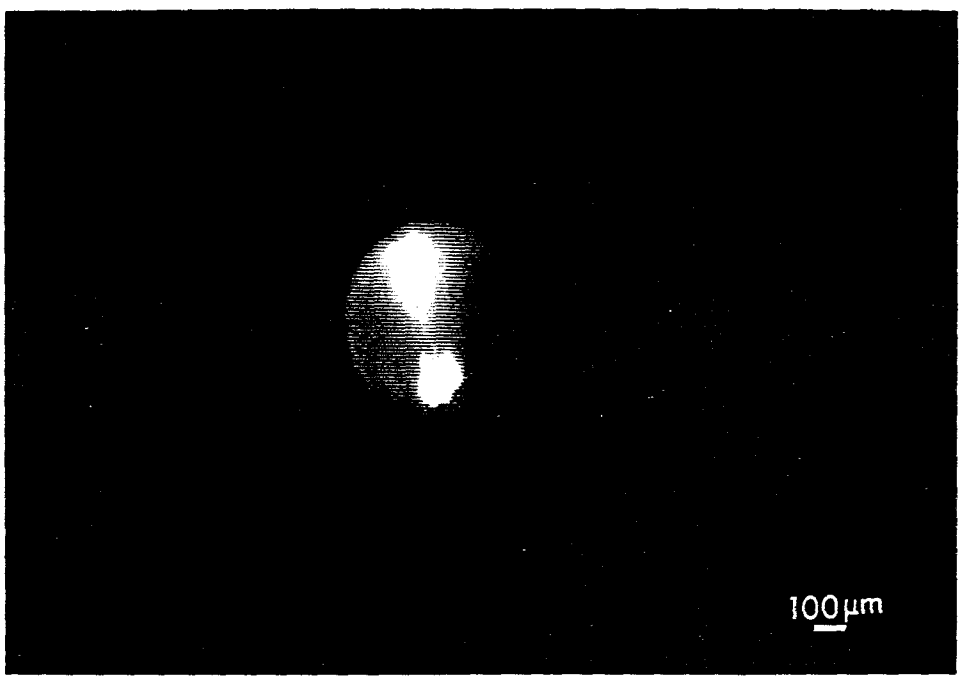

(b)

Fig. 4.6a Image of pyrite particle trapped in the electrodynamic balance
4.6b Cloud formation around the particle after a single laser pulse

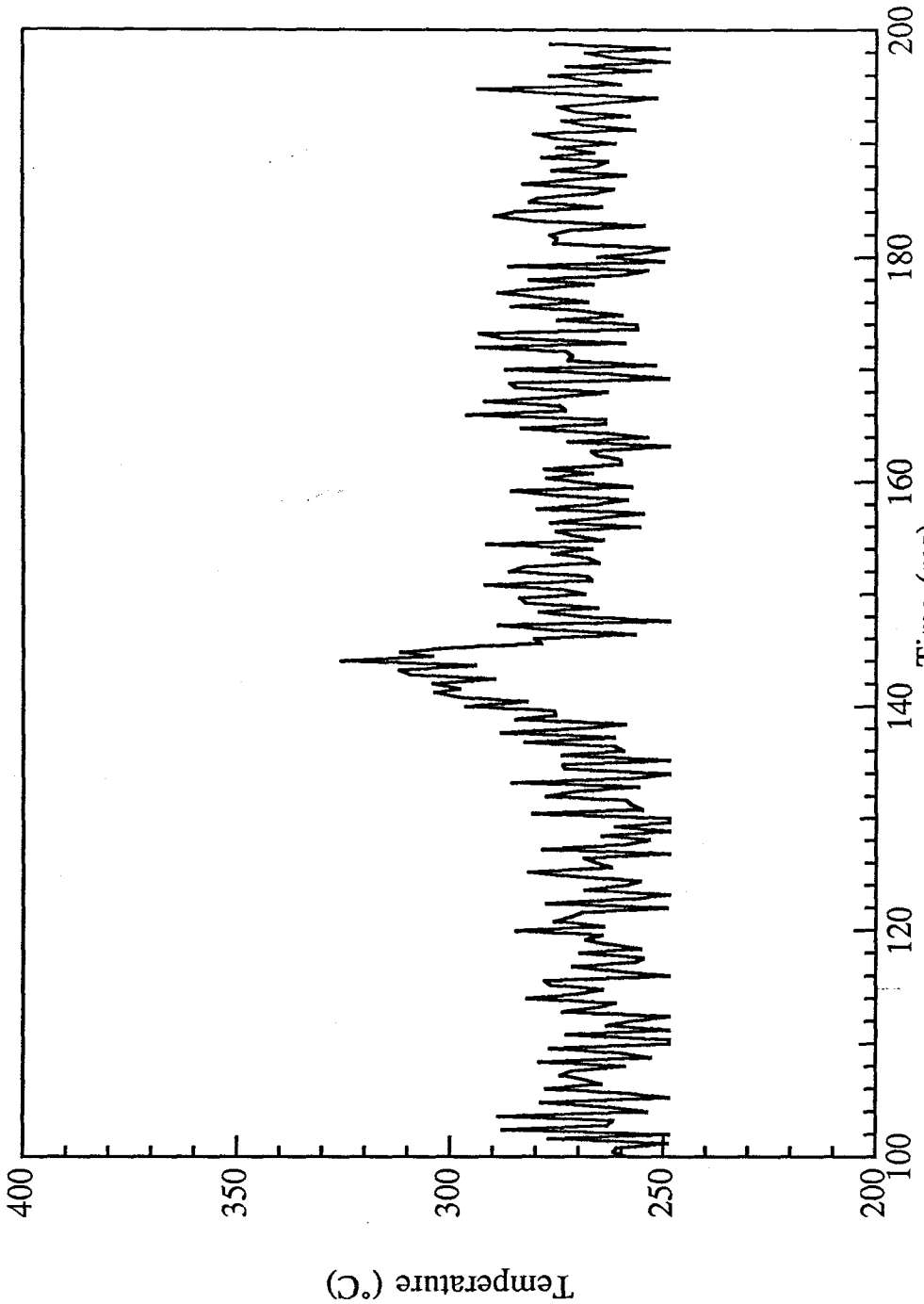

Fig. 4.6c Optically measured temperature profile for the laser pulse

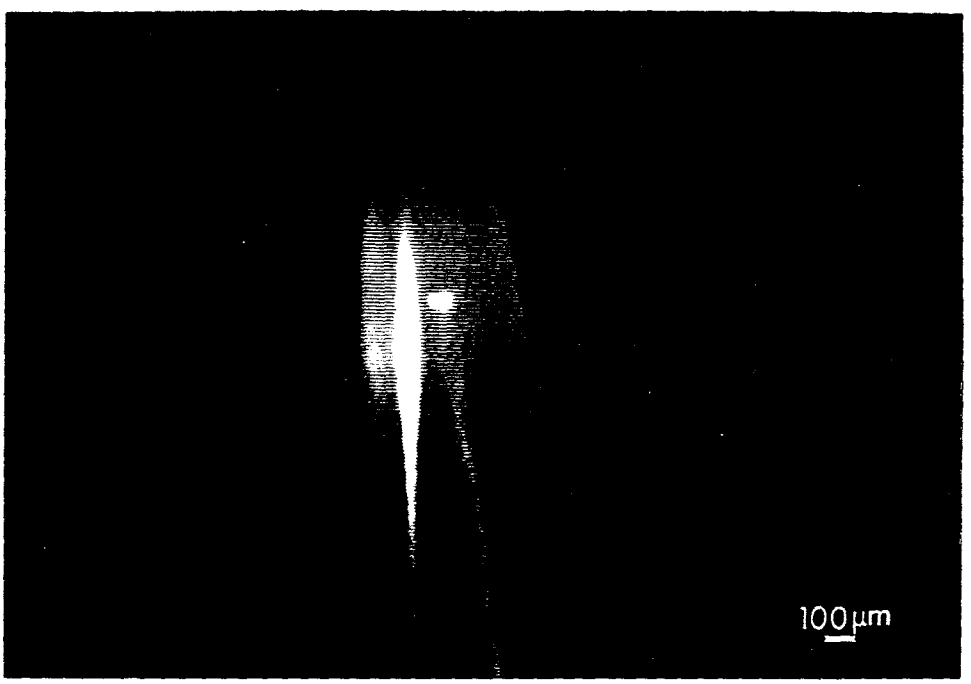

Fig. 4.7a Ignition of the pyrite particle by a single laser pulse

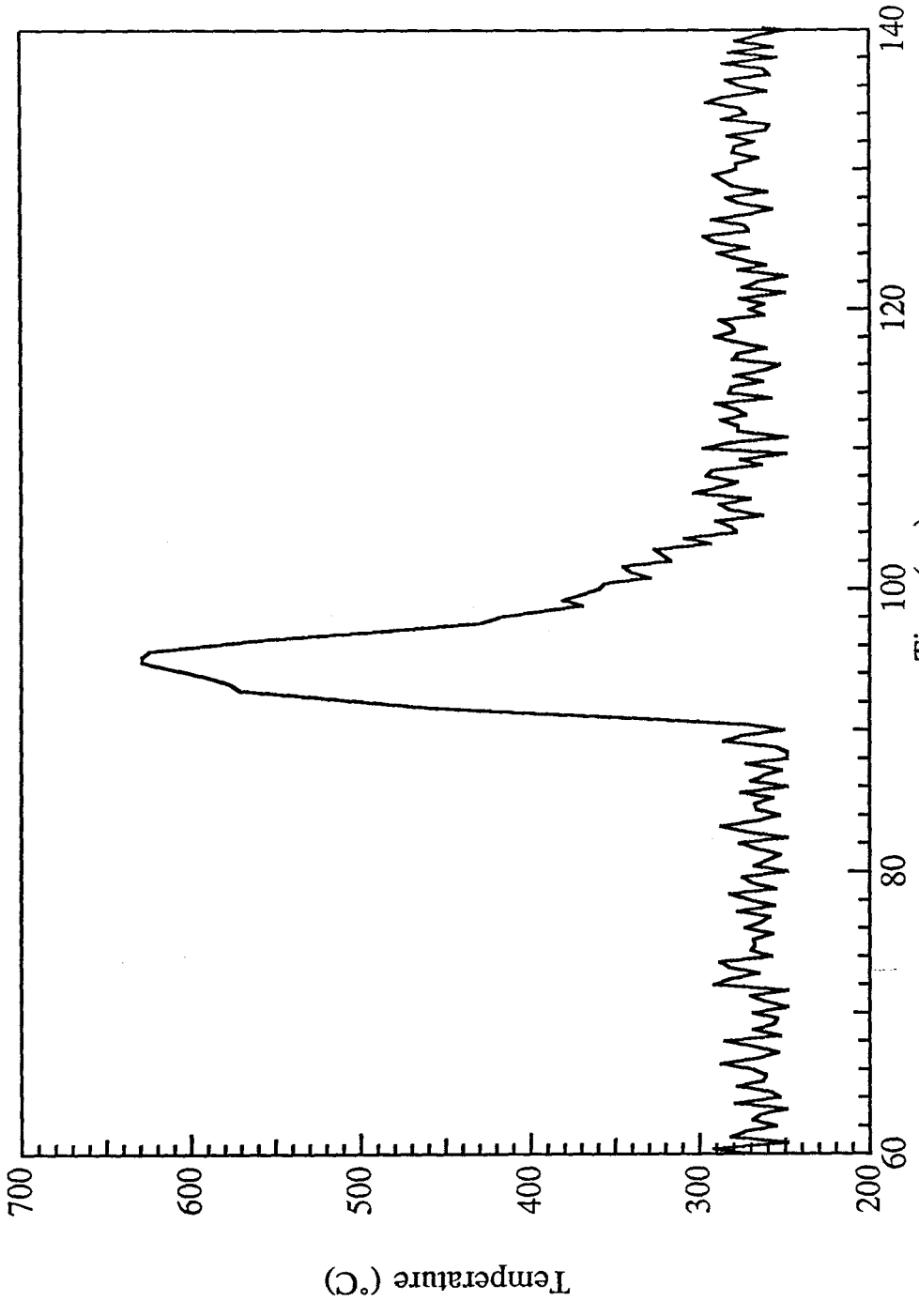

Fig. 4.7b Temperature history of the pyrite particle during the laser pulse

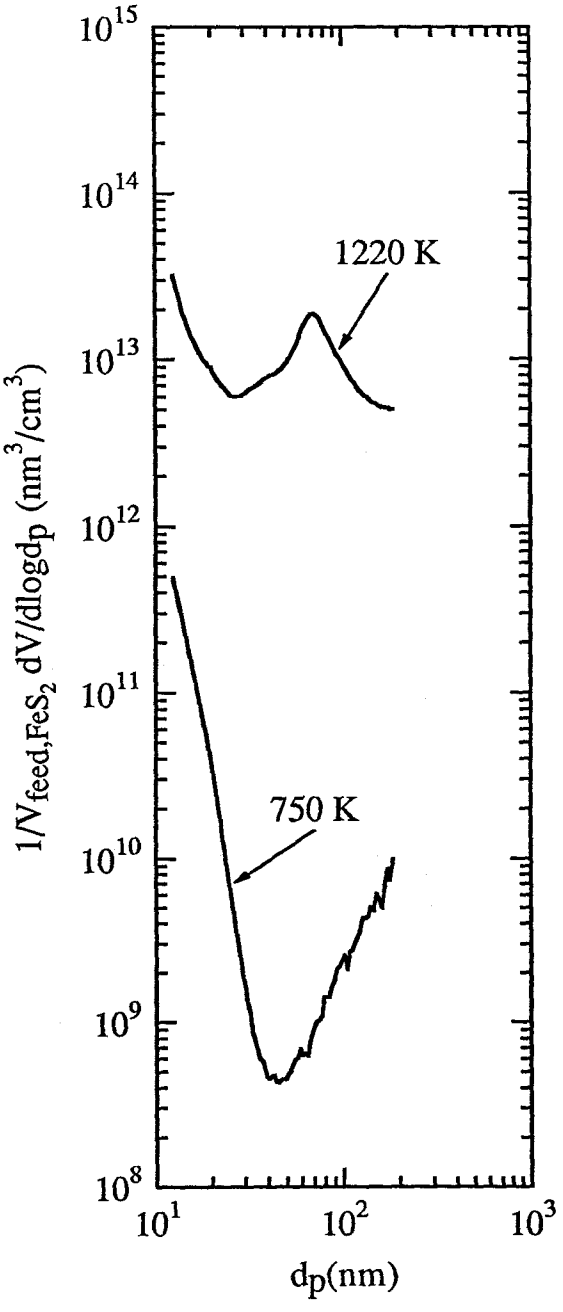

Fig. 4.8 Normalized particle volume distribution of the fume generated by reaction of natural pyrite in air

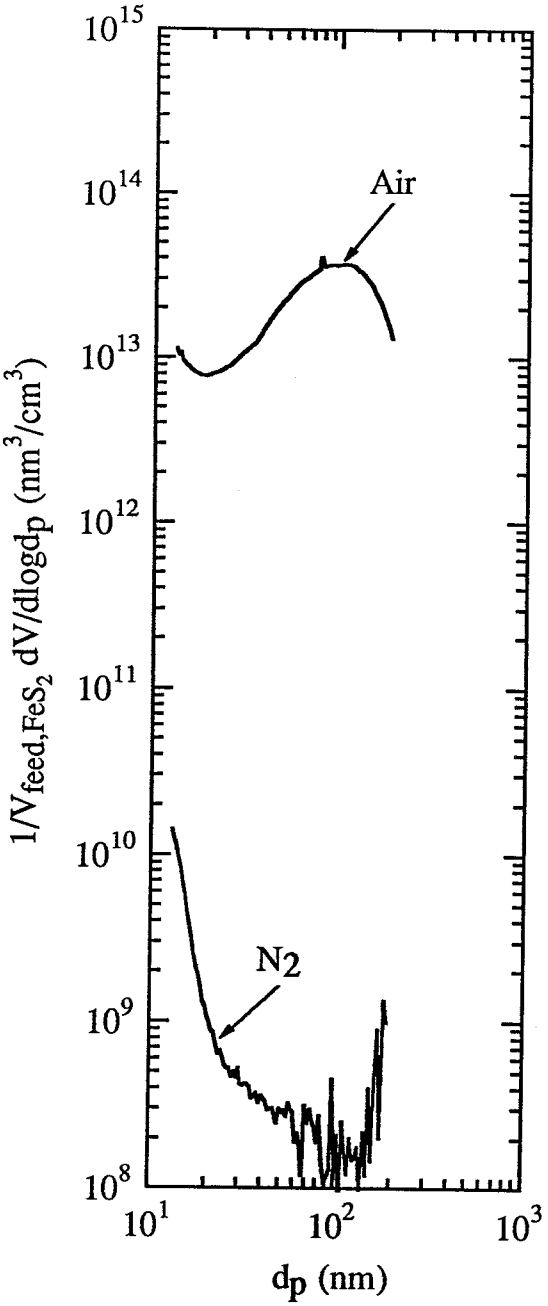

Fig. 4.9 Normalized particle volume distribution of the fume generated by reaction of synthetic pyrite at 873 K

(a)

50nm

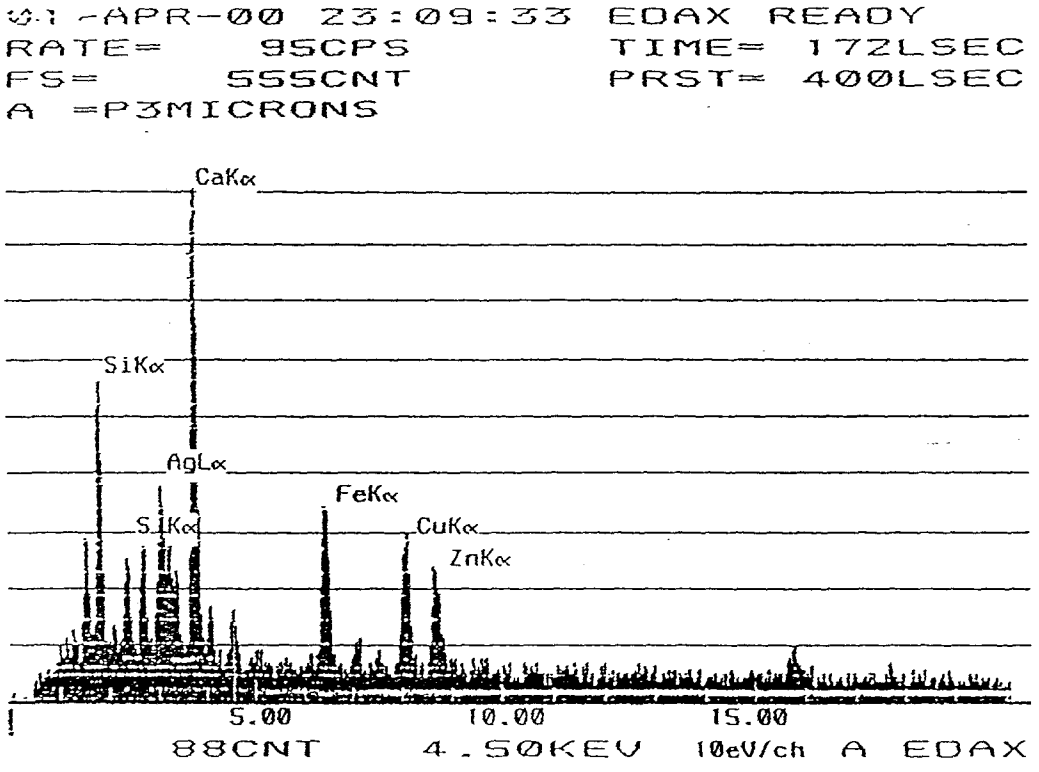

(b)

Fig. 4.10 Fume produced during reaction of natural pyrite in air at 1220K (a) Micrograph; (b) EDX spectrum of the low density material within the circle

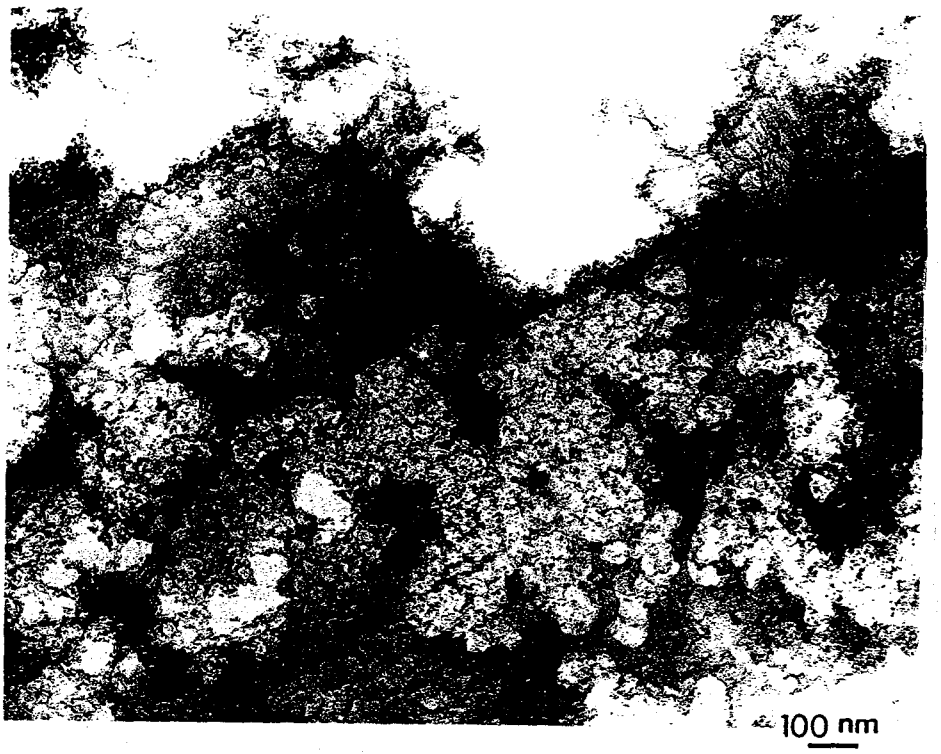

Fig. 4.11 Agglomerate particles produced during reaction of synthetic pyrite in N_2 at 1420K

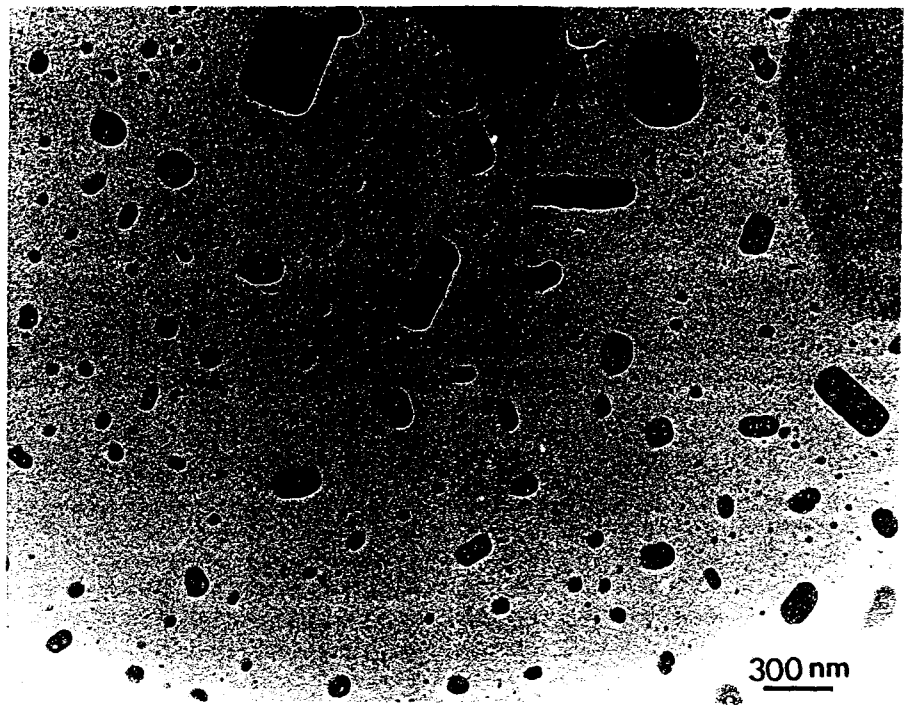

Fig. 4.12 Sulfur crystals produced by reaction of synthetic pyrite in air at 873K

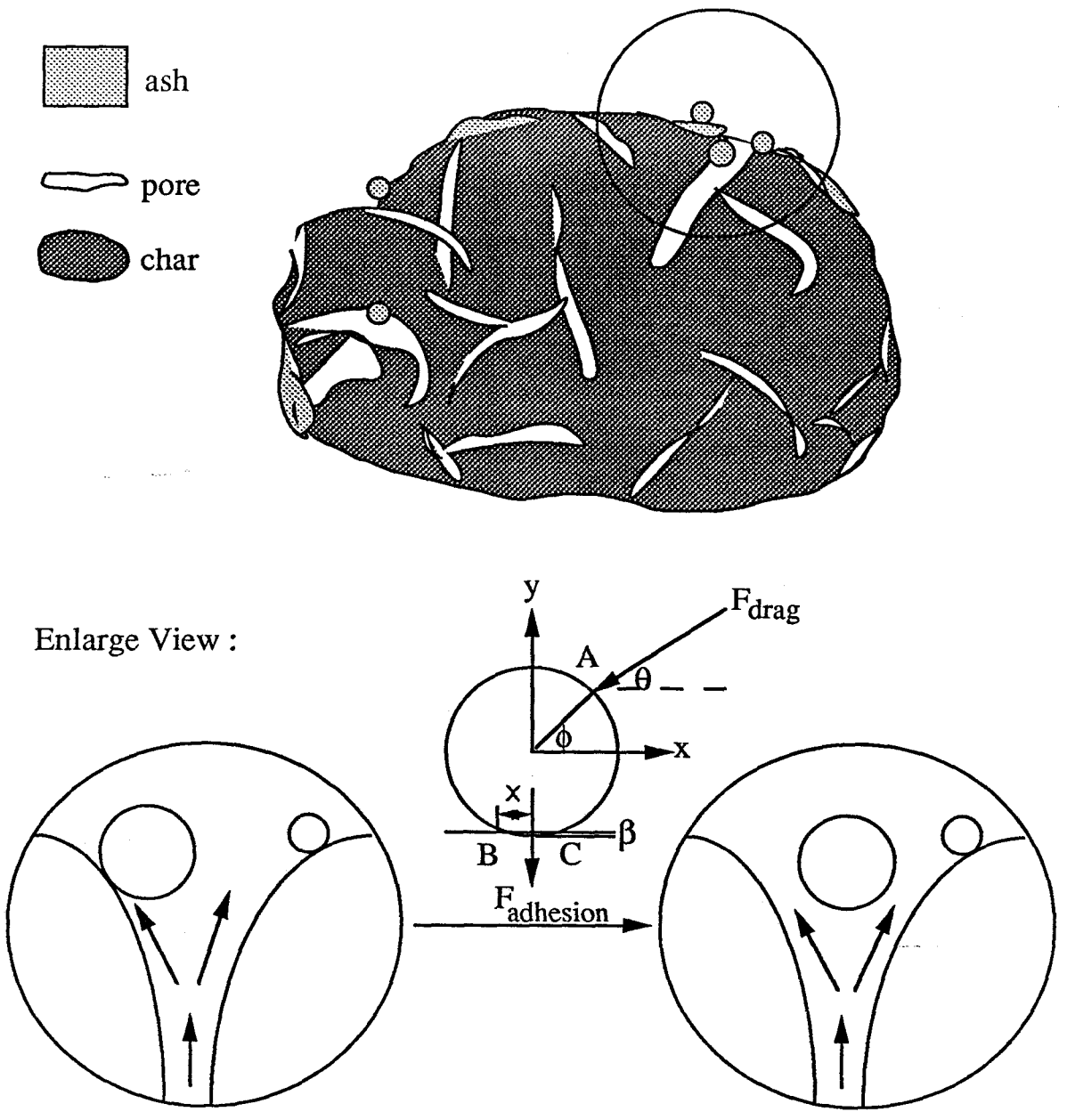

Fig. 4.13 The removal of an ash particle by drag force

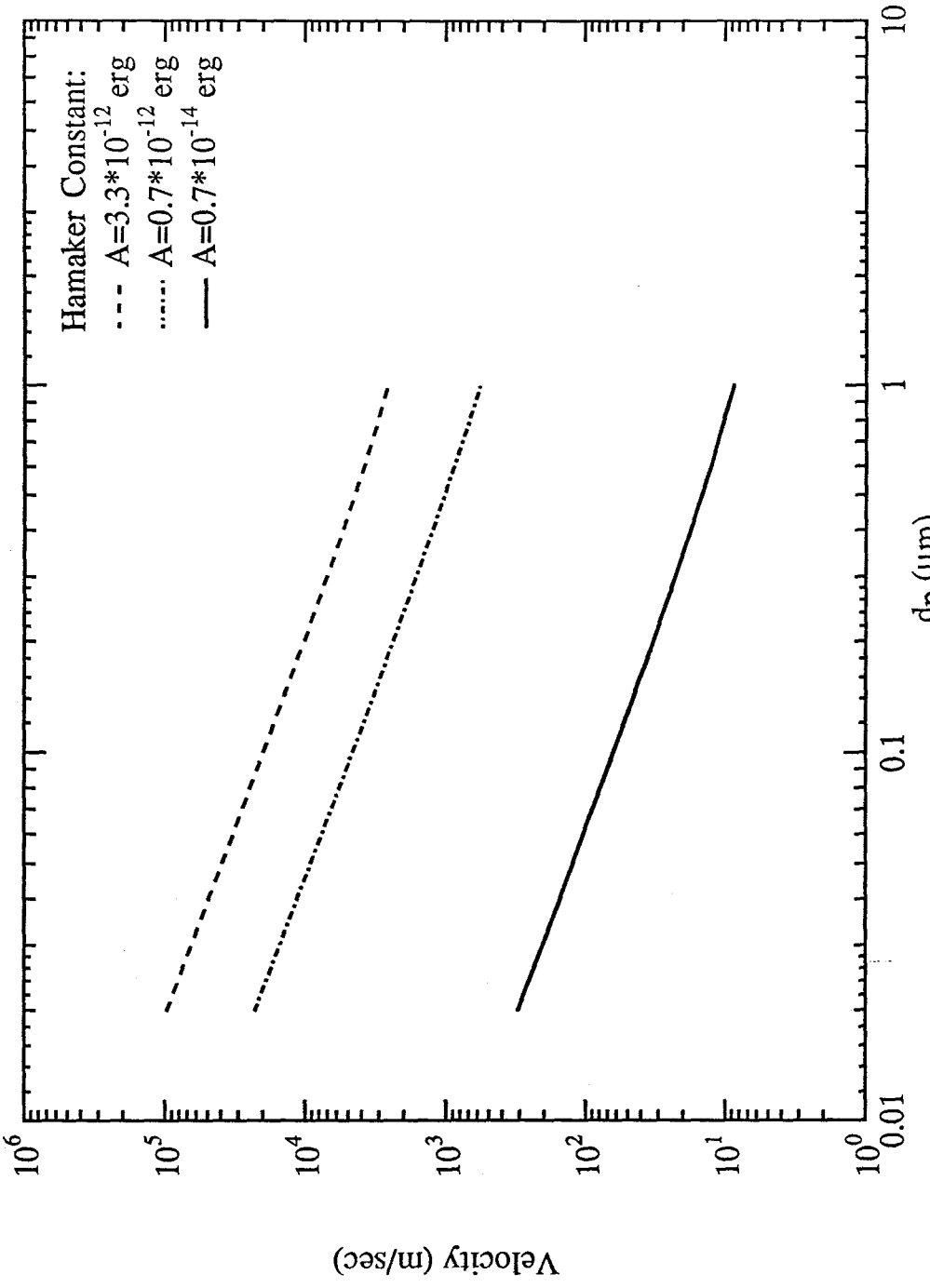

Fig. 4.14 Velocity calculated by drag force and surface energy (dp=100 μm)

CHAPTER 5

CONCLUSIONS AND RECOMMENDATIONS

5.1 Conclusions

The challenge of understanding coal combustion is attributable to the complex and variable chemical composition and physical structure of coal, the heterogeneous nature of the reactions, and the high temperature of the combustion process. Of more than 1200 coals categorized by petrographers at the Bituminous Coal Research Institute, no two coals were found to have the same elemental composition. Coal combustion involves gas-solid reactions and is, therefore, heavily influenced by mass and heat transfer. High temperature complicates the experimental apparatus, the measurements, and the sample collection.

Char oxidation and ash formation have been addressed in numerous papers. The novel contributions of the present work are: (1) focusing on the structural changes occurring on the short time scale of pulverized coal combustion, and on the effects of these changes on char reactivity; (2) carrying out experiments with the coal rather than char; (4) exploring the mechanism of ash particle formation both experimentally and theoretically. Many studies of char oxidation separate the char production from the combustion phases. Char is produced by pyrolysis of coal in an inert atmosphere. The generated char is later burned under controlled conditions in separate experiments. How the thermal history of char formation alters the char properties before significant oxidation begins has not been addressed. In the present study, coal was injected into the furnace. Coal pyrolysis and oxidation take place in a single reactor under an oxidizing atmosphere. In addition to more closely approximate the practical combustion environment, this experimental approach eliminates the time consuming char production and classification processes.

Coal particles undergo a series of structural changes when they are heated in a neutral or oxidizing atmosphere. Hollow spheres are formed, followed by particle

fragmentation. In 1 or 5% oxygen, oxidation proceeds both externally and internally at approximately constant diameter until the onset of fragmentation. For all of the chars, the surface area and the pore volume in the size range 15 to 120 Å increase dramatically within the first 100 ms. The ratio of carbon to hydrogen increases with residence time. Carbon conversion at 1600K also increases with increasing oxygen levels. But the char reactivity measured in the low temperature TGA experiments is decreased. Significant structural reorganization occurs either simultaneously with devolatilization or continuously after devolatilization, depending on the oxygen concentration. Oxygen appears to accelerate the structural changes and to change the reactivity of the char. The experimental results indicate a strong relation between char properties and experimental conditions. This relation could have important implications for the modeling of coal combustion and for combustion design and operation.

An experimental investigation of the reactions of pyrite has been undertaken to seek the sources of iron-rich fume in coal combustion with particular emphasis on the formation mechanism of iron-rich particles as postulated by Baxter and Mitchell. A fume was formed in low temperature reactions, but it contained virtually no iron. The primary constituents of the fume were impurities derived from the starting mineral and sulfur. When pyrite was oxidized in air at temperature below 1220K, or pyrolyzed in nitrogen at temperatures up to 1420K, a sulfur rich fume was generated. There was no direct evidence for the formation of an iron-rich fume during pyrolysis or oxidation of pyrite particles.

The ability of aerodynamic and centrifugal forces to remove particles held on a surface by van der Waals force has been examined. The velocities required to entrain submicron particles are too large for this mechanism to produce significant quantities of fine particles directly. However, fragments of order 1 to 10 μm in size or larger might be

released.

5.2 Recommendations for Future Experiments

In char oxidation experiments, the elemental analysis of various chars indicates variation in C/H ratio with experimental conditions. Further chemical structure analysis may need to be conducted in order to explain this variation. With gas chromatography-mass spectrometry combinations (GC-MS), complex mixtures of organic compounds can be separated, identified, and quantitatively measured. Infrared spectroscopy could give the very valuable information about the constitution of organic materials. Nuclear magnetic resonance (NMR) spectroscopy has been applied in coal research from basic studies of coal structure to compositional analyses of coal-conversion products. The study of chemical structural change may also shed light on the origins of physical structural changes, such as, surface area, pore size, with experimental conditions.

Previous coal combustion studies have shown substantial evidence for iron volatilization, but recent pyrite studies suggest that a mechanical mechanism may be responsible for the production of fine, iron-rich ash particles in coal combustion. The experimental evidence on which arguments for a mechanical mechanism for fine iron particle formation are based is the apparent loss of iron during coal combustion. Our attempts to measure such iron loss during reactions of pyrite alone revealed fine particle formation, but the fine particles contained no iron. If the physical release mechanism hypothesized by Baxter and Mitchell are real, the carbon reactions must play a role. Definitive experiments are needed to resolve this question. The particle size distribution, physical structures, and chemical composition of both coal and minerals may provide important insights into the observed iron loss. Synthetic char studies may simplify identification of the mechanisms involved.

APPENDIX A

INSTRUCTION FOR SURFACE AREA MEASUREMENT

A1 Introduction

The apparatus in Keck Lab, Room 218 was originally set up by Northrop (1988). Some modification has been made. It is used to measure gas adsorption isotherms by continuous addition of adsorbate gas to the sample. The surface area of the sample is obtained by interpreting the experimental data based on Brunauer-Emmett-Teller (BET) theory.

A2 Principles

A2.1 Gas Adsorption Isotherms by Continuous Adsorbate Addition

The system containing the sample is outgassed under vacuum. The adsorbate with a steady, known mass flow rate is continuously introduced to the system. The pressure is monitored by a microcomputer data acquisition system. The amount of gas adsorbed is simply the difference between the amount of gas introduced and the amount occupying the "dead volume".

$$n_{ad} = \int_0^t Q(t)\,dt - \frac{P(t)}{R}\int_0^{V_T}\frac{1}{T}\,dV \qquad \text{(A.1)}$$

where Q is the molar flow rate of gas, t is the time, P is the pressure, R is the gas constant, and V_T is the dead volume of system including sample holder. Both Q and P are the functions of time.

A2.2 Data Inversion

The BET theory is based on the assumptions of a homogeneous surface and no

adsorbate-adsorbate interaction. The adsorption at one site does not affect adsorption at neighboring sites (Daniels and Alberty, 1966). Since in physical adsorption molecules of vapor may be adsorbed to the depth of many monolayers, the theory further assumes that molecules can be adsorbed in second, third, ..., and nth layers with the surface area available for the nth layer equal to the coverage of the (n-1)th layer. The BET equation is

$$\frac{P}{v_{ad}(P_0-P)} = \frac{1}{v_m c} + \frac{(c-1)P}{v_m c P_0} \qquad \text{(A.2)}$$

where v_m is the volume of gas adsorbed when the entire adsorbent surface is covered with a complete unimolecular layer. The volume of gas adsorbed is represented by v_{ad}, and c is a constant at a given temperature. v_m and v_{ad} in Eq. A.2 can be replaced by n_m and n_{ad}, where n_m is the number of moles of gas adsorbed when the entire adsorbent surface is covered with a complete unimolecular layer.

The surface area of the solid material is estimated from the density of the liquefied adsorbate by assuming that the surface area is occupied by a single molecule of adsorbate on the surface, that the adsorbate molecules are spherical and that they are close packed in the liquid. The area occupied by a nitrogen molecule at -195° is estimated to be 16.2 Å. Therefore the total surface area of the sample is

$$S_T(m^2) = 6.022\times10^{23}\,\frac{molecule}{mole} \times 16.2\,\frac{\mathring{A}^2}{molecule} \times (10^{-10}\frac{m}{\mathring{A}})^2 \times n_m(mole) \qquad \text{(A.3)}$$

A3 Description of Operation

A schematic of the apparatus is shown in Fig. A.1. The sample is outgassed successively by a mechanical pump to 10^{-3}~10^{-2} torr and then isolated from the vacuum system. A small Dewar flask containing liquid nitrogen is placed around the sample tube.

The level of liquid nitrogen in the Dewar is maintained constant by periodically replenishing the liquid lost by evaporation. The adsorbate (high-purity nitrogen) passes through a filter to remove any dust particles and then flows through the orifice of 5 microns in diameter. The pressure of nitrogen cylinder is around 10 psi. During the period when the sample is cooling to liquid nitrogen temperature, nitrogen flows through the orifice and exits through the vacuum line. At the start of the run, the valve to vacuum is closed, the valve to the sample is opened, and data acquisition is initiated. The reason that nitrogen flows through the system before the sample measurement, is to eliminate the significant change of system pressure due to suddenly opening the valve. When the adsorption measurements are complete, the system is re-evacuated. The dead volume of the system, including the sample tube, is obtained by filling it with helium. The pressure is measured, then the valve to the calibration volume is opened. The pressure after expansion is recorded. This procedure is repeated twice. The dead volume is calculated by the ideal gas relation.

A4 Experimental Procedure

A4.1 System Setup

A4.1.1 Vacuum System

1. Close the valves to *Setra* gauge and to the sample holder, and open all the other valves. Turn on the pump and *Pirani* vacuum gauge. The vacuum starts to increase after a short time for a good vacuum system.
2. Place the big Dewar flask containing liquid nitrogen around the trap.

A4.1.2 Sample Preparation

1. Write the sample, number of the run, date, and sample filename on the data sheet (see **BET DATA SHEET**).
2. Make sure the sample holder is clean. Record the weight of the sample on the data sheet.
3. Grease the joint to the sample holder. Secure the holder in place in apparatus with the metal springs.
4. Open the valve to the sample holder **VERY SLOWLY** to outgas sample. (Watching the vacuum change may help to know how slow it should be.) After the valve is fully opened (about four half runs), evacuate the sample for couple of hours.
5. Close the valve to the calibration volume. Heat the sample to 50-140°C for a while in order to remove moisture.
6. Remove the heater. Ensure the sample is cool. Place the small Dewar flask containing liquid nitrogen around the sample. Close the valve to the sample.
   ALWAYS MAINTAIN LEVEL OF LIQUID N_2 IN SAMPLE DEWAR.

A4.1.3 Data Acquisition System

1. Put **DOS** disk in drive A. Turn on the computer. Set the correct date and time. Remove **DOS** disk from drive A.
2. Put **BET** disk in drive A and **DATA** disk in drive B.
3. Type **basica <CR>, <F3>**
   Show: **LOAD"** Type: **scan1 <CR>**
   OK

A4.2 Experimental Measurements

1. Turn on nitrogen and helium cylinders which are by the west wall (Regulators should be already adjusted. P_{N_2} ~ 10 psi, and P_{He} ~ 15 psi). Open the valve in front of the filter to nitrogen.
2. Switch the 3-way valve to nitrogen. Open the valve to the *Setra* gauge.

A4.2.1 Calibration

1. Hit **<F2>**.

   Show: **RUN**

   A/D Gain ? Type: **2 <CR>**

   Filename ? **pres <CR>**

   Scan Rate ? **5 (DO NOT PRESS <CR> NOW)**

2. Wait for the reading of *Setra* gauge reaching steady. Hit **<CR>** and Close the valve to the trap.
3. Hit **<F2>** to stop the data acquisition when the pressure of *Setra* gauge reaches **100** mbar. Open the valve to the trap to re-evacuate the system.

   Show: **Filename ?** Type: **b:cal1.dat <CR>**

   Mode ? **d <CR>**

   OK

4. Repeat steps 1 to 3. Give the new **Filename** as **b:cal2.dat.**
5. Repeat steps 1 to 3. But hit **<F2>** when the pressure reaches **300** mbar in order to obtain a measurement of adsorbate mass flow rate within the whole range. Give the new **Filename** as **b:f#.dat.**
6. Record the temperature during the calibrations on the data sheet.

A4.2.2 Sample Measurement

1. Repeat steps 1 and 2 in **4.2.1. AND OPEN THE VALVE TO THE SAMPLE HOLDER.** Hit **<F2>** when the pressure reaches **300** mbar. Give the new **Filename** as **b:filename. ALWAYS MAINTAIN LEVEL OF LIQUID N_2 IN SAMPLE DEWAR.**
2. Record the initial and final temperatures on the data sheet.

A4.2.3 Back to Calibration:

1. Close the valve to the sample holder. Repeat step 4 in **4.2.1.** Give the new **Filename** as **b:cal4.dat <CR>.**

A4.2.4 Dead Volume

1. Close the 3-way valve and the valve to *Setra* gauge. Open the valve to the sample holder **VERY SLOWLY.** Open the valve to the trap **VERY SLOWLY** to evacuate the sample completely, then close it. Open the valves to the calibration volume and to *Setra* gauge. Record the pressure on the data sheet as P_0.
2. Close the valve to the calibration volume. Switch 3-way valve to helium and close it. Record the pressure, P_1, on the data sheet.
3. Open the valve to the calibration volume. Record the new pressure, P_2, on the data sheet.
4. Repeat steps 2 and 3 twice. Using P_2 as P_0 for the next run.
5. Turn off nitrogen and helium cylinders.

A4.3 Data Inversion

1. Create a calibration data file from the file "**f#.dat**".

   Hit **<F3>**

Show:		Type:
	LOAD"	**chop <CR>**
	OK	**<F2>**
	RUN"	
	Input File ?	**b:f#.dat <CR>**
	Output File ?	**b:cal3.dat <CR>**
	Lowest X value ?	**0 <CR>**
	Highest X value ?	**100 <CR>**
	OK	

2. Calculate the mass flow rate of adsorbate.

   Hit **<F3>**

Show:		Type:
	LOAD"	**inflo <CR>**
	OK	**<F2>**
	RUN"	
	Gain ?	**2 <CR>**
	Input File ?	**b:f#.dat <CR>**
	Output File ?	**b:q#.dat <CR>**
	Temp. during Cal.?	the value of T (K) **<CR>**
	OK	

3. Differentiate the calibration data.

   Hit **<F3>**

Show:		Type:
	LOAD"	**poly2 <CR>**
	OK	**<F2>**
	RUN"	

Input File ?	**b:cal1.dat <CR>**
Order ?	**1 <CR>**
OK	

4. Record the second coefficient as **S1** on the data sheet.
5. Repeat steps 3 (from <F2>) to 4 to differentiate the files, **cal2.dat, cal3.dat**, and **cal4.dat**. Record the second coefficient as **S2** to **S4** on the data sheet. Hit **<F2>**.

   Show: RUN"

Input File ?	**b:q#.dat <CR>**
Order ?	**2 <CR>**
OK	

6. Record the three coefficients as **coef(1)** to **coef(3)** on the data sheet.
7. Create the data files, **iso#.dat, bet#.dat**, and **pore.dat**.

   Hit **<F3>**

Show:	LOAD"	Type: **inst <CR>**
	OK	**<F2>**
	RUN"	
	Gain ?	**2 <CR>**
	Input File ?	the sample filename **<CR>**
	Run Number ?	the number given to the measurement **<CR>**
	Initial Temp. ?	the value of initial T (K) **<CR>**
	Final Temp. ?	the value of final T (K) **<CR>**
	Effective Volume ?	the value V_{eff} on the data sheet **<CR>**
	Vapor Pressure ?	**750 <CR>**
	coef(1) ?	the value of F_c×coef(1) on the data sheet **<CR>**
	coef(2) ?	the value of F_c×coef(2) on the data sheet **<CR>**
	coef(3) ?	the value of F_c×coef(3) on the data sheet **<CR>**
	coef(4) ?	**0 <CR>**

coef(5) ? **0 <CR>**

coef(6) ? **0 <CR>**

Plot isothermal ? **y <CR>**

(run, plot, exit) ? **e <CR>**

OK

8. Calculate the BET surface area of the sample.

   Hit **<F3>**

   Show: LOAD" Type: **mono <CR>**

   OK **<F2>**

   RUN"

   Input File ? **b:bet#.dat <CR>**

9. Record the first value of the three under two coefficients on the screen.

A5 System Calibration

Whenever the system is reconnected, recalibration is necessary to be conducted. The procedure is as following:

1. Measure the volume with the same method of the "dead volume" measurement (see **4.2.4 Dead Volume**) except closing the valve to the sample holder. Repeat the measurements three times to get the average value (The last number obtained is 31.52 ml.). If the system is reconnected between the 3-way valve to the orifice, the volume between them needs to be estimated (The last value is 0.6 ml.). The old value of the sum of these two volumes needs to be replaced, which is on line 430 of the program "**INFLO.BAS**", and on line 710 of "**INST.BAS**" .
2. Do the whole measurement with an **EMPTY** sample tube. The surface area from the **bet#.dat** file should be very close to zero.

3. Use the known surface area material, γ-alumia, to recalibrate system (The last average result is 170 ± 0.2 m^2 gm^{-1}).

A6 Troubleshooting

A6.1 The system can not get vacuum.

1. If the pump runs quiet, turn off the *Pirani* gauge, then turn on again to ensure the gauge works properly.
2. Check the pump oil level. Change the oil if it is too dirty.
3. Check all connections.

A6.2 The surface area data is not reasonable.

1. Re-evacuate the sample overnight and heat it for a longer time or at a higher temperature, depending on the material, to ensure the sample has been outgassed properly.
2. Check the programs to ensure the volume value is correct.
3. Check the mass flow rate of adsorbate by reading the data from the file of "**q#.dat**", using the program "**READAT.BAS**". The data of second column should be ≤ 1.0. Check the pressure of nitrogen cylinder (P ≤ 10 psi) and the diameter of orifice (5 μm) if the data are much great than 1.0.

REFERENCES

Daniels, F. and Alberty, R. A., *Physical Chemistry*, 3rd Edition, 1966.

Northrop, P. S. (1988), *A Fundamental Study of Char Combustion: Changes in Particle Morphology during Oxidation*, Ph. D. Thesis, California Institute of Technology.

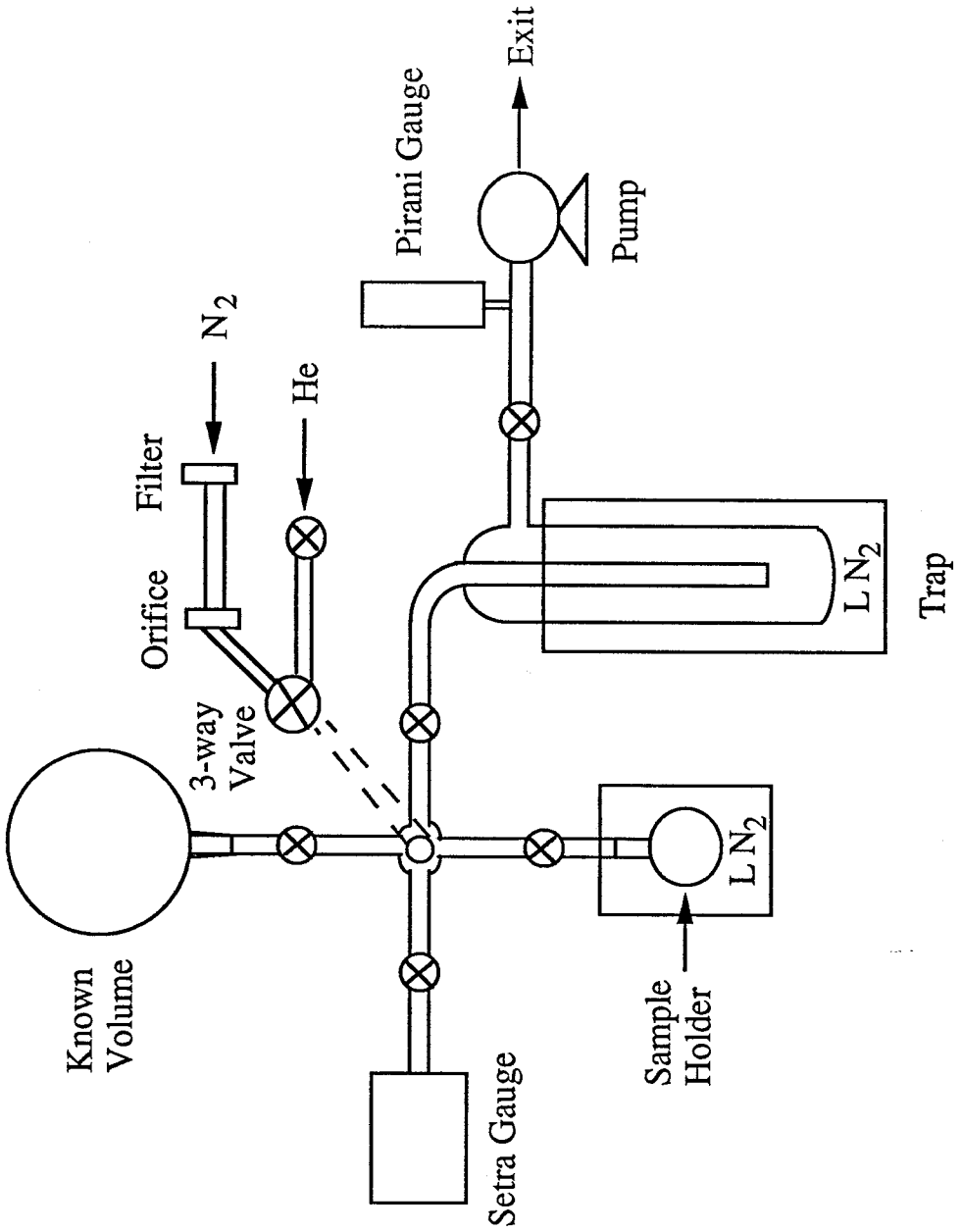

Fig. A.1 Schematic of BET system

BET DATA SHEET

Run Number: **Date:**

Sample:

Sample Filename:

Sample Weight:

Temperature during Calibration (K):

Temp. at beginning of Sample Measurement (K):

Temp. after Sample Measurement (K):

Calibration of Dead Volume:

P_0 (mbar)	P_1 (mbar)	P_2 (mbar)	$V=(\frac{P_2-P_0}{P_1-P_2} \times 271.2)$ (ml)

$$V_{eff.} = V + 0.6 =$$

Calibrated Parameters:

Cal1.dat: **S1 =**

Cal2.dat: **S2 =**

Cal3.dat: **S3 =**

Cal4.dat: **S4 =**

$$F_c = \frac{S1+S2+S3}{3 \times S4} =$$

Q#.dat: **coefficient(1) =** $F_c \times coef(1) =$

coefficient(2) = $F_c \times coef(2) =$

coefficient(3) = $F_c \times coef(3) =$

BET PROGRAMS

```
10   CLEAR, 32768!
20'*************************************************************************
30'*
40'*      SLOW REAL TIME PLOTTING AND LOGGING PROGRAM
50'* by RANAJIT SAHU  and  P.SCOTT NORTHROP              2/20/86
60'*************************************************************************
70   '
80   ' CALL NAME:     SCAN1.BAS
90   '
100  '   This program  allows the user to display a selected channel of the
110  'DT2801-A I/O  board and store the data on disk.
120  '
130  '
150  N = 6 * 60 * 5          'size of storage array :
160                          '1 sample /10 sec during 5 hours
170  '
180 GAIN(0)=1
190 GAIN(1)=2
200 GAIN(2)=4
210 GAIN(3)=8
220 INPUT "A/D GAIN (TYPE 0,1,2 OR 3)";ADGAIN
230 IF ADGAIN < 0 THEN GOTO 220
240 IF ADGAIN > 3 THEN GOTO 220
250  '
260 ADSCHANNEL=0
270 ADECHANNEL=7
280 NCONVERSIONS#=8
290  KEY OFF
300  TRUE = 1:FALSE = 0
310  CLS:SCREEN 0,0,0
320  PRINT "---------------------- REAL TIME ANALOG I/O PLOT ----------------------
--330  LOCATE 5,1
340  INPUT "ENTER SCREEN DISPLAY FILE AS [dsk:] filename (no extension) .
";FILX$
350  IF FILX$ = "" THEN 310
360  LOCATE 8,1
370  DIM C%(1)
552  C%(0)=TRUE
560  LOCATE 20,1:PRINT SPACE$(78);:LOCATE 20,1
570  INPUT "ENTER SCAN RATE IN SECONDS [1 to 3600] . ";SCANRATE%
580  IF SCANRATE% < 1 OR SCANRATE% > 3600 THEN 560
590  '
600  'Setup the display and load the display program and scale parameters.
610  '
620  DEF SEG = &H2000
630  OPEN "I",#1,"get.ADR":INPUT #1,BASADD%:CLOSE #1 'boards base address
640  '
650  'Load the screen display and set the parameters for data scaling
660  '
```

```
670  CLS:SCREEN 2
680  DEF SEG = &HB800                    'graphics display segment
690  BLOAD FILX$+".SCN"                   '.SCN is the screen display
700  DEF SEG
710  OPEN FILX$+".PAR" AS #1 LEN=30       'parameter file for .SCN
720  FIELD #1,15 AS PARX$, 15 AS PARY$    'single prescion fields
730  GET #1,1
740  SX = CVS(PARX$):SY = CVS(PARY$)      'scale factors
750  GET #1,2
760  DX = CVS(PARX$):DY = CVS(PARY$)      'slope variables for axis
770  GET #1,3
780  X2 = CVS(PARX$):Y2 = CVS(PARY$)      'X,Y maximum values on graph
790  GET #1,4
800  X1 = CVS(PARX$):Y1 = CVS(PARY$)      'X,Y minimum values on graph
810  GET #1,5
820  QX = CVS(PARX$):QY = CVS(PARY$)      'X,Y screen scale factor
830  GET #1,6
840  OX = CVS(PARX$):OY = CVS(PARY$)      'graph starting point
850  GET #1,7
860  XA = CVS(PARX$):YA = CVS(PARY$)      'data positional scale factors
870  GET #1,8
880  XE = CVS(PARX$):YE = CVS(PARY$)      'scale x,y resolution
890  CLOSE #1
900  '
910  '
920  '   This is the section where the data is scanned and plotted for each
930  'channel.  The display  sets a different  graphic character  for  each
940  'channel. This is added to the screen on line 23.
950  '
960  '
970  DIM OUT0%(N) , TIME%(N) , ADH%(8), ADL%(8)
990  STIME$ = TIME$:SDATE$ = DATE$        'start time/date
1000  LOCATE 23,10:PRINT "START TIME IS  ";STIME$;"    START DATE IS
";SDATE$;
1010  LOCATE 25,1:PRINT SPACE$(78);:LOCATE 25,1
1020  PRINT "F1 = SAVE SCREEN      F2 = END";
1030  ON KEY(1) GOSUB 1420
1040  ON KEY(2) GOSUB 1800
1050  KEY(1) ON:KEY(2) ON
1060  '
1070  'one second delay loop
1080  '
1090  DEF SEG = SG
1100  XAXIS =0
1110 GOTO 1180
1120 'Start loop :
1130  FOR SECDLY% = 1 TO SCANRATE%
1140  TEMT$=RIGHT$(TIME$,2)
1150  IF RIGHT$(TIME$,2)=TEMT$ THEN GOTO 1150
```

```
1160  NEXT SECDLY%
1170  '
1180  DEF SEG = &H2000
1190  GOSUB 3570
1220   PS = 1
1230   X = XA + SX * XAXIS *SCANRATE%
1240   Y = YA - SY * (ADL%(1)+ADH%(1)*256)
1250   IF X < 9 OR Y < 9 THEN PS = 0
1260   IF X > 271 OR Y > 151 THEN PS = 0
1270   IF PS = 0 THEN 1300
1280   CIRCLE (QX*X+OX,QY*Y+OY),I
1300  XAXIS = XAXIS + 1
1310  IF XAXIS = 32766 THEN GOTO 1800
1320  TIME%(XAXIS) = (XAXIS - 1) * SCANRATE%
1330  OUT0%(XAXIS) = ADL%(1)+ADH%(1)*256
1410  GOTO 1130
1420  LOCATE 25,1:PRINT SPACE$(78);:LOCATE 25,1
1430  INPUT ;"ENTER SCREEN NAME AS [dsk:] filename (no extension) -- ";SFLX$
1440  OPEN SFLX$+".PAR" AS #1 LEN=30
1450  FIELD #1,15 AS PARX$,15 AS PARY$
1460  FOR XX% = 1 TO 14:LSET PARX$ ="XXX":LSET PARY$ ="YYY":PUT
#1,XX%:NEXT XX%:CLOSE #1
1470  OPEN SFLX$+".PAR" AS #1 LEN=30
1480  FIELD #1,15 AS PARX$,15 AS PARY$
1490  LSET PARX$ = MKS$(SX)
1500  LSET PARY$ = MKS$(SY)
1510  PUT #1,1
1520  LSET PARX$ = MKS$(DX)
1530  LSET PARY$ = MKS$(DY)
1540  PUT #1,2
1550  LSET PARX$ = MKS$(X2)
1560  LSET PARY$ = MKS$(Y2)
1570  PUT #1,3
1580  LSET PARX$ = MKS$(X1)
1590  LSET PARY$ = MKS$(X2)
1600  PUT #1,4
1610  LSET PARX$ = MKS$(QX)
1620  LSET PARY$ = MKS$(QY)
1630  PUT #1,5
1640  LSET PARX$ = MKS$(OX)
1650  PUT #1,6
1660  LSET PARX$ = MKS$(XA)
1670  LSET PARY$ = MKS$(YA)
1680  PUT #1,7
1690  XE = 1/ABS(X2-X1):LSET PARX$ = MKS$(XE)
1700  XE = 1/ABS(Y2-Y1):LSET PARY$ = MKS$(YE)
1710  PUT #1,8
1720  CLOSE #1
1730  LOCATE 25,1:PRINT SPACE$(78);:LOCATE 25,1
```

```
1740  DEF SEG = &HB800                    'screen buffer
1750  BSAVE SFLX$+".SCN",0,&H4000         '16 k buffer
1760  DEF SEG
1770  PRINT "FILE ";SFLX$;"  SAVED   STRIKE ANY KEY TO
CONTINUE";:LOCATE 20,1
1780  KX$ = INKEY$:IF KX$ = "" THEN 1780
1790  RETURN 1800
1800  LOCATE 25,1:PRINT SPACE$(78);:LOCATE 25,1
1810  PRINT "      TERMINATED AT  ";TIME$;"    ON  ";DATE$;:LOCATE 23,1
1820  KEY(1) OFF:KEY(2) OFF
1830  CLS:SCREEN 0,0,0
1870  LOCATE 3,1
1880  INPUT "Enter name of storage data file [dsk:]filename.dat";FILDAT0$
1890  OPEN FILDAT0$ AS #1 LEN = 30
1900  FIELD #1, 15 AS X$, 15 AS Y$
1910  LOCATE 5,1
1920  INPUT "Line, Dot or No plot mode (L,D,N) ? ";A$
1930  IF A$="L" OR A$="l" THEN M=1:GOTO 1970
1940  IF A$="N" OR A$="n" THEN M=2:GOTO 1970
1950  IF A$="D" OR A$="d" THEN M=0:GOTO 1970
1960  LOCATE 11,1:PRINT"RE-ENTER":LOCATE 9,1:PRINT SPC(79):GOTO 1910
1970  CLS:LOCATE 12,24:PRINT"STORING DATA ON DISK"
1980  LSET X$ = MKS$(XAXIS):LSET Y$=MKS$(M)
1990  PUT #1,1
2000  FOR I=2 TO XAXIS+1
2010  LSET X$=MKS$(TIME%(I-1)):LSET Y$=MKS$(OUT0%(I-1))
2020  PUT #1,I
2030  NEXT I
2040  CLOSE #1
3550  CLS:LOCATE 12,28:PRINT"DONE":LOCATE 25,1
3560  END
3570   'READ A/D COMMAND
3580   '
3590   'THE A/D CONVERTER IS ASSUMED TO BE SET UP
3600   'FOR SE UNIPOLAR OPERATION
3610   '
3620   'THIS PROGRAM READS A BLOCK OF A/D CONVERSION
3630   '
3640   'THE CHANNELS USED AND THE NUMBER OF CONVERSIONS
3650   'DONE IS DETERMINED BY USER INPUT.
3660   '
3670   'DEFINE CONSTANTS
3680   '
3690   '
3710    BASE.ADDRESS    =&H2EC
3720    COMMAND.REGISTER    =BASE.ADDRESS+1
3730    STATUS.REGISTER     =BASE.ADDRESS+1
3740    DATA.REGISTER       =BASE.ADDRESS
3750    COMMAND.WAIT        =&H4
```

```
3760   WRITE.WAIT                =&H2
3770   READ.WAIT                 =&H5
3780  '
3790   CCLEAR                    =&H1
3800   CCLOCK                    =&H3
3810   CSAD                      =&HD
3820   CRAD                      =&HE
3830   CSTOP                     =&HF
3840    PERIOD#          =40000!
3850  '
3860   BASE.FACTOR#              =4096
3870   BASE.CHANNELS             =8
3875  GAIN(0)=1
3876  GAIN(1)=2
3877  GAIN(2)=4
3878  GAIN(3)=8
3880   NCONVERSIONS# = 8
3890  ' STOP AND CLEAR THE DT2801-A BOARD
3900   '
3910   OUT COMMAND.REGISTER, CSTOP
3920   TEMP = INP(DATA.REGISTER)
3930   WAIT STATUS.REGISTER, COMMAND.WAIT
3940   OUT COMMAND.REGISTER, CCLEAR
3950  '
3960  'SET CLOCK RATE
3970  '
3980   WAIT STATUS.REGISTER, COMMAND.WAIT
3990   OUT COMMAND.REGISTER, CCLOCK
4000  '
4010   PERIODH =INT(PERIOD#/256)
4020   PERIODL =PERIOD# - PERIODH*256
4030   WAIT STATUS.REGISTER, WRITE.WAIT, WRITE.WAIT
4040   OUT DATA.REGISTER, PERIODL
4050   WAIT STATUS.REGISTER, WRITE.WAIT, WRITE.WAIT
4060   OUT DATA.REGISTER, PERIODH
4080   WAIT STATUS.REGISTER, COMMAND.WAIT
4090   OUT COMMAND.REGISTER, CSAD
4100  '
4110   WAIT STATUS.REGISTER, WRITE.WAIT, WRITE.WAIT
4120   OUT DATA.REGISTER, ADGAIN
4130  '
4140  WAIT STATUS.REGISTER, WRITE.WAIT, WRITE.WAIT
4150   OUT DATA.REGISTER, ADSCHANNEL
4160  '
4170   WAIT STATUS.REGISTER, WRITE.WAIT, WRITE.WAIT
4180   OUT DATA.REGISTER, ADECHANNEL
4190  '
4200   NUMBERH = INT(NCONVERSIONS#/256)
4210   NUMBERL = NCONVERSIONS# - NUMBERH*256
```

```
4220   WAIT STATUS.REGISTER, WRITE.WAIT, WRITE.WAIT
4230   OUT DATA.REGISTER, NUMBERL
4240   WAIT STATUS.REGISTER, WRITE.WAIT, WRITE.WAIT
4250   OUT DATA.REGISTER, NUMBERH
4260   '
4270   WAIT STATUS.REGISTER, COMMAND.WAIT
4280   OUT COMMAND.REGISTER, CRAD
4290   '
4300   FOR LOOP = 1 TO NCONVERSIONS#
4310   WAIT STATUS.REGISTER, READ.WAIT
4320   ADL%(LOOP) = INP(DATA.REGISTER)
4330   WAIT STATUS.REGISTER, READ.WAIT
4340   ADH%(LOOP) = INP(DATA.REGISTER)
4350   NEXT LOOP
4360   '
4370   WAIT STATUS.REGISTER, COMMAND.WAIT
4380   STATUS = INP(STATUS.REGISTER)
4390   IF (STATUS AND &H80) THEN GOTO 4440
4400  RETURN
4435  RETURN
4440  ' Error.
4450  PRINT
4460  PRINT "error"
4470 RETURN
4480  END
```

```
10'*************************************************************************
20'*
30'*                    INSTANTANEOUS ORIFICE FLOW
40'*
50'*     by P. Scott Northrop                                      8-1-86
60'*
70'*************************************************************************
80 '  Call name:                    INFLO.BAS
90 '
92    PGH(0)=.5 :  PGH(1)=1 : PGH(2)=2 : PGH(3)=4
100  N = 1500         'size of the arrays
110 '
111  CLS:SCREEN 0,0,0:KEY OFF
112   LOCATE 3,1
114   INPUT "What was the gain "; GAIN#
116  FACTOR = PGH(GAIN#)
130  LOCATE 5,1
140  INPUT "Enter data to be differentiated as [dsk:]filename.dat  ";FILOLD$
150  LOCATE 7,1
160  INPUT "Enter name of output file as [dsk:]filename.dat       ";FILNEW$
170  DIM X(N) , Y(N) , Z(N)
180  LOCATE 9,1
190  INPUT "What was the temperature during calibration ";TEMP
200  LOCATE 11,1
210  PRINT "Reading old file..."
220  OPEN FILOLD$ AS #1 LEN = 30
230  FIELD #1, 15 AS X$, 15 AS Y$
240  GET #1,1
250  NPTS = CVS(X$)
260  M = CVS(Y$)
270  FOR I = 1 TO NPTS
280    GET #1,I+1
290    X(I) = CVS(X$)
300    Z(I) = CVS(Y$)
310  NEXT I
320  CLOSE #1
330 '
340  LOCATE 13.1
350  PRINT "Computing modifications..."
360   DEN = 12*(X(3)-X(2))*FACTOR
370 NEND = NPTS - 2
380 '
390 FOR I = 3 TO NEND
410 ' For 5 micron with nitrogen, vol. =40.00 cc. For micromoles/sec,
420 ' and psia gage, const. = 20 psi/10volt*51.7149 torr/psia *32.12 ml
422 ' /82.05 ml atm/gmol k /760torr/atm *10e6 micromoles/mole =12.701
430   Y(I) = (Z(I-2)-8*Z(I-1)+8*Z(I+1)-Z(I+2))*160.5655*32.12/(DEN*TEMP*40!)
433 ' Conversion factor for psi meter is 3.96017
435   X(I) = Z(I)/(3.96017*FACTOR)
```

```
440 NEXT I
450 NTOT=NPTS-5
460  LOCATE 15,1
470  PRINT "Writing new file..."
480  OPEN FILNEW$ AS #1 LEN = 30
490  FIELD #1, 15 AS X$, 15 AS Y$
500  LSET X$ = MKS$(NTOT) : LSET Y$ = MKS$(M)
505 NEND=NEND-1
510  PUT #1,1
520  FOR I = 3 TO NEND
530    LSET X$ = MKS$(X(I)) : LSET Y$ = MKS$(Y(I))
540    PUT #1,I-1
550  NEXT I
560  CLOSE #1
570  LOCATE 17,1
580  PRINT "Done."
590  LOCATE 24,1
600  END
```

```
100'*************************************************************************
110'*
120'*                  MODIFY A DATA FILE
130'*
140'*  by Sergio Edelstein                          4-8-85
150'*
160'*************************************************************************
170 '  Call name:                    CHOP.BAS
180 '
185  N = 2000         'size of the arrays
186 '
190  CLS:SCREEN 0,0,0:KEY OFF
200  LOCATE 5,1
210  INPUT "Enter name of file to be chopped off as [dsk:]filename.dat  ";FILOLD$
220  LOCATE 7,1
230  INPUT "Enter name of new file as [dsk:]filename.dat            ";FILNEW$
231  LOCATE 9,1
232  INPUT "Enter lowest X value  ";XMIN
233  LOCATE 11,1
234  INPUT "Enter highest X value ";XMAX
240  DIM X(N) , Y(N)
250  LOCATE 13,1
260  PRINT "Reading old file..."
270  OPEN FILOLD$ AS #1 LEN = 30
280  FIELD #1, 15 AS X$, 15 AS Y$
290  GET #1,1
300  NPTS = CVS(X$)
305  M = CVS(Y$)
306  NNEW = 1
310  FOR I = 1 TO NPTS
320    GET #1,I+1
330    X(NNEW) = CVS(X$)
340    Y(NNEW) = CVS(Y$)
341     IF X(NNEW) > XMAX OR X(NNEW) = XMAX GOTO 360
343     IF X(NNEW) > XMIN OR X(NNEW) = XMIN THEN NNEW = NNEW+1
350  NEXT I
360  CLOSE #1
390 '
485  LOCATE 15,1
490  PRINT "Writing new file..."
500  OPEN FILNEW$ AS #1 LEN = 30
510  FIELD #1, 15 AS X$, 15 AS Y$
520  LSET X$ = MKS$(NNEW) : LSET Y$ = MKS$(M)
530  PUT #1,1
540  FOR I = 1 TO NNEW
550    LSET X$ = MKS$(X(I)) : LSET Y$ = MKS$(Y(I))
560    PUT #1,I+1
570  NEXT I
580  CLOSE #1
```

```
590 LOCATE 17,1
600 PRINT "Done."
610 KEY ON
611 LOCATE 24,1
612 END
```

```
1000'*****************************************************************
1010'*
1020'*       FIFTH ORDER LEAST SQUARES POLYNOMIAL UTILITY
1030'* MetraByte Corporation                Rev. 1.10  8/16/83
1040'*****************************************************************
1041 ' Call name:                    POLY2.BAS
1050 '
1060 '     This program evaluates the coefficients C1-6 for the polynomial
1070 'approximation:-
1080 '
1090 '  Y = C1 + C2*X  +  C3*X^2  +  C4*X^3  +  C5*X^4  +  C6*X^5
1100 '
1110 '    such that the sum of the squares of the errors between the actual
1120 'value of Y and the polynomial value of Y for all data points entered
1130 'is minimised (i.e. curve fitting).
1140 '     This approximation is useful for linearizing transducer outputs.
1150 'e.g. flowmeters, thermocouples, tacho-generators etc.. The transducer
1160 'output is obtained from the A/D converter (suitably scaled if required)
1170 'as variable X and the linearized output from the transducer e.g. flow,
1180 'temperature, velocity etc. is calculated as variable Y. The coefficients
1190 'C1-6 are calculated from a set of Y,X data or calibration points.
1200 '     Type RUN(CR) to run the program. The prompts are self explanatory.
1205 'You should be prepared to provide the number of data points (N) and the
1210 'data (arrays X(N), Y(N)). The data is displayed and you may make any
1215 'changes to correct entry mistakes. The program then proceeds to perform
1220 'a regression analysis to calculate the coefficients of the polynomial.
1225 'You are prompted to select the order required, up to 5th. order. Usually
1230 '5th. order is the best option unless you want to experiment with trying
1235 'a lower order. After the analysis is finished, the coefficients are
1240 'displayed and you can check the conformance by inputting various values
1245 'of X and seeing how accurate Y is. If you wish, before exiting the
1250 'program, you can run the regression at another order on the same data
1255 'to see how good the conformance is with a different order polynomial.
1270 '
1280 '     Once the coefficients are evaluated the polynomial can be inserted
1290 'into your programs as a subroutine. The neatest way is to use a loop to
1300 'evaluate it as follows:-
1304 '
1305 '    xxx00 Y = COEF(1)
1310 '    xxx10 FOR CNT% = 5 TO 1 STEP -1
1320 '    xxx20 Y = Y + COEF(CNT% + 1) * X ^ CNT%
1330 '    xxx30 NEXT CNT%
1340 '    xxx40 RETURN
1350 '
1360 '
1500 '------ START - INITIALIZATION SECTION ----------------------------------
1505 SCREEN 0,0,0:KEY OFF:CLS:LOCATE 25,1:PRINT"POLYNOM";
1510 DIM COEF(6), MTX(6,7), SM(10), RT(6)
10000 '----- DATA POINT ENTRY -----------------------------------------------
```

```
10020 CLS:LOCATE 25,1:PRINT"POLYNOM - DATA FILE ENTRY";
10025 NP= 2000
10029 LOCATE 2,1
10030 INPUT "Enter name of file to be read as [dsk:]filename.dat ";FILOLD$
10040 DIM X(NP) , Y(NP)
10050 OPEN FILOLD$ AS #1 LEN = 30
10060 FIELD #1, 15 AS X$, 15 AS Y$
10065 GET #1,1
10070 N = CVS(X$)
10080 DUM = CVS(Y$)
10090 FOR I = 1 TO N
10100    GET #1,I+1
10110    X(I) = CVS(X$)
10120    Y(I) = CVS(Y$)
10125 PRINT I,X(I),Y(I)
10130 NEXT I
10140 CLOSE #1
20000 '------ PERFORM LINEAR REGRESSION ----------------------------------
20010 CLS:LOCATE 25,1:PRINT"POLYNOM - PERFORMING LINEAR
REGRESSION";
20030 LOCATE 2,1:INPUT"ORDER OF ANALYSIS REQUIRED (0-5)? ",ORD
20040 IF ORD <0 OR ORD>5 THEN GOTO 20030
20045 LOCATE 10,20:PRINT"WAIT - REGRESSION ANALYSIS IN PROGRESS"
20050 FOR I=1 TO 2*ORD
20060 SM(I)=0
20070 NEXT I
20080 FOR I = 1 TO ORD+1
20090 RT(I)=0
20100 NEXT I
20110 FOR PNT = 1 TO N
20120 FOR I= 1 TO ORD*2
20130 SM(I)=SM(I) + X(PNT)^I
20140 NEXT I
20150 FOR I = 1 TO ORD+1
20160 IF I=1 THEN RT(I)=RT(I) + Y(PNT)
20170 IF I<>1 THEN RT(I) = RT(I) + Y(PNT)*(X(PNT)^(I-1))
20180 NEXT I
20190 NEXT PNT
20200 MTX(1,1)=N
20210 FOR I=1 TO ORD+1
20220 MTX(I,ORD+2)=RT(I)
20230 FOR J=1 TO ORD+1
20240 IF I+J<>2 THEN MTX(I,J)=SM(I+J-2)
20250 NEXT J
20260 NEXT I
20270 FOR K = 1 TO ORD
20280 KTMP=K+1
20290 L=K
20300 FOR I=KTMP TO ORD+1
```

```
20310 IF ABS(MTX(I,K))>ABS(MTX(L,K)) THEN L=I
20320 NEXT I
20330 IF L=K THEN GOTO 20390
20340 FOR J=K TO ORD+2
20350 TMP=MTX(K,J)
20360 MTX(K,J)=MTX(L,J)
20370 MTX(L,J)=TMP
20380 NEXT J
20390 FOR I= KTMP TO ORD+1
20400 FTR = MTX(I,K)/MTX(K,K)
20410 FOR J= KTMP TO ORD+2
20420 MTX(I,J)=MTX(I,J) - FTR * MTX(K,J)
20430 NEXT J
20440 NEXT I
20450 NEXT K
20460 COEF(ORD+1) = MTX(ORD+1,ORD+2)/MTX(ORD+1,ORD+1)
20470 I=ORD
20480 ITMP= I+1
20490 TOT = 0
20500 FOR J= ITMP TO ORD+1
20510 TOT=TOT + MTX(I,J)*COEF(J)
20520 NEXT J
20530 COEF(I)=(MTX(I,ORD+2)-TOT)/MTX(I,I)
20540 I=I-1
20550 IF I>=1 THEN GOTO 20480
20560 '------ DISPLAY COEFFICIENTS ------------------------------------
20565 CLS:LOCATE 1,1
20570 FOR I=1 TO ORD+1
20580 PRINT"COEF(";I;") = ";COEF(I)
20590 NEXT I
20600  RESID = 0
20610  FOR I = 1 TO NPTS
20620  P = X(I)
20630   Q = COEF(6)
20640  FOR CNT% =  5 TO 1 STEP -1
20650   Q = Q * P + COEF(CNT%)
20670  NEXT CNT%
20680  RESID = RESID + ABS( Y(I) - Q )
20690   NEXT I
20700   PRINT RESID
30000 '-------- TEST FIT ------------------------------------------------
30010 LOCATE 25,1:PRINT SPC(79):LOCATE 25,1:PRINT"POLYNOM - TEST
CONFORMANCE";
30015 LOCATE 9,1:PRINT"TEST CONFORMANCE":PRINT"----------------"
30020 LOCATE 12,1:PRINT SPC(79);:LOCATE 12,1:INPUT "X VALUE (type Q to
quit)? ",A$
30030 IF A$="Q" OR A$="q" THEN GOTO 30100
30040 X=VAL(A$)
30045 Y = COEF(1)
```

```
30050 FOR CNT%= 5 TO 1 STEP -1
30060 Y = Y + COEF(CNT%+1) * X^CNT%
30070 NEXT CNT%
30080 LOCATE 14,1:PRINT SPC(79):LOCATE 14,1:PRINT"Calculated Y (output) =
";Y;"  for X (input) = ";X
30090 GOTO 30020
30100 LOCATE 14,1:PRINT SPC(79):LOCATE 14,1:INPUT "TRY REGRESSION
WITH A DIFFERENT ORDER (Y/N)? ",A$
30110 IF A$="y" OR A$="Y" THEN GOTO 30130
30120 LOCATE 25,1:PRINT SPC(79):LOCATE 20,1:END
30130 ERASE SM, MTX, RT, COEF
30140 DIM COEF(6), MTX(6,7), SM(10), RT(6)
30150 GOTO 20000
30160 END
```

```
10'*************************************************************************
20'*
30'*              CREATE ADSORPTION INFORMATION FILES
40'*
50'*  by P. Scott Northrop                        6-27-85
60'*
70'*************************************************************************
75 '  Call name:                    INST.BAS
80 '
90   PGH(0)=.5 : PGH(1)=1 : PGH(2)=2 : PGH(3)=4
100  N = 1500         'size of the arrays
110 '
120  CLS:SCREEN 0,0,0:KEY OFF
121  LOCATE 1,1
123  INPUT "What was the gain "; GAIN#
125  IF GAIN#<0 OR GAIN#>3 GOTO 121
127  FACTOR=PGH(GAIN#)
130  LOCATE 3,1
140  INPUT "Enter name of data file to be read as [dsk:]filename.dat  ";FILOLD$
150 LOCATE 5,1
160 PRINT "The new data files will be sent to drive b: "
170  LOCATE 7,1
180  INPUT "Enter run number of this experiment ";RUNNUM$
190  FILNEW1$ = "b:iso"+RUNNUM$+".dat"
200  FILNEW2$ = "b:bet"+RUNNUM$+".dat"
210  FILNEW3$ = "b:pore"+RUNNUM$+".dat"
220  DIM X(N) , Y(N) , COEF(6) ,Z(N)
230  LOCATE 9,1
240  PRINT "Reading data..."
250  OPEN FILOLD$ AS #1 LEN = 30
260  FIELD #1, 15 AS X$, 15 AS Y$
270  GET #1,1
280  NPTS = CVS(X$)
290  M = CVS(Y$)
300  FOR I = 1 TO NPTS
310    GET #1,I+1
320    X(I) = CVS(X$)
330    Y(I) = CVS(Y$)
340  NEXT I
350  CLOSE #1
420  LOCATE 11,1
430  PRINT "Smoothing data..."
440  FOR K = 1 TO NPTS
450   Z(K) = Y(K)
460  NEXT K
470 ' Smooth the data by using appropriate weights of local points.
480 NMOD = NPTS - 2
490 FOR N = 3 TO NMOD
500     Y(N) = (-3*Z(N-2)+12*Z(N-1)+17*Z(N)+12*Z(N+1)-3*Z(N+2))/35
```

```
510 NEXT N
520 ' Now that the data is smoothed, calculate the isotherm.
530 LOCATE 13,1
540 INPUT "Enter initial temperature in k " ; TEMP1
544 LOCATE 14,1
546 INPUT "Enter final temperature in k " ; TEMP2
550 LOCATE 15,1
560 INPUT "Enter total effective volume in ml " ; VOL
570  LOCATE 16,1
580  INPUT "What was the vapor pressure of adsorbate ";PFIN
590  LOCATE 17,1
600 ' Read coefficients for instantaneous flow rate as a function of pressure:
610  INPUT "Enter first rate coefficient ";COEF(1)
620  INPUT "Enter second coefficient";COEF(2)
630  INPUT "Enter third coefficient ";COEF(3)
640  INPUT "Enter fourth coefficient ";COEF(4)
650  INPUT "Enter fifth coefficient ";COEF(5)
660  INPUT "Enter sixth coefficient ";COEF(6)
670 CLS
680 LOCATE 13,1
690 PRINT "Computing Isotherm..."
695  ' Pressure = bits/4096*20psi*0.01934torr/psi
700   P0 = Y(1)/(3.96017*FACTOR)
710  DVOL=32.12
720  ' The initial amount of gas is that in the dead volume at t=0.
730  TOTMOL=P0*DVOL*16.0364/TEMP1
740 TIME = X(2)-X(1)
750  FOR I = 2 TO NPTS
760  P = Y(I)/(3.96017*FACTOR)
770  Q = COEF(6)
780  FOR CNT% = 5 TO 1  STEP - 1
790  Q = Q * P + COEF(CNT%)
800  NEXT CNT%
810 '
815  TEMP = TEMP1 + (TEMP2-TEMP1)*(X(I)-X(0))/(X(NPTS)-X(0))
820  TOTMOL=TOTMOL + Q * TIME
830  ADSMOL=TOTMOL-P*VOL*16.0364/TEMP
840  X(I) = P
850   Y(I) = ADSMOL
860  NEXT I
870  X(1)=P0 : Y(1)=0
880  LOCATE 19,1
890  PRINT "Creating data files:"
900  OPEN FILNEW1$ AS #1 LEN = 30
910  FIELD #1, 15 AS X$, 15 AS Y$
920  LSET X$ = MKS$(NPTS) : LSET Y$ = MKS$(M)
930  PUT #1,1
940  FOR I = 1 TO NPTS
950   LSET X$ = MKS$(X(I)) : LSET Y$ = MKS$(Y(I))
```

```
960   PUT #1,I+1
970  NEXT I
980  CLOSE #1
990 PRINT FILNEW1$
1000 ' Now create a BET file.
1010 OPEN FILNEW1$ AS #2 LEN = 30
1020 FIELD #2, 15 AS X$, 15 AS Y$
1030 GET #2,1
1040 NPTS = CVS(X$)
1050 M = CVS(Y$)
1060  NNEW = 1
1070  FOR I = 1 TO NPTS
1080  GET #2, I+1
1090    X(NNEW) = CVS(X$)
1100    Y(NNEW) = CVS(Y$)
1110  PHI=.31*PFIN
1120  PLO=.04*PFIN
1130      IF X(NNEW) > PHI OR X(NNEW) = PHI GOTO 1160
1140      IF X(NNEW) > PLO OR X(NNEW) = PLO THEN NNEW = NNEW + 1
1150  NEXT I
1160  CLOSE #2
1170  OPEN FILNEW2$ AS #1 LEN = 30
1180  FIELD #1, 15 AS X$ , 15 AS Y$
1190  LSET X$ = MKS$(NNEW) : LSET Y$ = MKS$(M)
1200  PUT #1,1
1210  FOR I = 1 TO NNEW
1220   X(I) = X(I)/PFIN
1230   Y(I) = X(I)/(Y(I)*(1-X(I)))*1000000!
1240   LSET X$ = MKS$(X(I))
1250   LSET Y$ = MKS$(Y(I))
1260   PUT #1,I+1
1270  NEXT I
1280  CLOSE #1
1290  PRINT FILNEW2$
1300  OPEN FILNEW1$ AS #1 LEN = 30
1310  FIELD #1, 15 AS X$, 15 AS Y$
1320  GET #1,1
1330  NPTS = CVS(X$)
1340  M = CVS(Y$)
1350  NNEW = 1
1360   FOR N =  1 TO NPTS
1370      GET #1, N+1
1380  X(NNEW) = CVS(X$)
1390  Y(NNEW) = CVS(Y$)
1400  HIEND = .92*PFIN
1410  LOEND = .5*PFIN
1420    IF X(NNEW) > HIEND OR X(NNEW)=HIEND GOTO 1450
1430   IF X(NNEW) > LOEND OR X(NNEW)=LOEND THEN NNEW=NNEW+1
1440 NEXT N
```

```
1450 CLOSE #1
1460 OPEN FILNEW3$ AS #2 LEN = 30
1470 FIELD #2, 15 AS X$, 15 AS Y$
1480 LSET X$ = MKS$(NNEW) : LSET Y$ =  MKS$(M)
1490 PUT #2,1
1500  FOR J = 1 TO NNEW
1510   Z(J) = Y(J)
1520  NEXT J
1530 NLAST = NNEW - 2
1540  Y(1)=0:X(1)=0:Y(2)=0:X(2)=0
1550  Y(NLAST+2)=0:X(NLAST+2)=0:Y(NLAST+1)=0:X(NLAST+1)=0
1560  FOR I=3 TO NLAST
1570   ARG = X(I)/PFIN
1580   IF ARG < 0 OR ARG = 0 THEN GOTO 1690
1590   DEN = -1*LOG(ARG)
1600 ' Surface Tension nitrogen = 8.5 dynes/cm, v = 34.65 cm^3/gmole.
1610   PRAD = 1.018E-07/DEN
1620 ' For freon, gamma = 18 dynes/cm, v=73.15cm^3/gmole,T=282 K.
1630 '  PRAD = 1.123E-07/DEN
1640   X(I) = LOG(PRAD)/2.303 + 6
1650   Y(I) = (Z(I-2)-8*Z(I-1)+8*Z(I+1)-Z(I+2))*3.465E-05/(12*(X(I)-X(I-1)))
1660 LSET X$ = MKS$(X(I))
1670 LSET Y$ = MKS$(Y(I))
1680 PUT #2, I-1
1690 NEXT I
1700 CLOSE #2
1710 PRINT FILNEW3$
1720 SCREEN 0,0,0
1730 DIM FL$(1)
1740  INPUT "Do you wish to plot the isotherm ";ANS$
1750  IF ANS$="y" OR ANS$="Y" THEN FL$(1)=FILNEW1$ ELSE GOTO 1790
1760 YLBL$= "Micromoles "
1770  XLBL$= "Pressure  (torr)"
1780  GOTO 1830
1790  INPUT "Do you wish to see the BET plot "; ANS$
1800  IF ANS$="y" OR ANS$="Y" THEN FL$(1)=FILNEW2$  ELSE GOTO 2060
1810  YLBL$= "BET plot"
1820  XLBL$= "Rel. Pres.  (P/P0)"
1830  PRINT "Working...."
1840  NOF = 1
1850 OPEN "RLINPLT.LNK" AS #1 LEN = 30
1860 FIELD #1, 30 AS RFLD$
1870 FOR I = 1 TO 21:LSET RFLF$ = "XXXXXXXXXX":PUT #1,I:NEXT I:CLOSE #1
1880 OPEN "RLINPLT.LNK" AS #1 LEN = 30
1890 FIELD #1, 30 AS RFLD$
1900 GET #1,1
1910 LSET RFLD$ = MKI$(NOF)
1920 PUT #1,1
1930 GET #1,2
```

```
1940 LSET RFLD$ = YLBL$
1950 PUT #1,2
1960 GET #1,3
1970 LSET RFLD$ = XLBL$
1980 PUT #1,3
1990 FOR I = 1 TO NOF
2000   GET #1,I+3
2010   LSET RFLD$ = FL$(I)
2020   PUT #1,I+3
2030 NEXT I
2040 CLOSE #1
2050 CHAIN "LINPLT.BAS"
2060 END
```

```
1000'*************************************************************************
1010'*
1020'*        FIFTH ORDER LEAST SQUARES POLYNOMIAL UTILITY
1030'* MetraByte Corporation                  Rev. 1.10  8/16/83
1040'*************************************************************************
1045 ' Call name:                    MONO.BAS
1050 '
1060 '     This program evaluates the coefficients C1-6 for the polynomial
1070 'approximation:-
1080 '
1090 '  Y = C1 + C2*X  +  C3*X^2  +  C4*X^3  +  C5*X^4  +  C6*X^5
1100 '
1110 '    such that the sum of the squares of the errors between the actual
1120 'value of Y and the polynomial value of Y for all data points entered
1130 'is minimised (i.e. curve fitting).
1140 '     This approximation is useful for linearizing transducer outputs.
1150 'e.g. flowmeters, thermocouples, tacho-generators etc.. The transducer
1160 'output is obtained from the A/D converter (suitably scaled if required)
1170 'as variable X and the linearized output from the transducer e.g. flow,
1180 'temperature, velocity etc. is calculated as variable Y. The coefficients
1190 'C1-6 are calculated from a set of Y,X data or calibration points.
1200 '     Type RUN(CR) to run the program. The prompts are self explanatory.
1205 'You should be prepared to provide the number of data points (N) and the
1210 'data (arrays X(N), Y(N)). The data is displayed and you may make any
1215 'changes to correct entry mistakes. The program then proceeds to perform
1220 'a regression analysis to calculate the coefficients of the polynomial.
1225 'You are prompted to select the order required, up to 5th. order. Usually
1230 '5th. order is the best option unless you want to experiment with trying
1235 'a lower order. After the analysis is finished, the coefficients are
1240 'displayed and you can check the conformance by inputting various values
1245 'of X and seeing how accurate Y is. If you wish, before exiting the
1250 'program, you can run the regression at another order on the same data
1255 'to see how good the conformance is with a different order polynomial.
1270 '
1280 '     Once the coefficients are evaluated the polynomial can be inserted
1290 'into your programs as a subroutine. The neatest way is to use a loop to
1300 'evaluate it as follows:-
1304 '
1305 '    xxx00 Y = COEF(1)
1310 '    xxx10 FOR CNT% = 5 TO 1 STEP -1
1320 '    xxx20 Y = Y + COEF(CNT% + 1) * X ^ CNT%
1330 '    xxx30 NEXT CNT%
1340 '    xxx40 RETURN
1350 '
1360 '
1500 '------ START - INITIALIZATION SECTION ----------------------------------
1505 SCREEN 0,0,0:KEY OFF:CLS:LOCATE 25,1:PRINT"POLYNOM";
1510 DIM COEF(6), MTX(6,7), SM(10), RT(6)
10000 '----- DATA POINT ENTRY ------------------------------------------------
```

```
10025 NP= 2000
10029 LOCATE 2,1
10030 INPUT "Enter name of file to be read as [dsk:]filename.dat ";FILOLD$
10040 DIM X(NP) , Y(NP)
10050 OPEN FILOLD$ AS #1 LEN = 30
10060 FIELD #1, 15 AS X$, 15 AS Y$
10065 GET #1,1
10070 N = CVS(X$)
10080 DUM = CVS(Y$)
10090 FOR I = 1 TO N
10100    GET #1,I+1
10110    X(I) = CVS(X$)
10120    Y(I) = CVS(Y$)
10125 PRINT I,X(I),Y(I)
10130 NEXT I
10140 CLOSE #1
20000 '------ PERFORM LINEAR REGRESSION ----------------------------------
20010 CLS:LOCATE 25,1:PRINT"POLYNOM - PERFORMING LINEAR
REGRESSION";
20030 ORD = 1
20045 LOCATE 10,20:PRINT"WAIT - REGRESSION ANALYSIS IN PROGRESS"
20050 FOR I=1 TO 2*ORD
20060 SM(I)=0
20070 NEXT I
20080 FOR I = 1 TO ORD+1
20090 RT(I)=0
20100 NEXT I
20110 FOR PNT = 1 TO N
20120 FOR I= 1 TO ORD*2
20130 SM(I)=SM(I) + X(PNT)^I
20140 NEXT I
20150 FOR I = 1 TO ORD+1
20160 IF I=1 THEN RT(I)=RT(I) + Y(PNT)
20170 IF I<>1 THEN RT(I) = RT(I) + Y(PNT)*(X(PNT)^(I-1))
20180 NEXT I
20190 NEXT PNT
20200 MTX(1,1)=N
20210 FOR I=1 TO ORD+1
20220 MTX(I,ORD+2)=RT(I)
20230 FOR J=1 TO ORD+1
20240 IF I+J<>2 THEN MTX(I,J)=SM(I+J-2)
20250 NEXT J
20260 NEXT I
20270 FOR K = 1 TO ORD
20280 KTMP=K+1
20290 L=K
20300 FOR I=KTMP TO ORD+1
20310 IF ABS(MTX(I,K))>ABS(MTX(L,K)) THEN L=I
20320 NEXT I
```

```
20330 IF L=K THEN GOTO 20390
20340 FOR J=K TO ORD+2
20350 TMP=MTX(K,J)
20360 MTX(K,J)=MTX(L,J)
20370 MTX(L,J)=TMP
20380 NEXT J
20390 FOR I= KTMP TO ORD+1
20400 FTR = MTX(I,K)/MTX(K,K)
20410 FOR J= KTMP TO ORD+2
20420 MTX(I,J)=MTX(I,J) - FTR * MTX(K,J)
20430 NEXT J
20440 NEXT I
20450 NEXT K
20460 COEF(ORD+1) = MTX(ORD+1,ORD+2)/MTX(ORD+1,ORD+1)
20470 I=ORD
20480 ITMP= I+1
20490 TOT = 0
20500 FOR J= ITMP TO ORD+1
20510 TOT=TOT + MTX(I,J)*COEF(J)
20520 NEXT J
20530 COEF(I)=(MTX(I,ORD+2)-TOT)/MTX(I,I)
20540 I=I-1
20550 IF I>=1 THEN GOTO 20480
20560 '------ DISPLAY COEFFICIENTS ----------------------------------------
20565 CLS:LOCATE 1,1
20570 FOR I=1 TO ORD+1
20580 PRINT"COEF(";I;") = ";COEF(I)
20590 NEXT I
20600 RECIP = 1/(COEF(1)+COEF(2))
20610 AREA  = 16.2 * 6022 * RECIP
20611  NM= RECIP
20612  C=COEF(2)/COEF(1) + 1
20620 RESID = 0
20630 FOR I =1 TO N
20640    RESID = RESID +ABS(Y(I)-COEF(2)*X(I)-COEF(1))
20650 NEXT I
20660 PRINT AREA,RECIP,C,RESID
30160 END
```

```
100'*************************************************************************
110'*
120'*                    READ A DATA FILE
130'*
140'*  by P. Scott Northrop                          6-27-85
150'*
160'*************************************************************************
170 '  Call name:                    READAT.BAS
180 '
185  N = 2000          'size of the arrays
186 '
190  CLS:SCREEN 0,0,0:KEY OFF
200  LOCATE 5,1
210  INPUT "Enter name of file to be read as [dsk:]filename.dat  ";FILOLD$
220 '
230 '
240  DIM X(N) , Y(N)
250  LOCATE 9,1
260  PRINT "Loading buffer..."
270  OPEN FILOLD$ AS #1 LEN = 30
280  FIELD #1, 15 AS X$, 15 AS Y$
290  GET #1,1
300  NPTS = CVS(X$)
305  M = CVS(Y$)
310  FOR I = 1 TO NPTS
320    GET #1,I+1
330    X(I) = CVS(X$)
340    Y(I) = CVS(Y$)
350  NEXT I
360  CLOSE #1
370 '
375  LOCATE 11.1
390 '
400 '
410 '---------------- INSERT DESIRED ALGORITHM HERE ----------------------
420 '
430  FOR I = 1 TO NPTS
440 '
450    PRINT I,X(I),Y(I)
460 '
470  NEXT I
480 '
610  KEY ON
611  LOCATE 24,1
612  END
```